Development and Evaluation of Binderless Coconut Husk Boards

Effects of Hot-Pressing Conditions on Bending Performance and Board Integrity

J. Lubbers

Delft University of Technology

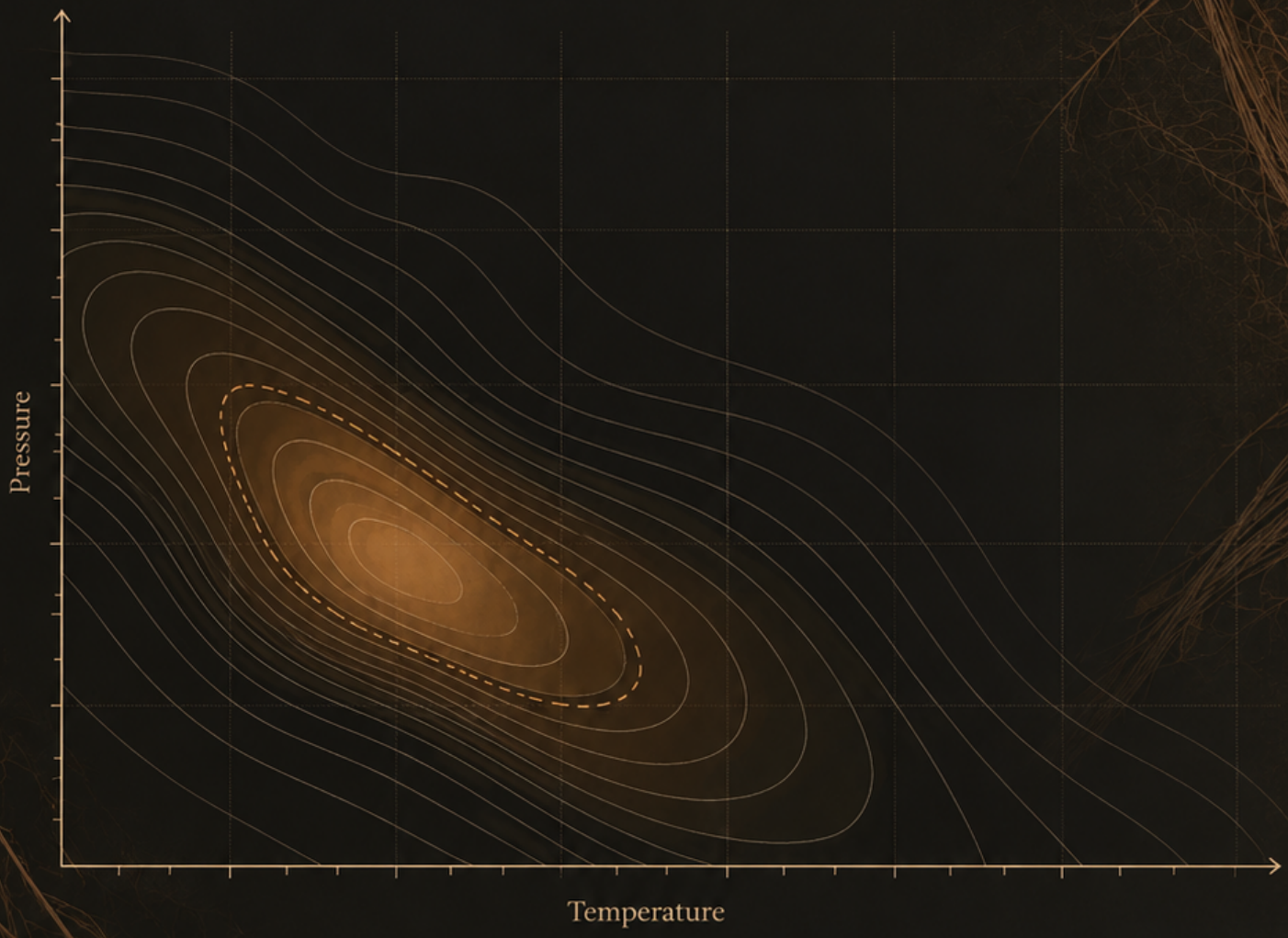

TU Delft

Development and Evaluation of Binderless Coconut Husk Boards

Effects of Hot-Pressing Conditions on Bending Performance and Board Integrity

by

J. Lubbers

to obtain the degree of Master of Science
at the Delft University of Technology,
to be defended publicly on Friday December 4, 2026 at 13:00.

Student number:	5880513	
Project duration:	March, 2026 – December, 2026	
Thesis committee:	Prof. dr. K. Hooman,	TU Delft, responsible supervisor
	Dr. L. L. Cutz Ijchajchal,	TU Delft, supervisor
	Dr. ir. J. Jovana,	TU Delft

An electronic version of this thesis is available at http://repository.tudelft.nl/.

TU Delft

Preface

This report was written as part of my thesis project on the development of bio-based materials from coconut husk. The project originated from discussions between TU Delft and CoEco about the potential of coconut husk as a raw material for pressed products. Earlier trials by CoEco had shown that board-like and packaging-related products could be formed from the material, but achieving consistent product quality within a relatively short pressing cycle remained a challenge. This provided the starting point for investigating the behaviour of coconut husk during hot pressing in more detail.

The experimental work developed towards binderless flat boards made from mechanically flattened coconut husk sheets. Rather than milling the entire husk into a homogeneous furnish, the sheets were retained so that much of the original fibre-pith structure remained intact and the material processing could be limited. The research focused on how pretreatment and hot-pressing conditions affected board consolidation, bending behaviour and visible defects. As the work progressed, the interfaces between the individual husk sheets became an important part of the study, leading to additional exploratory trials using pith and bio-oil between the layers.

I would like to thank Prof. Dr. K. Hooman and Dr. L. L. Cutz IJchajchal at TU Delft for their guidance, feedback and support throughout this project. I would also like to thank CoEco for providing the coconut husk material used in the experiments.

Finally, I would like to thank everyone who contributed through discussions, laboratory support or feedback during the preparation of this thesis. Their help was valuable throughout the experimental work and the development of this report.

J. Lubbers
Delft, October 2026

Abstract

Coconut husk contains long coir fibres and lignin-rich pith, making it a potential raw material for binderless board production. Instead of milling the husk, this study investigated the production of binderless flat boards by stacking and hot-pressing four mechanically flattened husk sheets that retain their original fibre-pith structure. The influence of material preparation and hot-pressing conditions on bending performance and visible defects was examined.

Pretreatment screening compared untreated coconut husk with immersion in demineralised water at $80\,^{\circ}$C for 1 h and immersion for 1 h in 1 wt% NaOH solution. Based on the results, the hot-water treatment (Demi80) was selected for the main design of experiments (DOE). Eighteen boards, each consisting of four flattened husk sheets, were manufactured using three temperature levels (170, 180 and $190\,^{\circ}$C) and three nominal pressure levels (9, 12 and 15 MPa), with a prescribed 4.5 min pressing cycle. Six additional boards were produced at the model-selected best condition of $185\,^{\circ}$C and 14.2 MPa. Two unmodified boards were used to compare measured performance with the model predictions, while four boards containing either bio-oil or additional pith between the sheets were produced to explore potential improvements.

Across the main experiment, modulus of rupture (MOR) ranged from 9.53 to 33.74 MPa and apparent modulus of elasticity (MOE) from 0.266 to 1.887 GPa. Higher pressure was generally associated with better average bending performance, while temperature effects were less consistent. Neither quadratic bending model was statistically significant overall. At the selected setting, predicted MOR and apparent MOE (22.59 MPa and 1.497 GPa) were broadly comparable to the unmodified confirmation means (18.43 MPa and 1.73 GPa), but this local comparison did not validate the models. The follow-up experiments identified added pith as a promising route for improving bending performance, with mean MOR and apparent MOE 85.3% and 51.8% higher than the confirmation board references, respectively. Bio-oil also showed potential, although the observed improvements were smaller. These exploratory findings require further investigation. The confirmation follow-up boards achieved a mean MOR above the numerical JIS A 5905 Type 15 benchmark, and both added-pith specimens exceeded the EN 622-5 bending-strength benchmark.

The results demonstrate the feasibility of producing binderless boards from retained coconut husk sheets. However, variability in bending performance, interlayer defects and the adapted testing procedure indicate that further development is needed before product compliance can be established.

Nomenclature

Abbreviations

Abbreviation	Meaning
ASTM	ASTM International
DOE	Design of experiments
EN	European Standard
FTIR	Fourier-transform infrared spectroscopy
IB	Internal bond strength
ISO	International Organization for Standardization
JIS	Japanese Industrial Standard
MC	Moisture content
MDF	Medium-density fibreboard
MOE	Modulus of elasticity; reported as apparent MOE in the present bending tests
MOR	Modulus of rupture
N.S.	Not specified
PLA	Polylactic acid
SD	Sample standard deviation
SE	Standard error
TGA	Thermogravimetric analysis
TS	Thickness swelling
WA	Water absorption

Experimental Designations

Designation	Meaning
Demi80	Demineralised-water treatment at $80\,^{\circ}$C for 1 h
C185-14	Follow-up condition at $185\,^{\circ}$C and 14.2 MPa
C185-14-O	Follow-up condition with bio-oil at the sheet interfaces
C185-14-P	Follow-up condition with additional pith at the sheet interfaces

Symbols

Symbol	Meaning	Unit
A_0	Nominal initial lay-up area	mm^2
b	Specimen width	mm
c_m	Machine-compliance coefficient	$\mathrm{mm\,N^{-1}}$
F	Applied force	N or kN
F_max	Selected structural failure load	N
k	Force–displacement slope	$\mathrm{N\,mm^{-1}}$
L	Bending support span	mm
l	Specimen length	mm
m	Mass	g
m_{70}	Mass after drying at $70\,^\circ\mathrm{C}$	g
m_dry	Estimated dry mass	g
m_target	Target mass at the specified moisture content	g
P	Nominal pressing pressure	MPa
T	Nominal platen temperature	°C
T_rel	Relative FTIR transmittance	%
t	Specimen thickness	mm
ρ	Apparent density	$\mathrm{kg\,m^{-3}}$
δ	Crosshead displacement	mm
δ_mc	Machine-compliance-corrected displacement	mm
δ_rel	Displacement relative to the 5 N reference point	mm
ΔA	Differential FTIR absorbance	–
λ	Thermal conductivity	$\mathrm{W\,m^{-1}\,K^{-1}}$
β	Regression coefficient	response-dependent
ε	Regression residual	response-dependent
R^2	Coefficient of determination	–

Notation

Notation	Meaning
wt.%	Percentage by mass
w/w	Mass-to-mass ratio

Contents

Preface i

Abstract ii

Nomenclature iii

1 Introduction 1
- 1.1 Background and motivation . . . 1
- 1.2 Material characteristics and binderless board formation . . . 2
- 1.3 Product context and selected manufacturing route . . . 3
- 1.4 Research problem and aim . . . 4
- 1.5 Relevant parameters . . . 4
- 1.6 Scope and limitations . . . 5

2 Literature Review 6
- 2.1 Purpose and research topics . . . 6
- 2.2 Literature search strategy . . . 6
- 2.3 Coconut husk as a variable input material . . . 7
  - 2.3.1 Variance depending on region . . . 7
  - 2.3.2 Variance depending on age . . . 7
  - 2.3.3 Comparison . . . 9
- 2.4 Temperature-time effects and thermal degradation . . . 10
- 2.5 Pretreatment approaches relevant to flattened husk sheets . . . 10
- 2.6 Route 1: Low-density insulation boards . . . 11
  - 2.6.1 Effects of fibre treatment and binder addition . . . 11
  - 2.6.2 Interpretation . . . 12
  - 2.6.3 Process window . . . 12
- 2.7 Route 2: Binderless flat boards . . . 12
  - 2.7.1 Interpretation . . . 15
  - 2.7.2 Process window . . . 16
- 2.8 Route 3: Moulded binderless products . . . 16
  - 2.8.1 Interpretation . . . 16
  - 2.8.2 Process window . . . 16
- 2.9 Requirements for products . . . 17
- 2.10 Selection of the experimental route . . . 18
  - 2.10.1 From literature conditions to the experimental approach . . . 18
- 2.11 Knowledge gap . . . 19
- 2.12 Main research question . . . 19
- 2.13 Subquestions . . . 19

3 Methodology 20
- 3.1 Experimental Approach . . . 20
- 3.2 Materials and Equipment . . . 21
- 3.3 Husk Preparation and Dry-Mass Allocation . . . 22
  - 3.3.1 Sheet Preparation and Reference Drying . . . 22
  - 3.3.2 Parent-Sheet Moisture and Smaller-Sheet Mass . . . 23
  - 3.3.3 Grading and Initial Board Allocation . . . 23
- 3.4 Preliminary Trials and Pretreatment Selection . . . 23
  - 3.4.1 Development of the Manufacturing Procedure . . . 23
  - 3.4.2 Exploratory Pretreatment Screening . . . 24
  - 3.4.3 Exploratory FTIR Characterisation . . . 25

3.5 Final DOE and Board Manufacture . . . 25
3.5.1 Post-Treatment Material Preparation . . . 25
3.5.2 Factorial Design and Production Order . . . 26
3.5.3 Lay-Up and Nominal Pressure . . . 26
3.5.4 Temperature Control and Pressing Cycle . . . 27
3.5.5 Cooling and Board Inspection . . . 27
3.5.6 Post-DOE Confirmation and Interlayer Trials . . . 28
3.6 Specimen Preparation and Physical Measurements . . . 29
3.6.1 Whole-Board Measurement Schedule and Rationale . . . 29
3.6.2 Whole-Board Density, Mass Change and Post-Pressing Thickness Recovery . . . 30
3.6.3 Interpretation of Post-Pressing Thickness Recovery . . . 30
3.6.4 Sequential Dry Cutting . . . 31
3.6.5 Cut-Specimen Dimensions and Apparent Density . . . 32
3.7 Three-Point Bending and Mechanical Data Processing . . . 32
3.7.1 Test Geometry and Loading . . . 32
3.7.2 Failure Load and Modulus of Rupture . . . 33
3.7.3 Displacement Reference and Modulus of Elasticity . . . 33
3.7.4 Failure Observations . . . 34
3.8 Visual Observations and Preliminary Cutting Check . . . 34
3.9 Statistical Analysis . . . 34
3.9.1 Data Organisation and Reporting . . . 34
3.9.2 Spreadsheet Processing and JMP Outputs . . . 34
3.9.3 Response Surface Modelling . . . 35
3.10 Practical Challenges and Experimental Adaptations . . . 35

4 Results 37
4.1 Pretreatment Screening . . . 37
4.1.1 Mechanical Screening Results . . . 37
4.1.2 Selection of Demi80 for the Main Experiment . . . 37
4.1.3 FTIR Comparison of Pretreated Material . . . 37
4.2 Material Preparation and Moisture Condition . . . 39
4.2.1 Dry-Mass Determination and Moisture Conditioning . . . 39
4.2.2 Material Loading for the Main DOE . . . 39
4.2.3 Material Loading and Moisture at the Model-Selected Best Condition . . . 40
4.3 Board Production and Physical Properties . . . 40
4.3.1 Recorded Pressing Conditions . . . 40
4.3.2 Board Mass, Thickness and Density . . . 41
4.3.3 Post-Pressing Mass and Dimensional Changes . . . 41
4.4 Three-Point Bending Results . . . 43
4.4.1 Load-Displacement Behaviour . . . 43
4.4.2 Modulus of Rupture . . . 43
4.4.3 Modulus of Elasticity . . . 43
4.4.4 Observed Load Drops and Recovery . . . 43
4.5 Effects of Pressing Temperature and Pressure . . . 44
4.5.1 Measured MOR and MOE by DOE Condition . . . 44
4.6 Statistical Analysis and Fitted Responses . . . 46
4.6.1 Quadratic Regression Models . . . 46
4.6.2 Model Fits and Estimated Effects . . . 47
4.6.3 Model Diagnostics . . . 47
4.6.4 Fitted MOR and MOE Responses . . . 47
4.7 Visual Board Quality . . . 49
4.7.1 Distribution of Delamination Scores . . . 49
4.7.2 Representative Delamination Observations . . . 49

4.8 Desirability-Based Selection of the Follow-up Condition . . . 50
4.9 Boards Produced at the Model-Selected Best Condition . . . 51
4.9.1 Material Additions and Visual Quality . . . 51
4.9.2 Comparison of Unmodified and Interlayer Variants . . . 51
4.9.3 Numerical Comparison with Development Benchmarks . . . 54
4.10 Summary of Main Findings . . . 54

5 Discussion **55**
5.1 Pretreatment Choice and FTIR Interpretation . . . 55
5.2 Pressing Conditions and Mechanical Response . . . 55
5.2.1 Interpretation of the Model-Selected Best Condition . . . 56
5.2.2 Reduced Bending Geometry and Possible Shear Effects . . . 56
5.3 Consolidation and Changes after Pressing . . . 56
5.3.1 Layer Integrity and Vapour Escape . . . 56
5.4 Exploratory Interlayer Additions . . . 57
5.5 Comparison with Existing Boards and Product Requirements . . . 57
5.6 Limitations and Remaining Uncertainty . . . 57

6 Conclusions **59**
6.1 Material Pretreatment . . . 59
6.2 Pressing Conditions and Mechanical Performance . . . 59
6.3 Supporting Physical Changes and Board Integrity . . . 59
6.4 Exploratory Interlayer Additions . . . 60
6.5 Overall Conclusion . . . 60

7 Recommendations **61**
7.1 Priority 1: Interlayer Bonding and Controlled Pith Addition . . . 61
7.2 Priority 2: Bending Geometry, Failure Mode and Reproducibility . . . 61
7.3 Priority 3: Post-Pressing Recovery and Vapour Management . . . 61
7.4 Priority 4: Mechanical and Product Validation . . . 62

A Supporting comparison data for non-coconut lignocellulosic materials **63**
A.1 Purpose of the appendix . . . 63
A.2 Reference materials and relevance . . . 63
A.3 Bagasse comparison from the Panyakaew and Fotios study . . . 63
A.4 High-frequency and dielectric-heating reference studies . . . 64

B Supplementary Quadratic Regression Results **65**

1

Introduction

Declaration on the Use of AI

Generative AI tools were used to assist with language editing. The author reviewed and revised the resulting text and is responsible for the experimental procedures, data analysis, interpretations and references presented in this thesis. Some schematics and illustrative figures such as Figure 1.2 have been prepared with AI assistance.

1.1. Background and motivation

Coconut husk is a lignocellulosic residue generated during processing of the fruit of *Cocos nucifera*. Long coir fibres and a finer pith fraction remain together in the husk, offering a potential raw material for pressed bio-based products. Established uses include ropes, mats, brushes and horticultural substrates, while research into board manufacture offers another possible use for this agricultural material [1, 2].

CoEco, which supplied the coconut husk for this research, had previously produced board-like and moulded products without a conventional synthetic binder. However, reproducible products had required a pressing cycle of approximately 30 min. This motivated the investigation of a shorter laboratory pressing procedure. The present work uses a 4 min pressure hold within a prescribed 4.5 min press operation (15 s loading, 240 s holding and 15 s unloading), excluding material handling and other preparation time. The earlier CoEco process was not examined in a controlled comparison, so the shorter operation does not demonstrate equivalent performance or an industrial reduction in total cycle time.



Figure 1.1: Examples of traditional uses and product streams associated with coconut husk [1].

1.2. Material characteristics and binderless board formation

The husk forms the fibrous outer part of the coconut (Figure 1.2). Its fibre–pith distribution, moisture condition and local structure can vary with origin, maturity and handling [3, 4]. Such variation matters when individual husk pieces are assembled into a board: similar overall material masses do not necessarily provide the same fibre orientation, thickness or surface contact.

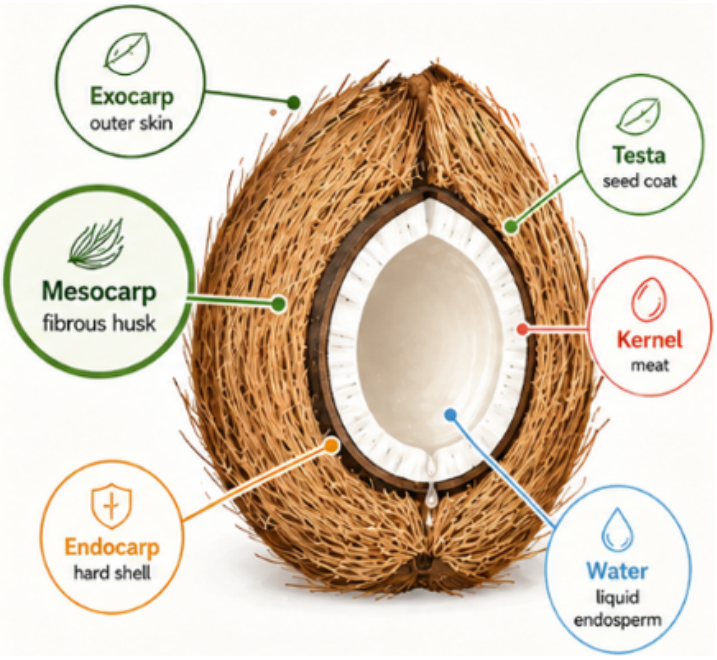

Figure 1.2: Anatomical structure of the coconut, including the fibrous husk.

Coconut cultivation is concentrated in tropical regions, including Indonesia, the Philippines and India. Husk availability could support regional material processing, although local quality, supply volumes and competing uses vary [2]. Figure 1.3 gives a literature-derived production overview, not a current forecast.

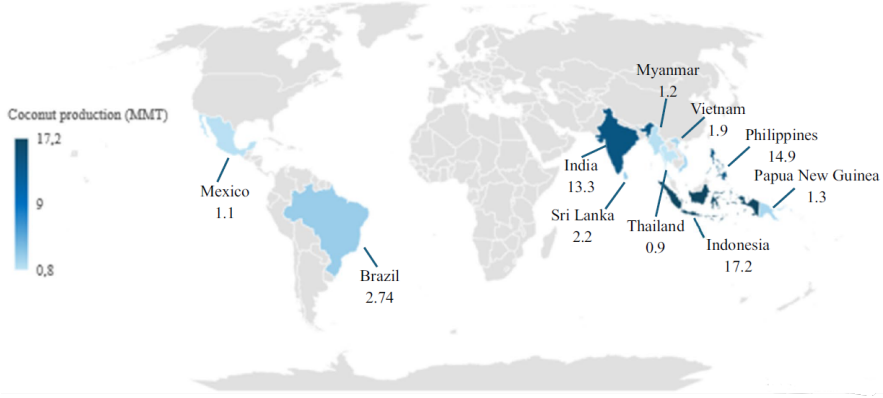

Figure 1.3: Coconut-producing countries and reported production volumes, based on the literature source used to prepare the figure [2].

Coconut husk contains cellulose, hemicellulose and lignin (Figure 1.4). The coir fibres provide a potential reinforcing structure, whereas the finer pith contains lignin and may contribute to intrinsic bonding during hot pressing [5, 6]. Heat, moisture and pressure influence deformation and contact between the constituents. The extent to which any particular physical or chemical bonding mechanism operates cannot be determined from bending measurements alone.

Applied pressure can bring fibre-rich and pith-rich regions into closer contact, but a denser board is

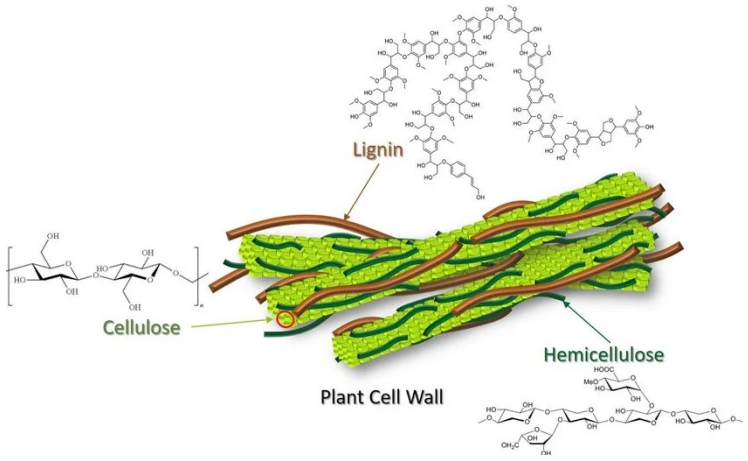

Figure 1.4: Principal structural constituents of lignocellulosic biomass [7].

not necessarily a better bonded board. Inadequate local contact and moisture- or pressure-related defects can contribute to cracking, blistering and separation [3, 8]. For this reason, bending performance must be considered alongside visible integrity and supporting physical measurements.

1.3. Product context and selected manufacturing route

The literature describes different applications for pressed coconut husk, including low-density insulation boards, denser flat boards and three-dimensional moulded products. Their required properties and processing conditions differ [9, 3, 8, 10]. Figure 1.5 gives two illustrative material examples; neither was manufactured or tested in this project.



(a) Illustrative insulation board



(b) Illustrative denser board

Figure 1.5: Illustrative coconut-husk-related products from two different application routes; these images do not document specimens made in the present experiments.

This study focuses on *binderless flat boards manufactured from mechanically flattened husk sheets*. In contrast to approaches that mill the husk and redistribute the fibres and pith into a mat, the retained-sheet method preserves much of the original fibre–pith arrangement. Four sheets form one board, with three original sheet-to-sheet interfaces. Retaining long fibres may offer a reinforcement opportunity and avoids extensive milling in the investigated preparation route, but neither a mechanical advantage over milled furnish nor a lower overall industrial processing cost was established.

The main DOE boards were manufactured without an externally added binder. Bio-oil and additional pith were investigated separately in exploratory follow-up trials.

Figure 1.6 illustrates the material form and retained-sheet preparation route used in this study. The photographs show the flattened coconut husk, selected sheets before stacking and a board after pressing.



(a) Flattened coconut husk (b) Selected sheets before stacking (c) Board after hot pressing

Figure 1.6: Experimental material and retained-sheet board preparation: (a) mechanically flattened coconut husk, (b) selected sheets before stacking and (c) a board after hot pressing.

1.4. Research problem and aim

The challenge is to produce mechanically coherent boards with a short pressure hold despite natural material heterogeneity and three sheet interfaces that must transfer load. Nominal pressure and platen temperature may affect both consolidation and bending behaviour, but the relationship need not be direct: boards of similar density may differ in fibre arrangement, interface contact and local defects.

The aim of this study is to investigate how material preparation, nominal pressing pressure and platen temperature relate to the bending performance and visible integrity of retained-sheet coconut husk boards. Modulus of rupture (MOR) and apparent bending modulus of elasticity (MOE) are the main mechanical responses. Supporting physical measurements are used to examine consolidation and post-pressing changes, while exploratory follow-up trials compare unmodified boards with boards containing bio-oil or additional pith at the sheet interfaces. Figure 1.7 provides an overview of the investigated inputs, possible mechanisms and measured responses.

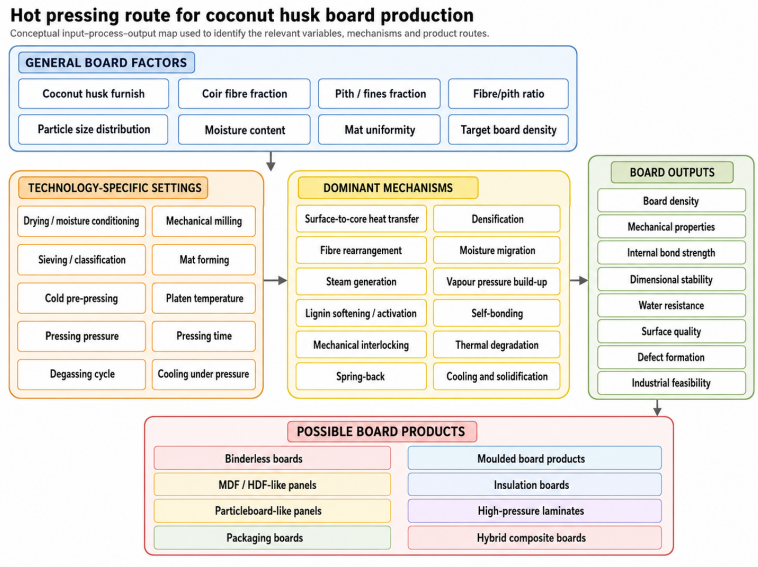

Figure 1.7: Conceptual input–process–output framework for hot pressing coconut husk. The indicated links represent possible mechanisms and responses, not effects established by this experiment.

1.5. Relevant parameters

Material preparation involves selecting intact sheets, screening hot-water and alkaline pretreatments, drying, moisture adjustment and lay-up. The final design of experiments (DOE) varies *nominal press-*

ing pressure and *platen temperature*, while the pressing hold and estimated moisture target remain approximately common. MOR and apparent MOE are the primary measured responses. Cut-specimen density, post-pressing mass and dimensional changes, and visible defect observations provide context about the manufacturing process; density is not treated as an independent product-quality objective.

1.6. Scope and limitations

The experimental programme included preliminary pressing trials, pretreatment screening and an 18-board pressure–temperature design of experiments (DOE). Six additional boards were manufactured at the *model-selected best condition* to explore the effects of bio-oil and additional pith at the sheet interfaces, alongside unmodified confirmation boards. Modulus of rupture (MOR) and apparent bending modulus of elasticity (MOE) were the primary mechanical responses. Physical measurements and visual observations provided supporting information on consolidation, post-pressing changes and board integrity.

The investigation was limited to small laboratory-manufactured boards, with one longitudinal bending specimen obtained per board. The specimens and 60 mm support span were smaller than those specified for standard bending tests of wood-based panels under EN 310 [11]. The resulting measurements were therefore used for comparative evaluation rather than product qualification. Internal bond strength, water-immersion swelling, water absorption, reaction-to-fire performance and long-term durability were not assessed. Industrial-scale production, dielectric heating and controlled-mould pressing also remained outside the experimental programme.

The Literature Review establishes the context and research questions. The Methodology describes the experiments, followed by Results, Discussion, Conclusions and Recommendations.

2

Literature Review

This chapter reviews coconut husk as a raw material for pressed products. Section 2.3 first examines reported variation in composition, including differences associated with material origin, maturity and the fibre and pith fractions.

The review then compares three product routes: low-density insulation boards in Section 2.6, dense binderless flat boards in Section 2.7, and moulded binderless products in Section 2.8. For each route, the available studies are considered in terms of material preparation, pressing conditions, measured properties and reported processing difficulties.

The comparison provides the basis for selecting the experimental route in Section 2.10. The remaining knowledge gap is defined in Section 2.11, followed by the main research question and subquestions. Chapter 3 describes how the selected route was developed into the laboratory experiments.

2.1. Purpose and research topics

Building on Chapter 1, this review provides a technical reference for pressed coconut husk products. It focuses on reported material composition, fibre-pith ratio, pretreatment, pressing conditions and product properties, including density, thermal conductivity, mechanical performance and defect formation.

The reviewed coconut-husk product routes are:

1. low-density insulation boards;
2. high-density binderless flat boards;
3. moulded binderless products.

Conventional hot pressing is treated as the baseline process. High-frequency dielectric heating is not treated as a separate product route, because the reviewed high-frequency studies are mainly based on rice straw, MDF or wood-based materials rather than coconut husk. These non-coconut studies are used only as supporting process references and are placed in Appendix A.

2.2. Literature search strategy

The literature review was conducted mainly through Google Scholar, using keyword combinations that linked the raw material, processing method and product type. The main search terms included *coconut husk binderless board*, *coir fibreboard*, *coconut pith lignin binder*, *hot pressing coconut husk*, *coconut husk insulation board*, *binderless lignocellulosic board*, *thermo-compressive processing biomass*, *coir fibre thermal degradation* and *high-frequency heating wood composites*.

The search was expanded by checking the reference lists of relevant papers and technical reports. Forward citation searching was also used to identify later studies that cited the key coconut husk board publications. This was important because several relevant studies are connected through project reports, pilot-scale work and follow-up publications.

Sources were selected when they provided information on coconut husk composition, fibre-pith ratio, pretreatment, moisture content, density, pressing temperature, pressing time, pressure, degassing, board properties or defect formation. Sources that focused on unrelated coconut products or heavily resin-bonded composites were excluded, unless they were useful as comparison material. The se-

lected literature was then organised into three product routes: low-density insulation boards, binderless flat boards and moulded binderless products.

2.3. Coconut husk as a variable input material

Coconut husk is a heterogeneous lignocellulosic material. It consists of long coir fibres and a finer pith fraction. Van Dam et al. reported that coconut husk contains approximately 30 wt.% fibre and 70 wt.% pith [3]. This distinction is important because the two fractions have different functions during pressing. The purpose of this section is to define the chemical components and the variability of the components depending on region, age and storage conditions. Section 2.3.1 describes the regional variance, while section 2.3.2 shows the variance in age and storage conditions.

2.3.1. Variance depending on region

Coconut husk composition varies between studies and between material sources. D'Almeida and Albuquerque reported regional differences in cellulose, hemicellulose and lignin content. The values reported in their review ranged from 23.4 to 41.0% cellulose, 0.23 to 26.0% hemicellulose and 21.3 to 45.7% lignin [2]. Table 2.1 lists the values reported for each region. These ranges show that coconut husk should be treated as a variable agricultural feedstock rather than a uniform industrial raw material.

Table 2.1: Regional variation in reported coconut husk composition values compiled by [2]. Values are reported in wt.%.

Origin	Cellulose	Hemicellulose	Lignin
South Minahasa, Indonesia	26.6	17.7	41.2
Maceió, Brazil	24.7	12.3	40.1
Costa Rica	37.6	15.2	41.3
Sabak Bernam, Malaysia	41.0	16.3	31.2
Manado, Indonesia	23.4	15.3	30.4
Taichung Market, Taiwan	30.2	11.0	40.9
Pernambuco, Brazil	33.5	0.23	45.7
India	34.1	26.0	32.6
Rio Grande do Norte, Brazil	34.0	10.2	21.3
Range	**23.4-41.0**	**0.23-26.0**	**21.3-45.7**

2.3.2. Variance depending on age

Maturity is another relevant source of raw-material variation. During ripening, the extractives content decreases strongly, from approximately 45 wt.% to below 15 wt.%, while the relative amount of lignin and polysaccharides increases [10]. This trend is shown in Figure 2.1a, where the blue fraction represents extractives and the dark red fraction represents lignin. Younger husks of 6-7 months were associated with lower board quality than mature husks. The same source reported that the 6- and 7-month nuts still contained a soft shell, making separation of shell and husk impractical [10].

The effect of maturity on chemical composition is quantified in Table 2.2. The values show that the extractives fraction decreases with maturity. In whole husk, extractives decrease from approximately 45 wt.% at 6 months to approximately 13 wt.% at 11 months. In fibres, extractives decrease from approximately 27 wt.% at 6 months to approximately 9 wt.% at 11 months. At the same time, lignin and polysaccharides increase in both whole husk and fibres.

Coconut variety also influences the available husk yield. The six investigated varieties were Tagnanan Tall (TAGT), Baybay Tall (BAYT), Laguna Tall (LAGT), Catigan Green Dwarf (CATD), Rennell Island Tall (RIT) and Agta Tall (AGAT). The average coconut weight ranged from 1488 to 1933 g. The average husk weight ranged from 481 to 718 g. The husk fraction ranged from 26 to 40% of total coconut weight [10]. This variation is shown in Figure 2.1b.

Table 2.2: Approximate chemical composition variation of coconut husk and fibres with maturity, estimated from the graph reported by [10]. Values are in wt.%.

Component	Husk 6m	Husk 7m	Husk 11m	Fibre 6m	Fibre 7m	Fibre 11m
Extractives	45	42	13	27	20	9
Lignin	17	18	34	22	25	31
Uronic acids	2	2	2	2	2	2
Polysaccharides	28	30	39	40	43	49

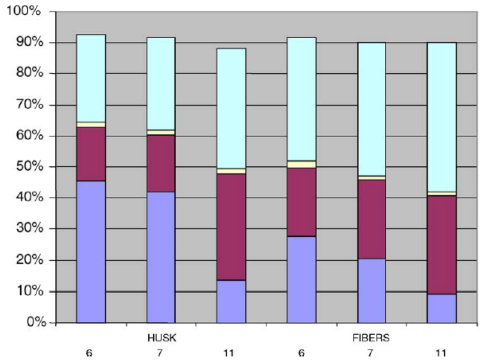

(a)

Var.	Coconut (g)	Husk (g)	Husk (%)
TAGT	1932	571	30
BAYT	1867	481	26
LAGT	1674	502	30
CATD	1488	534	36
RIT	1933	517	27
AGAT	1803	718	40
Range	**1488-1933**	**481-718**	**26-40**

(b)

Figure 2.1: Sources of raw-material variation in coconut husk. (a) Chemical composition of LAGT coconut husk and fibres at 6, 7 and 11 months of maturity. In (a), blue indicates extractives, dark red lignin, yellow uronic acids and light blue polysaccharides. (b) Husk fraction of six coconut varieties. Both are adapted from [10].

Storage and conditioning effects

Snijder et al. indicate that the condition of the husk before processing affects handling and preparation. Moisture content is the main reported storage-related input condition. Coconut husk with a moisture content of about 30% caused milling problems and jamming. Drying to approximately 12% moisture content improved the dry milling step [10]. This shows that storage and pre-drying conditions change the practical input state of the material before pressing.

The report also discusses conditioning of pressed boards under different humidity conditions. This is relevant because coconut husk boards can absorb moisture after pressing. For this literature review, storage and conditioning are therefore treated as input-condition variables rather than as a separate chemical composition category. The main reported storage-related value is the moisture condition before milling and pressing.

2.3.3. Comparison

Table 2.3 shows that coconut husk cannot be treated as a single fixed raw material. The reported regional composition already shows a wide range, with cellulose varying from 23.4 to 41.0 wt.%, hemicellulose from 0.23 to 26.0 wt.% and lignin from 21.3 to 45.7 wt.%. Maturity also changes the composition. In the reported age comparison, extractives decrease from 45 to 13 wt.% in whole husk and from 27 to 9 wt.% in fibres between 6 and 11 months. At the same time, lignin and polysaccharides increase with maturity.

The comparison also shows that the reported values depend on how the material is divided and analysed. Some sources report whole husk, while others report fibre and pith separately. Some report cellulose, hemicellulose and lignin, while others report holocellulose, polysaccharides or separate lignin fractions. These categories are related, but not identical. The table should therefore be interpreted as a comparison of reported material states, not as one fully uniform chemical dataset.

The reported variation means that pressing conditions should be interpreted together with the condition and preparation of the raw material. Moisture content, fibre-pith distribution and material structure are relevant when comparing studies, but the available composition values do not define the properties of every coconut husk supply.

For the present work, these findings identify possible sources of material variability rather than provide a measured composition for the supplied sheets. Material selection, dry-mass allocation and moisture conditioning are used to limit some differences between assemblies, as described in Chapter 3. Local variation within the sheets remains a limitation, and the experiments do not establish whether the selected pressing conditions are transferable to other material sources.

Table 2.3: Comparison of reported coconut husk, fibre and pith composition values. Values are reported in wt.% unless stated otherwise. Regional min and max represent the lowest and highest values across the regional composition data compiled by [2]. Maturity values are approximate values estimated from the maturity-composition graph in [10]. Missing values are indicated by -.

Component	Regional min	Regional max	Husk 6m	Husk 7m	Husk 11m	Fibre 6m	Fibre 7m	Fibre 11m	Coconut fibre	Coconut pith	RIT fibre	RIT pith
Cellulose	23.4	41.0	-	-	-	-	-	-	-	-	-	-
α-cellulose	-	-	-	-	-	-	-	-	51.12	48.21	36.3	21.0
Hemicellulose	0.23	26.0	-	-	-	-	-	-	-	-	-	-
Holocellulose	-	-	-	-	-	-	-	-	67.63	58.82	-	-
Polysaccharides	-	-	28	30	39	40	43	49	-	-	-	-
Uronic acids	-	-	2	2	2	2	2	2	-	-	-	-
Lignin	21.3	45.7	17	18	34	22	25	31	36.73	45.12	32.7[a]	24.5[a]
Extractives	-	-	45	42	13	27	20	9	-	-	12.4[b]	29.5[b]
Ash	-	-	-	-	-	-	-	-	-	-	3.4	4.5

[a] RIT lignin is calculated as acid-insoluble lignin plus acid-soluble lignin from [5]. [b] RIT extractives are NaOH extractives from [5]. Holocellulose represents cellulose and hemicellulose together. Polysaccharides represent the carbohydrate fraction in the maturity-composition data and are therefore not identical to holocellulose.

2.4. Temperature-time effects and thermal degradation

Pressing temperature should be interpreted together with exposure time. During hot pressing, the core temperature of the mat usually lags behind the platen temperature. The relevant thermal load is therefore determined by the maximum temperature reached inside the mat and the time at that temperature.

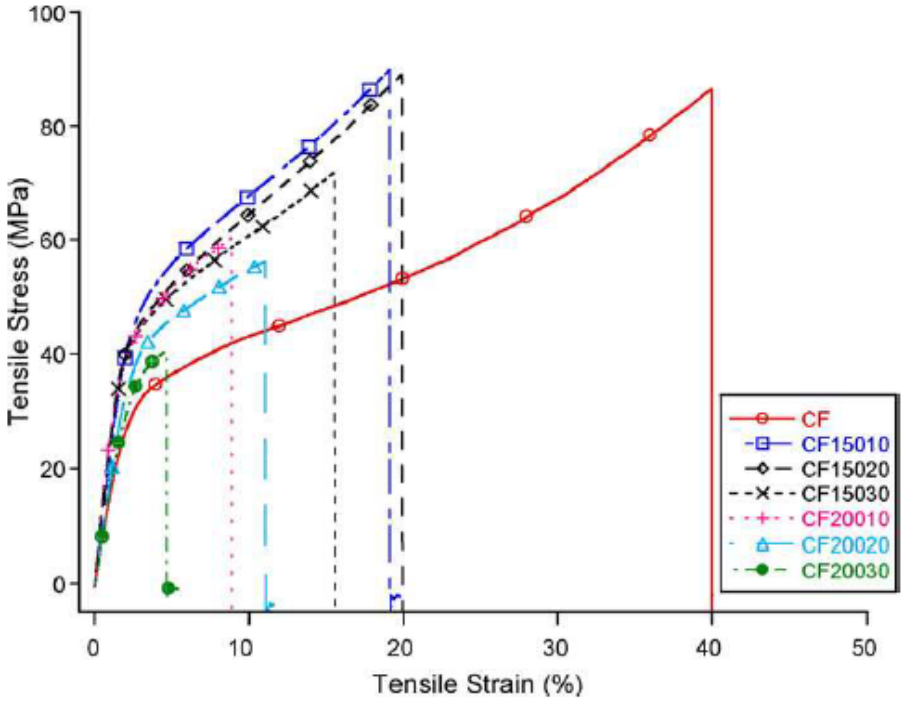

Figure 2.2: Effect of heat treatment on the tensile behaviour of coir fibres, showing the influence of temperature and exposure time on fibre performance [12].

Figure 2.2 shows that untreated coir fibres reached the highest strain before failure, while heat-treated fibres generally failed at lower strain. Some treated fibres reached a higher initial stiffness and, in some cases, a higher stress at low strain, but the overall failure strain clearly decreased with increasing temperature and exposure time.

Heating therefore has both positive and negative effects. Van Dam et al. [5] reported an irreversible exothermic event around 140 °C for coconut husk material, which was related to lignin reactions. This indicates that lignin-related self-bonding may start around this temperature. However, excessive thermal exposure can damage the reinforcing coir fibres. Ezekiel et al. [12] heated coir fibres at 150 and 200 °C for 10, 20 and 30 min. They reported a decrease in ultimate tensile strength of 1.17-44.00%, a decrease in elongation at break of 15.28-81.93%, and an increase in Young's modulus of 6.3-25.0%. This means that heat treatment can make coir fibres stiffer, but also weaker and more brittle.

2.5. Pretreatment approaches relevant to flattened husk sheets

Pretreatment can modify the surface characteristics and chemical composition of coconut fibres, potentially affecting their behaviour during subsequent consolidation. Faria et al. [13] investigated several coconut fibre pretreatments, including immersion in deionised water at 80 °C for 2 h and treatment with 5 wt.% NaOH at 95 °C for 1 h. Their study provides a basis for considering hot-water and alkaline treatments as contrasting preparation methods. However, the treated fibres were incorporated into polyurethane composites, so the results cannot be directly transferred to binderless boards.

Alharbi et al. [14] investigated 1 and 3 wt.% NaOH pretreatments of coconut coir before milling and hot pressing the material into binderless compacts. The alkaline solutions were heated to 95 °C, followed by washing and neutralisation. This study is particularly relevant because it demonstrates the use of low-concentration alkaline treatment in binderless coconut coir materials, although the treatment

conditions and milled material structure differ from those investigated here.

Based on these studies, the present work examined two exploratory pretreatments: immersion in demineralised water at $80\,^{\circ}C$ for 1 h and immersion in 1 wt.% NaOH at room temperature for 1 h. These conditions were selected for preliminary screening rather than as direct replications of published procedures. Their suitability for the retained-sheet approach was evaluated primarily through measured bending performance, with FTIR providing supporting information on changes in the material's spectral response.

2.6. Route 1: Low-density insulation boards

Few sources were identified for the insulation route. Panyakaew and Fotios provide the most detailed account of binderless insulation boards, while Espinoza et al. offer a comparison involving fibre treatment and binder addition. Table 2.4 summarises the material preparation, pressing conditions and results reported by Panyakaew and Fotios. Section 2.6.2 discusses these findings, followed by a summary of the reported processing conditions in Section 2.6.3.

Table 2.4: Raw material, pretreatment, process conditions and results reported by Panyakaew and Fotios [9]. N.S. = not specified.

Raw material			
Material	**Coconut fibre(%)**	**Coconut pith(%)**	**Bagasse(%)**
Lignin	36.73	45.12	19.19
Holocellulose	67.63	58.82	76.31
α-cellulose	51.12	48.21	56.94
Pretreatment			
Step	**Pretreatment**	**Starting condition**	**Reported changed value**
1	Drying	80 °C	Coconut husk 11-13%
2	Fibre cutting	dried	Fibre length reduced to 8-10 mm
3	Fibre-pith blending	N.S.	Fibre:Pith ratio 80:20 by weight
Process conditions			
Parameter	**Value 1**	**Value 2**	**Value 3**
Target density	250 kg/m^3	350 kg/m^3	450 kg/m^3
Pressure	14.7 MPa	-	-
Temperature	180 °C	200 °C	220 °C
Time	7 min	10 min	13 min
dimensions	t = 25 mm	l = 450 mm	b = 450 mm
Results			
Property	**Group 1 (density)**	**Group 2**	**Group 3**
Thermal conductivity	0.046-0.068 W/mK	0.046-0.068 W/mK	N.S.
Internal bond (max)	N.S.	0.002	N.S.
MOE	102 MPa	392 MPa	957 MPa
MOR (max)	0.12 MPa	0.68 MPa	1.94 MPa
Densities	230-270 kg/m^3	340-360 kg/m^3	440-480 kg/m^3
moisture content	6.3-9.3%	N.S.	N.S.
Thickness swelling (TS)	N.S.	21.7% (Lowest at 220°C / 13 min)	N.S.

2.6.1. Effects of fibre treatment and binder addition

Espinoza Montero et al. [15] investigated the thermal conductivity of coconut fibre insulation panels produced using different fibre treatments and PLA addition. Untreated coconut fibre panels showed the lowest mean thermal conductivity of 0.03320 W/(m·K), compared with 0.07916 W/(m·K) for acetone-treated fibres and 0.13302 W/(m·K) for acetosol-treated fibres.

The panels containing untreated fibres combined with PLA had a mean thermal conductivity of 0.06926 W/(m·K), although considerable variation was reported for this formulation. None of the investigated modifications resulted in a lower mean thermal conductivity than the untreated panels.

In contrast to the binderless insulation boards investigated by Panyakaew and Fotios [9], Espinoza Montero et al. [15] explored fibre treatments and the addition of a polymeric binder. The results suggest that these modifications do not necessarily improve thermal insulation performance, illustrating the need to evaluate material treatments in relation to the intended application.

2.6.2. Interpretation

The results in Table 2.4 show that low-density coconut husk insulation boards are technically feasible, but mainly limited by mechanical performance and dimensional stability. The reported thermal conductivity was 0.046-0.068 W/mK. This is close to conventional insulation materials, but it was obtained at relatively high densities of 250-350 kg/m^3. Therefore, the insulation performance is promising, but the mass efficiency is still limited.

Density was the dominant process variable. Increasing density improved MOR, MOE and internal bond strength. The maximum MOR increased from 0.12 MPa at 250 kg/m^3 to 1.94 MPa at 450 kg/m^3. The 250 kg/m^3 boards also showed delamination at 180 °C and 7-10 min, indicating insufficient internal cohesion at low density and mild pressing conditions.

Panyakaew and Fotios used JIS A 5905:2003 as reference standard for insulation fibreboards [9]. This standard requires a minimum MOR of 1 MPa. Based on Table 2.4, only the 450 kg/m^3 boards reached this requirement. These results make density a useful organising variable for the insulation route: the 250 kg/m^3 boards were at the mechanically weaker end of the investigated range, while 350-450 kg/m^3 provides a reference range for further insulation-board development. These are literature-derived considerations, not the experimental settings selected for this thesis.

2.6.3. Process window

Table 2.5: Process window for binderless coconut husk insulation boards based on Panyakaew and Fotios [9].

Variable	Reported range or setting	Implications for the insulation route
Target density	250-450 kg/m^3	Lead variable. The full range is technically possible, but 250 kg/m^3 is mechanically weak. A practical window is 350-450 kg/m^3.
Actual density	230-480 kg/m^3	Actual boards deviated around the target density groups. This range should be used when comparing measured output properties.
Moisture content before pressing	11-13%	Conditioning range used for coconut husk in the reported insulation-board process.
Fibre:pith ratio	80:20 by weight	Fixed fibre-pith formulation used in the reported insulation-board process.
Fibre length	8-10 mm	Fixed pretreatment condition. Short fibres were used to form the low-density mat.
Pressing pressure	14.7 MPa	Fixed pressure reported for this insulation-board process, rather than a pressure selected for the present experiments.
Pressing temperature	180-220 °C	Secondary variable. Higher temperatures improved cohesion and reduced thickness swelling. The practical range is 200-220 °C.
Pressing time	7-13 min	Secondary variable. Longer pressing improved mechanical properties and dimensional stability. The practical range is 10-13 min.
Board thickness	25 mm	Fixed board thickness in the reported insulation-board process.

2.7. Route 2: Binderless flat boards

Route 2 focuses on the production of binderless flat boards from whole coconut husk. In contrast to Route 1, this route does not aim for low-density thermal insulation, but for denser board materials with sufficient mechanical strength for board-like applications. The bonding mechanism is mainly based on the lignin-rich coconut husk fraction, which can act as an intrinsic binder when exposed to heat and pressure.

Three studies are compared in this section. Van Dam et al. [3] introduced the basic high-density

binderless board route and compared different opening methods, including extrusion, steam explosion and milling. Snijder et al. [10] further developed this process towards pilot-scale production and gave more detailed information on milling, drying and pressing conditions. Böger et al. [8] later investigated a more industrially realistic process with lower board densities and a controlled degassing step to reduce blistering and delamination.

The raw material, pretreatment steps, process conditions and reported results from these studies are summarised in Tables 2.6, 2.7 and 2.8. These results are interpreted in Section 2.7.1 and converted into a process window in Section 2.7.2.

Table 2.6: Raw material, pretreatment, process conditions and results reported by van Dam et al. [3]. N.S. = not specified.

Raw material			
Composition		**Fibre wt%**	**Pith wt%**
α-Cellulose		36.3	21.0
NaOH-extractives		12.4	29.5
Ethanol/toluene extractives		4.9	23.6
95% ethanol extractives		1.7	0.4
Hot-water extractives		4.3	15.0
Klason lignin,AIL		31.9	24.1
Klason lignin,ASL		0.8	0.4
Ash		3.4	4.5
Pretreatment			
Step	**Pretreatment**	**Starting condition**	**Reported changed value**
1	Husk separation	Whole coconut	Husk separated from nut
2	Extrusion	Whole husk	N.S.
2*	Steam explosion	Whole husk	N.S.
2**	Milling	Whole husk	N.S. best results
Process conditions			
Parameter	**Lower value**	**Upper value**	**Note**
Temperature	180°C	N.S.	optimal 180°C
Time	3 min	30 min	Reported pressing-time range; limited influence on board properties
Press force	300 kN	750 kN	Contact pressure cannot be inferred without the loaded area
Moisture content	N.S.	N.S	Significant influence
Dimensions	N.S.	N.S.	not given in report
Results			
Property	**Lower value**	**Upper value**	**Note**
Density	1300	1400	kg/m^3; coconut board range
MOR	15	50	MPa; particleboard and coconut board, respectively
MOE	3	5	GPa; particleboard and coconut board, respectively
TS (24 h)	8	21	%; coconut board and particleboard, respectively; MDF was 17%
Water absorption	8	65	%; coconut board and particleboard, respectively; MDF was 24%

Van Dam et al. [3] showed that whole coconut husk can be converted into high-density binderless boards by hot pressing after mechanical opening of the husk. Extrusion, steam explosion and milling were compared as pretreatment methods, and all produced material that could be pressed into boards. However, milling gave the best results and was therefore considered the most suitable route. This is likely because milling creates a more homogeneous mixture of short fibres and lignin-rich pith, improving contact between both fractions during pressing. The study also indicates that pressing temperature

and material moisture content are more important than pressing time and pressure. The resulting boards reached high densities of approximately 1300-1400 kg/m^3, showing that this route is mainly suitable for dense board products rather than low-density insulation boards.

Table 2.7: Raw material, pretreatment, process conditions and results reported by Snijder et al. [10]. N.S. = not specified.

Raw material			
Composition	**Pith range**	**Fibre range**	**Note**
Polysaccharides	31-33 wt.%	44-45 wt.%	Approximate range from CAT and TAG varieties
Uronic acids	5-6 wt.%	4 wt.%	Approximate range from CAT and TAG varieties
Lignin	36-37 wt.%	33-34 wt.%	Approximate range from CAT and TAG varieties
Extractives	13-15 wt.%	5 wt.%	Approximate range from CAT and TAG varieties
Pretreatment			
Step	**Pretreatment**	**Starting condition**	**Reported changed value**
1	Husk opening	Whole coconut husk	N.S.
2*	Milling	Coconut husk at 30% MC	Milling caused jamming
2	Drying	30% MC	12% MC
3	Dry milling	Dried coconut husk	Mesh size of 2.5 and 8 mm
Process conditions			
Parameter	**Lower value**	**Upper Value**	**Note**
Time	15 min	N.S.	only optimum time specified
Temperature	125°C	230°C	typical value 150°C optimal 180°C
Pressure	42 bar	400 bar	typical value 40 bar optimum 150 bar
Target density	N.S.	N.S.	N.S.
Results			
Property	**Reported value**	**Unit**	**Note**
MOR	50 MPa	N.S.	
MOE	5 GPa	N.S.	

Table 2.8: Raw material, pretreatment, process conditions and results reported by Böger et al. [8]. N.S. = not specified.

Raw material			
Material	**Starting value**	**Relevant property**	**Note**
Raw coconut husk	N.S.	N.S.	Used for binderless boards
Pretreatment			
Step	**Pretreatment**	**Starting condition**	**Reported changed value**
1	Kiln drying	Raw coconut husk	Dried at 60 °C for 48 h to 15% MC
2	Hammer milling with screen	Dried coconut husk	5 mm
3	Sieving analysis	Hammer milled husk	65% w/w of particles below 0.310 mm. 50% w/w between 0.125 and 0.310 mm. Fibres between 5-20 mm
4	Drum blender	Hammer milled husk	Loose mat density about 90-100 kg/m^3
Process conditions			
Parameter	**Lower value**	**Upper value**	**Note**
Pressure	4 MPa	9,5 MPa	max values for 1000-1200 density respectively
Temperature	150 °C	170 °C	2 stages
Time	step 1: 150s	step 2: 250	
Target density	700 kg/m^3	1200 kg/m^3	N.S.
dimensions	t = 5-12 mm	l = 1m	b = 2 m
Moisture content	6%	25%	min and max, with acceptable defects
Results			
Property	**Lower value**	**Upper value**	**Note**
MOR	4.4 MPa	37.4 MPa	
MOE	467 MPa	4762 MPa	
IB	0.63 MPa	1.5 MPa	for densities between 913 - 1082 kg/m^3
TS	12.2%	21%	
Densities	700 kg/m^3	1200 kg/m^3	

2.7.1. Interpretation

The studies by van Dam et al., Snijder et al. and Böger et al. show that whole coconut husk can be processed into binderless flat boards using different preparation and pressing procedures [3, 10, 8]. Their results provide useful reference conditions, but the reported densities, mechanical properties and defect levels need to be interpreted within each manufacturing route.

Material preparation is one relevant difference. The reviewed routes use mechanically opened or milled husk, creating a different distribution of fibres, pith and contact surfaces from a stack of flattened sheets. The high-density boards described by van Dam et al. reached approximately 50 MPa MOR and 5 GPa MOE at reported densities around 1300–1400 kg/m^3 [3]. In a different milled-husk process, Böger et al. reported 19.3$\pm$3.1 MPa MOR for 12 mm boards near 900 kg/m^3 ($n = 10$), as well as extensive work on approximately 5 mm boards [8]. These results must not be combined into a direct ranking: furnish structure, density, board thickness, pressing cycle and test conditions differed.

Retention of long fibres could, in principle, favour longitudinal reinforcement and reduce the need for extensive milling. Conversely, milling can redistribute pith and expose contact surfaces, whereas stacked sheets contain distinct interfaces that must be consolidated. The literature therefore establishes the performance potential of *milled* coconut husk but does not show that a retained-sheet board is stronger. A matched comparison at controlled material loading, density and test geometry would be needed to determine whether fibre retention offers a mechanical advantage.

Moisture management and pressure release also receive attention in the reviewed work. In particular, Böger et al. investigated a staged process that included controlled pressure release to limit blistering and delamination [8]. This provides a reason to consider vapour release during process development, but does not establish one required pressing cycle for all board geometries and material preparations.

2.7.2. Process window

The conditions reported in Tables 2.6, 2.7 and 2.8 provide a literature reference for selecting experimental settings. They should not be combined into a single validated operating window for flattened-sheet boards. Table 2.9 summarises the main considerations when applying this literature to the present study.

Table 2.9: Considerations for transferring the reviewed binderless flat-board processes to a flattened-sheet approach.

Parameter	Implication for process selection
Material preparation	Mechanical opening and milling are used in the reviewed routes. Their results provide context, but do not directly establish suitable conditions for a layered sheet assembly.
Density	Reported density helps contextualise mechanical performance. It should not be treated as a universal quality threshold independent of material structure and pressing procedure.
Moisture content	Moisture condition needs to be considered together with material preparation, heating and pressure release. Comparisons also require attention to the reported moisture basis.
Temperature and pressure	The literature provides reference settings, while preliminary trials are needed to assess their suitability for the available sheets and pressing arrangement.
Pressing duration	Reported times belong to particular board geometries and pressing cycles. A duration selected for the laboratory boards requires its own experimental justification.
Degassing and cooling	Controlled pressure release and cooling procedures are relevant process options. Their contribution to the sheet-based route cannot be established without testing them separately.

2.8. Route 3: Moulded binderless products

Route 3 considers three-dimensional moulded products made from coconut husk. This route is mentioned in the literature as a possible extension of binderless coconut husk board production. Van Dam et al. [3] state that, besides flat boards, 3D moulded products can also be produced from whole coconut husk. Snijder et al. [10] similarly describe the possibility of producing moulded products such as beams, laminates, cups, trays, plant pots and pallets.

However, the moulding route is not described as a separate experimental route. The available sources do not report moulding-specific values for density, pressure, temperature, pressing time, wall thickness, demoulding behaviour or dimensional stability. Therefore, Route 3 is treated as a feasible but insufficiently defined extension of Route 2.

2.8.1. Interpretation

The literature supports the technical feasibility of moulded binderless coconut husk products, but does not provide enough data to evaluate this route independently. The most likely bonding mechanism is the same as for flat boards: the lignin-rich pith fraction contributes to self-bonding when the milled husk is exposed to heat and pressure. The reviewed sources do not give enough moulding-specific process information to establish how closely their pressing conditions matched those used for flat boards.

This makes Route 3 promising for future product development, but less suitable as the main experimental route of this thesis. Product geometry, wall thickness and steam release are expected to become more important than in flat boards, and these effects would need to be investigated experimentally.

2.8.2. Process window

No validated process window can be defined for Route 3 from the available literature. For future moulding trials, one possible initial reference is the flat-board combination discussed above: dry-milled whole coconut husk, moisture content below approximately 12%, a pressing temperature around 180 °C, pres-

sure around 150 bar and a pressing time around 15 min. This is an assumed reference for possible future work, not the procedure selected for the experiments in this thesis.

These values should not be presented as a confirmed moulding window, but as an assumed starting window derived from binderless flat-board production.

2.9. Requirements for products

Insulation boards and MDF-like flat boards require different success criteria. For insulation boards, low thermal conductivity, low density and basic board integrity are most important. For MDF-like flat boards, bending strength, stiffness, internal bond strength and dimensional stability are more important.

Panyakaew and Fotios [9] used JIS A 5905:2003 insulation fibreboards as the reference for mechanical and dimensional requirements, while thermal conductivity was measured according to ISO 8301. The relevant insulation-board targets are given in Table 2.10.

Table 2.10: Relevant requirements and targets for coconut husk insulation boards.

Property	**Requirement / target**	**Reference or reason**	**Unit**
Thermal conductivity	$\lambda \leq 0.070$	Based on reported values measured according to ISO 8301	W m^{-1} K^{-1}
Density	< 400	Target for low-density insulation products	kg m^{-3}
MOR / bending strength	≥ 1.0	JIS A 5905:2003 insulation fibreboard reference used by Panyakaew and Fotios [9]	MPa
Thickness swelling, 24 h	≤ 10	JIS A 5905:2003 insulation fibreboard reference used by Panyakaew and Fotios [9]	%
Board integrity	No major delamination or breakage	Practical requirement for successful board formation	-

For dense flat boards, published fibreboard standards provide numerical *development benchmarks*. EN 622-5:2009 specifies requirements for dry-process MDF. For general-purpose MDF used in dry conditions with nominal thickness greater than 4 mm and up to 6 mm, Table 3 lists bending strength of at least 23 MPa, bending MOE of at least 2700 MPa, internal bond strength of at least 0.65 MPa and 24 h immersion thickness swelling no greater than 30% [16]. The swelling limit is specific to this thickness class: it is not a general limit for every board below 8 mm.

JIS A 5905:2022 is the current Japanese fibreboard standard. For general-purpose Type 15 MDF, the published industry summary lists bending strength of at least 15 MPa and internal bond strength of at least 0.30 MPa; a bending modulus of 1300 MPa is presented as an *informative reference value*, not a mandatory MOE requirement [17, 18]. The Japanese and European classifications are not assumed to be interchangeable. Table 2.11 selects benchmarks relevant to boards near 5 mm thickness.

Table 2.11: Numerical development benchmarks for approximately 5 mm fibreboard-like products. These values do not establish product classification or compliance for the experimental retained-sheet boards.

Property	**EN 622-5:2009, MDF, dry, $>$ 4-6 mm**	**JIS A 5905:2022, general-purpose MDF Type 15**
Bending strength (MOR)	≥ 23 MPa	≥ 15 MPa
Bending modulus (MOE)	≥ 2700 MPa	≥ 1300 MPa (informative only)
Internal bond strength	≥ 0.65 MPa	≥ 0.30 MPa
Thickness swelling, 24 h water immersion	$\leq 30\%$	$\leq 17\%$ for boards ≤ 7 mm

The historical insulation-board comparison of Panyakaew and Fotios uses the 2003 edition of JIS A 5905 because it was the edition cited in their 2011 publication [9]. It should not be substituted for the current

2022 edition when describing present-day development benchmarks.

These requirements show that insulation and MDF-like flat boards are evaluated using different property combinations. Density is a useful manufacturing descriptor, but not a substitute for bending strength, internal bond strength, dimensional stability, water resistance or reaction-to-fire performance. The last two application-relevant properties were not tested in this thesis.

EN 310:1993 is a three-point bending *test method* for wood-based panels, including fibreboards; it is not a strength classification for solid timber [11]. Its conventional span is 20 times the nominal thickness, with 50 mm-wide specimens, and it refers to the bending modulus as an *apparent* modulus because the measured response also includes shear deformation. These method requirements must be distinguished from the MDF product benchmarks in EN 622-5 and JIS A 5905. The present study used an adapted ASTM D1037-based procedure with smaller specimens and crosshead-derived displacement, as described in the Methodology.

All numerical requirements are used as reference targets rather than compliance claims. The present tests did not follow all of the procedures, specimen sizes, conditioning regimes or additional checks prescribed by these product standards. The experimental work measures bending performance, density, short-term dimensional changes and visible specimen integrity. Internal bond strength, water absorption and immersion thickness swelling are not determined.

The results may be compared numerically with MOR and MOE benchmarks, but neither the adapted ASTM D1037 bending tests nor the unmeasured internal-bond and water-immersion responses establish EN 622-5 or JIS A 5905 compliance [19, 11]. Similarly, thickness recovery during storage in laboratory air should not be interpreted as 24 h water-immersion thickness swelling.

2.10. Selection of the experimental route

The three reviewed routes address different product requirements. Low-density insulation boards are relevant where thermal performance is the main objective, while denser flat boards place greater emphasis on bending properties and cohesion. Moulded products offer further application possibilities, but introduce questions about forming, wall thickness, demoulding and shape retention.

Binderless flat boards are selected as the main experimental route for this thesis. The reviewed studies provide a basis for comparing material preparation, pressing conditions and mechanical properties [3, 10, 8]. A flat geometry also allows consolidation and bending behaviour to be investigated without introducing the additional forming requirements of a three-dimensional product. This makes the route suitable for examining the relationship between pressing conditions and board quality using the available laboratory methods.

This selection does not exclude insulation or moulded products as future applications. It limits the experimental work to one product form so that its processing behaviour can be examined in more detail. Results from flat boards may help identify questions for later development, but cannot establish suitable manufacturing conditions or performance for the other routes.

2.10.1. From literature conditions to the experimental approach

The material supplied for this study consisted of mechanically flattened coconut husk sheets. The experiments therefore examine a sheet-based version of the flat-board route rather than reproducing the milled-material processes described in the literature. Four sheets are assembled into each board, retaining much of their original fibre and pith arrangement. This approach reduces the extent of size reduction required before pressing and preserves the long coir-fibre structure that would otherwise be disrupted by extensive milling. The present study does not directly compare sheet-based and milled boards, so any mechanical advantage associated with retaining the longer fibres remains to be established.

Retaining the sheets also introduces a different consolidation problem. Instead of forming a redistributed mat of fibre and pith, the board contains distinct sheet-to-sheet interfaces across which contact and load transfer must develop. The experimental route therefore examines whether this less extensively processed material structure can be consolidated into a coherent binderless board and how the selected processing conditions influence its quality and defect formation.

Literature conditions provide guidance for the initial pressing trials, while the workable board format, lay-up and pressing duration are established experimentally. The main design varies nominal pressing pressure and platen temperature. Moisture content was initially considered as a third factor but was

kept near a common target after the number of usable husk sheets proved insufficient for a larger replicated experiment. Pressing force was controlled rather than final board thickness, so density was measured as an outcome rather than imposed as an independent target.

Pretreatment screening is used to select a common preparation procedure before the pressure-temperature experiment. Separate follow-up trials examine additional pith and bio-oil at the sheet interfaces. These exploratory comparisons are kept distinct from the main factorial experiment. The manufacturing procedure, experimental levels and practical constraints are described in Chapter 3.

2.11. Knowledge gap

The reviewed studies establish that coconut husk can be converted into binderless flat boards and identify material preparation, moisture condition and pressing parameters as relevant to their performance [3, 10, 8]. These routes generally rely on mechanical opening or milling before board formation. Less is known about whether coconut husk can instead be used in a flattened-sheet form that retains much of its original long-fibre and pith structure while reducing the extent of size reduction before pressing. The reported processing conditions for milled materials cannot therefore be assumed to transfer directly to this retained-sheet architecture.

In a four-sheet assembly, consolidation involves both compression within the husk and contact between adjacent sheets. The resulting density does not, by itself, establish whether the interfaces remain intact or whether the board has consistent bending properties. Physical measurements, bending tests and visible edge observations are therefore needed to assess different aspects of board quality.

The specific gap addressed here concerns how a controlled preparation route and nominal pressing pressure and platen temperature relate to MOR and apparent MOE of flattened-sheet boards, with density, post-pressing recovery and visible defects providing supporting context. Preliminary pretreatment screening supports the choice of material preparation, while separate interlayer trials explore possible modifications to the sheet interfaces. The study is intended to identify useful processing trends and further experimental needs, rather than establish a general optimum for all coconut husk materials.

2.12. Main research question

The main research question of this study is:

> *How do material preparation and hot-pressing conditions influence the mechanical performance and defect formation of binderless coconut husk boards?*

2.13. Subquestions

The subquestions address the pretreatment screening, pressure–temperature DOE, supporting physical measurements, visual observations and exploratory interlayer trials:

1. What differences in bending performance are observed between untreated coconut husk boards and boards treated with demineralised water at $80\,^{\circ}\mathrm{C}$ or 1 wt.% NaOH during pretreatment screening?
2. How do nominal pressing pressure and platen temperature relate to the modulus of rupture and apparent modulus of elasticity of retained-sheet coconut husk boards?
3. What do cut-specimen density and short-term changes in whole-board mass and thickness indicate about board consolidation and post-pressing recovery?
4. How are nominal pressing pressure and platen temperature associated with visible post-cut delamination scores, and how do these observations relate to bending performance?
5. How does the bending performance of boards with additional pith or bio-oil at the sheet interfaces compare with unmodified confirmation boards at the model-selected best condition?

3

Methodology

3.1. Experimental Approach

The experimental programme began with preliminary pressing trials, followed by pretreatment screening and a factorial hot-pressing experiment. The trials established a workable board size, four-sheet lay-up and pressing cycle. The supply contained enough coconut husk for preliminary work, but fewer intact and reasonably uniform sheets than expected. The original three-factor design considered nominal pressing pressure, platen temperature and prepress moisture content. The limited number of usable sheets meant that this design could not be replicated adequately. Moisture content was therefore held near a common target, and the DOE was reduced to the two varied factors–pressure and temperature–with two independently manufactured boards per condition. Untreated, hot-water-treated and NaOH-treated sheets were then compared to select the pretreatment used in the main experiment.

The final design of experiments (DOE) comprised nine temperature-pressure combinations. The primary responses were modulus of rupture (MOR) and apparent modulus of elasticity (MOE), obtained from one longitudinal three-point bending specimen per board. Density, post-pressing dimensional and mass changes, and visible delamination were recorded as supporting observations to help interpret the mechanical behaviour. An overview is given in Figure 3.1. Following the DOE, six separate boards were manufactured at the selected pressing condition: two unmodified references, two with a bio-oil interlayer and two with additional coconut husk pith. These follow-up boards were analysed separately from the factorial series.

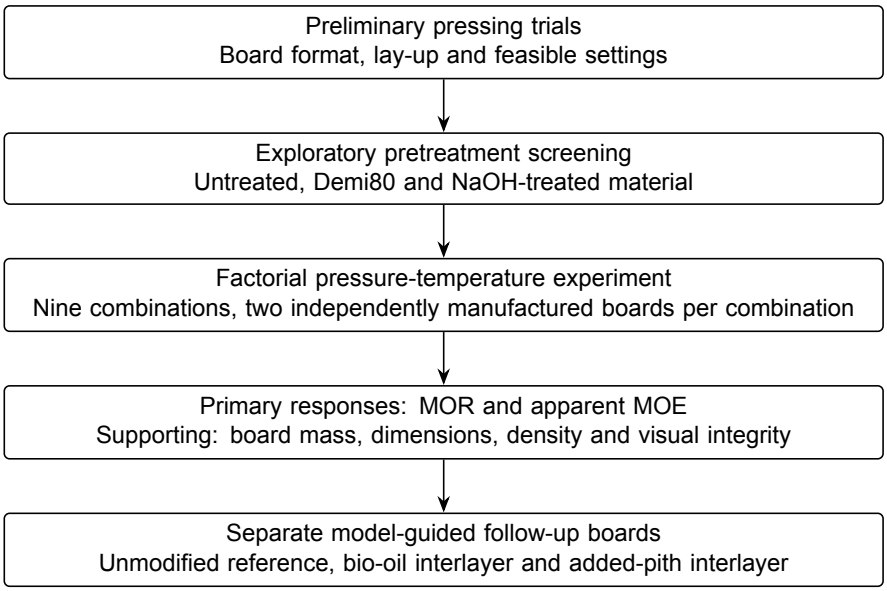

Figure 3.1: Sequence of completed experimental work and the board-level responses considered in this study.

3.2. Materials and Equipment

Coconut husk was supplied by CoEco in Indonesia. Before delivery, the husks had been mechanically flattened by rolling into sheet-like sections that retained both coir fibres and pith (Figure 3.2). The harvesting date and the conditions and duration of storage before delivery were not documented.
The material was stored in its original shipping box in a conditioned laboratory storeroom. The temperature and relative humidity at the storage location were not logged. The sheets were subsequently cut, dried at $70\,^{\circ}\mathrm{C}$ and exposed to ambient laboratory air for at least 24 h. Before pressing, their masses were adjusted towards a calculated moisture target as described in Section 3.3. No external binder was used for the factorial DOE; bio-oil was introduced only in a separate follow-up trial.



Figure 3.2: Flattened coconut husk supplied for board preparation.

Table 3.1 identifies the main instruments. The Joos press controlled applied force rather than final board thickness. Its platens were heated independently, and the sheets were pressed without lateral confinement, allowing material to spread beyond its initial footprint.

Table 3.1: Equipment used for material preparation, manufacture and characterisation.

Operation	Instrument	Relevant specification
Drying	Vötsch VTL60/60	Operated at $70\,^{\circ}\mathrm{C}$
Mass measurement	Mettler Toledo XSR204 DeltaRange; VWR LA Classic	Reported resolution: 0.1 mg; capacities: 220 and 120 g, respectively
Residual moisture	ADAM PMB 53	Moisture analyser
Hot pressing	Joos LAP 50	Maximum force: 500 kN; platen area: 600×600 mm
Specimen cutting	Compcut ACS 600	Dry cutting; blade manually wiped with acetone between cuts
Dimensions	Whitworth digital calliper	Resolution: 0.01 mm
Three-point bending	Zwick and Roell Proline	10 kN load cell; 60 mm support span
FTIR characterisation	PerkinElmer Spectrum 100 FTIR Spectrometer	16 scans; 4000-600 cm^{-1}



(a) Joos LAP 50 hot press.



(b) Unconfined lay-up before pressing.

Figure 3.3: Hot-press equipment and sheet placement used during board manufacture.

3.3. Husk Preparation and Dry-Mass Allocation

3.3.1. Sheet Preparation and Reference Drying

The coconut husk was first cut into 200×40 mm parent sheets. Each sheet was dried at $70\,^{\circ}$C for 24 h and weighed to obtain its reference mass (m_{ref}). The drying period was selected after repeated weighings showed two consecutive relative mass changes below 0.05%, separated by at least 2 h (Figure 3.4). Residual moisture was measured using representative material taken from seven locations within the husk supply, avoiding repeated moisture-analyser measurements of every production sheet.

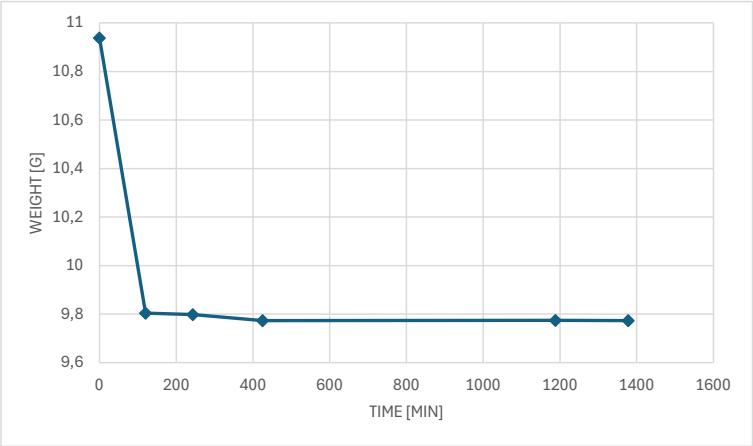

Figure 3.4: Mass development during drying at $70\,^{\circ}$C, used to assess the selected 24 h reference period.

Representative samples that had undergone the $70\,^{\circ}$C drying procedure were analysed with an ADAM PMB 53 moisture analyser. The recorded programme ramped towards $95\,^{\circ}$C over 5 min and stopped when the mass change was below 0.002 g over 30 s. The analyser output was expressed relative to the initial sample mass on a wet basis (%M). The measurement was therefore used as a reference mass-loss correction for material dried at $70\,^{\circ}$C.

For a measured wet-basis residual moisture content $MC_{70,\mathrm{wb}}$, the estimated dry mass was calculated as

$$m_{\mathrm{dry}} = m_{70}\left(1 - \frac{MC_{70,\mathrm{wb}}}{100}\right), \tag{3.1}$$

where m_{70} is the mass after drying at $70\,^{\circ}$C. The measured residual value was 4.49%, giving a correction factor of 0.9551. This factor was applied to the reference-dried sheet masses used in material allocation and subsequent moisture calculations.

Initially, the 4.49% moisture-analyser output was mistakenly treated as a dry-basis percentage. The dry mass was consequently estimated using $m_{\mathrm{dry,initial}} = m_{70}/(1 + MC_{70}/100)$, whereas the analyser reading was on a wet basis and requires Equation 3.1. The originally calculated mean prepress moisture content was approximately 10.01% (dry basis). After correcting the dry-mass reference, the estimated mean increased to 10.255% (dry basis). This was a retrospective correction to the mass calculations; no measured masses or manufactured boards changed. The error was associated with the difference between wet-basis and dry-basis definitions, not with a later physical change in the boards. All moisture values reported in the Results use the corrected dry-mass estimates. The sheets were then left in ambient laboratory air for at least 24 h before the final mass adjustment. Their moisture equilibrium state was not determined.

3.3.2. Parent-Sheet Moisture and Smaller-Sheet Mass

Some parent sheets contained missing corners or openings in the fibre-pith structure. To obtain more complete material sections, the intended sheet size was reduced from 200×40 to 90×40 mm. This reduced the amount of otherwise usable husk that had to be discarded and allowed sheets with visible through-thickness gaps to be excluded. The smaller sheets still provided sufficient material for a 70 mm bending specimen tested over a 60 mm span. Local differences in fibre distribution, pith content and thickness remained.

The reduced number of suitable sheets also influenced the experimental design. Three pressure levels and three temperature levels were retained, providing nine conditions with two independently manufactured boards per condition. Pressing time was fixed at 4 min following the preliminary trials described in Section 3.4.

Immediately before cutting, each parent sheet was weighed again. Its dry-basis moisture content was calculated from the measured mass and its estimated dry mass:

$$MC_{\text{parent}} = \frac{m_{\text{parent}} - m_{\text{dry,parent}}}{m_{\text{dry,parent}}} \times 100. \tag{3.2}$$

The 90×40 mm pieces were then weighed separately. Their estimated dry masses were calculated using the moisture content of the parent sheet:

$$m_{\text{dry,90}} = \frac{m_{\text{90,measured}}}{1 + MC_{\text{parent}}/100}. \tag{3.3}$$

This calculation assumes that moisture was distributed uniformly within each parent sheet and that cutting caused negligible moisture change.

3.3.3. Grading and Initial Board Allocation

Before allocation, each 90×40 mm sheet was examined against the light. Sheets were accepted when they covered the nominal rectangular area without missing corners or visible through-thickness openings. Material with see-through gaps was excluded.

This screening reduced conspicuous defects at the lay-up stage, while differences in local sheet thickness and fibre–pith distribution were still present. Figure 3.5 shows the cut-sheet format before visual grading and allocation.

Four accepted sheets were initially assigned to each board using a target estimated dry mass of 17.5 g. Groups were assembled to limit differences in material loading and to avoid placing prominent defects directly above one another. After pretreatment, the sheets were weighed and regrouped because the original assemblies differed more in mass than intended (Section 3.5.1).



Figure 3.5: Cut coconut husk sheets before visual grading and allocation.

3.4. Preliminary Trials and Pretreatment Selection

3.4.1. Development of the Manufacturing Procedure

Preliminary pressing trials varied the amount of husk, board dimensions, lay-up arrangement, pressure, platen temperature and pressing duration. The resulting boards were examined for incomplete consolidation, cracking, delamination, lateral spreading, darkening and scorching. These observations guided the manufacturing decisions listed in Table 3.2. None of the preliminary boards were included in the factorial dataset.

Table 3.2: Manufacturing decisions informed by preliminary trials and practical constraints.

Constraint or observation	Decision	Rationale
Insufficient intact 200×40 mm sheets; local gaps and missing corners	Select 90×40 mm sheets with full area coverage and no see-through openings	Retain more usable material while excluding gaps and incomplete corners
Limited suitable sheets for replication	Remove moisture content as the third DOE factor; retain pressure and temperature	Test nine combinations with two independent boards per combination at approximately common moisture
Local thickness and material variation	Use four sheets per board	Distribute fibre-rich and pith-rich regions and avoid aligned defects
Coherent boards within a short cycle; darkening at more severe exposure	Fix the hold at 4 min	Retain pressure and temperature as the two DOE factors
Poorer consolidation near unconfined edges	Progressively trim each board to a bending specimen	Remove outer material by a consistent cutting procedure
No time to develop a lateral-confinement mould	Press without lateral restraint and calculate nominal pressure from the initial footprint	Board spreading and spatially uneven consolidation could occur
Feasible consolidation around 12 MPa and $180\,^{\circ}$C	Test three levels around this centre	Examine responses within a practical process window

The selection of pressing conditions also considered literature on binderless coconut husk boards. Snijder et al. reported short pressing cycles under suitable processing conditions [10], while heat exposure has been associated with changes in coir fibre tensile behaviour [12]. The experimental centre of $180\,^{\circ}$C and 12 MPa was selected from the preliminary trials within the ranges reported for coconut husk board manufacture [3, 10, 8].

The preliminary boards tended to consolidate less effectively near their unconfined edges, where lateral spreading was visible. The later cutting procedure therefore used a fixed sequence of trimming operations rather than choosing a visually favourable area from each board.

3.4.2. Exploratory Pretreatment Screening

The pretreatment screening compared untreated husk with sheets treated in hot demineralised water or a dilute NaOH solution (Table 3.3). Screening boards had a nominal 90×40 mm footprint and an initial target dry-material mass of 17.5 g. Measured MOR and MOE, together with visible board integrity, informed selection of the treatment for the DOE. The unequal numbers of control and treated measurements were sufficient for an initial process decision but not a statistically replicated treatment comparison.

Table 3.3: Pretreatment conditions used in the preliminary screening.

Condition	Treatment	Reported sample count
Untreated	No water or alkaline treatment	Two control measurements
Hot water	Demineralised water, $80\,^{\circ}$C, 1 h	One board
NaOH	1 wt.% solution, 1 h at room temperature; demineralised-water rinse	One board

All screening boards were pressed at nominal settings of 12 MPa and $180\,^{\circ}$C with a 4 min hold. For the hot-water treatment, 800 mL of demineralised water was heated in a vessel with magnetic stirring. Water temperature was monitored with a thermometer, and the husk sheets were kept submerged at $80\,^{\circ}$C for 1 h.

For the alkaline treatment, the sheets were submerged in a 1 wt.% NaOH solution for 1 h at room temperature. They were then rinsed with demineralised water until the rinse water remained visually clear. Surface water was absorbed with paper before drying. The rinse endpoint was based on appearance; residual alkalinity was not measured.

Hot demineralised water was chosen as a relatively mild treatment that could remove some water-soluble material while retaining the sheet structure. Ferraz et al. [20] used coir fibres immersed in water at $80\,^{\circ}$C for 90 min in cement-bonded composites; this provided a treatment precedent but not an exact recipe or a binderless-board prediction. A 1 wt.% NaOH treatment for 1 h at room temperature provided a deliberately mild contrasting alkaline condition. The papers of Setyanto et al. [21] and Xiong et al. [22] used 5% NaOH and examined isolated fibres or subsequent alginate treatment, rather than intact flattened sheets. Their results therefore support the rationale for screening alkaline treatment, not the specific concentration selected in this study. The treatment liquids were not chemically analysed, and visually clear rinse water was not taken as evidence of neutral pH or complete removal of alkali.

After treatment, the hot-water and NaOH sheets were dried at $70\,^{\circ}$C for 24 h and exposed to ambient laboratory air for at least 24 h. Their target mass at 10% dry-basis moisture was calculated as

$$m_{\text{target}} = m_{\text{dry}}(1 + MC_{\text{target}}/100). \tag{3.4}$$

Immediately before pressing, each assembly was weighed against its calculated target. When the measured mass was too high, the material was returned briefly to the $70\,^{\circ}$C oven and reweighed. This was repeated until its mass was as close as practicable to the target. Moisture content was estimated from mass rather than measured directly in every assembled board.

Demi80, defined as immersion in demineralised water at $80\,^{\circ}$C for 1 h, was selected for the factorial series on the basis of the screening results. The measured bending properties and observed board condition supporting this choice are presented in Section 4.1.

3.4.3. Exploratory FTIR Characterisation

Fourier-transform infrared spectroscopy (FTIR) was used as an exploratory characterisation method to examine whether the Demi80 and NaOH pretreatments produced detectable spectral changes relative to untreated coconut husk. Untreated coconut husk was used as the background reference, after which Demi80- and NaOH-treated material were measured relative to this reference. The resulting spectra therefore represent differences between the treated and untreated materials rather than absolute FTIR spectra of each material.

Measurements were performed using a PerkinElmer Spectrum 100 FTIR Spectrometer. Each measurement consisted of 16 scans over a wavenumber range of 4000-600 cm^{-1}.

The measured relative transmittance was converted to differential absorbance according to

$$\Delta A = -\log_{10}\left(\frac{T_{\text{rel}}}{100}\right), \tag{3.5}$$

where T_{rel} is the transmittance measured relative to the untreated coconut husk reference, expressed as a percentage. A value of $\Delta A = 0$ therefore represents no difference in absorbance relative to the untreated material. Positive ΔA values indicate higher absorbance after pretreatment, while negative values indicate lower absorbance relative to the untreated reference.

The FTIR comparison was used to support interpretation of possible pretreatment-related chemical changes. It was not used to select the Demi80 treatment for the main DOE, as that selection was based on the preliminary bending measurements.

3.5. Final DOE and Board Manufacture

3.5.1. Post-Treatment Material Preparation

All DOE sheets received the selected Demi80 treatment followed by drying at $70\,^{\circ}$C for 24 h. Residual moisture was measured on representative material dried alongside the sheets, and estimated sheet dry masses were calculated using Equation 3.1.

The original four-sheet groups showed greater differences in post-treatment mass than intended. Each treated sheet was therefore weighed individually and assigned to a new group of four, targeting an estimated dry mass of 16.4 g per board. This replaced the original 17.5 g allocation target after the material losses associated with pretreatment.

The resulting DOE comprised 18 four-sheet assemblies, with two boards allocated to each temperature-pressure combination. The recorded estimated dry masses and prepress moisture contents were calculated from the corrected moisture reference and individual sheet masses. The board-level values

and their variation are reported in the Results chapter. The six C185-series follow-up assemblies were prepared and recorded separately.

Regrouping made the total material loads more consistent, but it did not eliminate local differences in fibre, pith or sheet thickness. The moisture estimates also relied on a representative residual-moisture value for the sheet material.

Following at least 24 h of exposure to laboratory air, each four-sheet assembly was weighed shortly before pressing. Its mass was compared with the target corresponding to 10% dry-basis moisture (Equation 3.4). Assemblies above the target were briefly returned to the $70\,^{\circ}$C oven, sometimes for only a few seconds, and carried to a balance elsewhere in the laboratory for reweighing. These steps were repeated until the measured mass approached the target. The cooling interval and sheet temperature at weighing were not recorded, and the procedure controlled estimated total water mass rather than the within-sheet moisture distribution.

3.5.2. Factorial Design and Production Order

The DOE crossed nominal pressures of 9, 12 and 15 MPa with platen temperatures of 170, 180 and $190\,^{\circ}$C (Table 3.4). Each of the nine conditions was manufactured once on each production day, giving 18 independent boards. Each board supplied one bending specimen. Repeated dimension measurements and offcuts were treated as subsamples rather than independent boards.

Table 3.4: Final factorial design. Each temperature cell contains one board from each production day. Force is calculated from the initial 90×40 mm footprint; row order does not indicate production order.

Nominal pressure	Force	$170\,^{\circ}$C	$180\,^{\circ}$C	$190\,^{\circ}$C
9 MPa	32.4 kN	2 boards	2 boards	2 boards
12 MPa	43.2 kN	2 boards	2 boards	2 boards
15 MPa	54.0 kN	2 boards	2 boards	2 boards

The press was run from 170 to 180 to $190\,^{\circ}$C within each production day to avoid repeated heating and cooling. Pressure order was randomised within each temperature block. Production day was recorded for each board but was not included as a factor in the DOE analysis. The influence of possible day-to-day variation on the measured board properties was therefore not evaluated separately.

Table 3.5 summarises the preparation, pressing and testing conditions held constant throughout the DOE. Moisture content was controlled towards a target rather than varied as a DOE factor.

Table 3.5: Common manufacturing and testing conditions.

Parameter	Procedure or setting
Pretreatment	Demineralised water, $80\,^{\circ}$C, 1 h
Post-treatment drying	$70\,^{\circ}$C, 24 h
Ambient exposure	At least 24 h after drying
Prepress moisture target	Nominal 10% on a dry-mass basis; the initial dry-mass reference contained a wet/dry-basis conversion error (corrected retrospective mean: 10.255%)
Lay-up and initial footprint	Four sheets; 90×40 mm
Material loading	Target estimated dry mass 16.4 g per board after pretreatment; achieved mean 16.346 g across the 18 DOE boards
Press positioning	Centred; no lateral confinement
Pressing hold	4 min, excluding loading and unloading ramps of 15 s each
Post-press storage	24 h under ambient laboratory conditions
Target bending geometry	70×20 mm; 60 mm support span
Crosshead rate	1 mm min^{-1}

3.5.3. Lay-Up and Nominal Pressure

Four sheets were stacked with the intention of distributing thick and thin regions and avoiding aligned discontinuities. The lay-up was placed centrally between the press platens (Figure 3.6).



(a) Top side (b) Back side

Figure 3.6: Four-sheet lay-up used to distribute local material variation.

The target press force was calculated using the nominal initial lay-up area:

$$A_0 = 90 \times 40 = 3600\ \mathrm{mm}^2, \qquad F = P_{\mathrm{nom}} A_0. \tag{3.6}$$

The corresponding forces are given in Table 3.4. These pressures are nominal values based on the initial footprint. Since the lay-ups were unconfined and spread laterally, the local pressure during pressing was not determined from the final board area. A lateral-confinement mould was not implemented because of the available experimental-development time; the resulting variation in geometry is considered when interpreting differences between whole-board and cut-specimen density.

3.5.4. Temperature Control and Pressing Cycle

The displayed mean of the separately heated upper and lower platen temperatures was used to decide when to begin pressing. This allowed the process to start near the intended DOE level even when the controller setpoints differed from the measured platen temperatures. The usual acceptance range was $\pm 2\,^{\circ}\mathrm{C}$.

Upper and lower platen temperatures were recorded at the start of pressing and after 2 and 4 min. Their average was used to describe the recorded platen temperature at each time point. The DOE factors remained the nominal levels of 170, 180 and $190\,^{\circ}\mathrm{C}$; their measured values are reported separately in Results.

The prescribed press operation consisted of a 15 s increase to the target force, a 4 min pressure hold and a 15 s release, totalling 4.5 min from the start of loading to the end of unloading (Figure 3.7). Material positioning, removal, handling and temperature stabilisation were not included in this interval. The linear ramps shown in the schematic are prescribed guides rather than a measured force history.

3.5.5. Cooling and Board Inspection

Boards were removed from the press and cooled in ambient laboratory air. Whole-board mass and dimensions were recorded at approximately 5 and 30 min and 24 h after pressing; the measurement procedure and rationale are given in Section 3.6.1. The first measurement was not taken at the instant of unloading. Temperature and relative humidity during storage were not logged, and the 24 h interval was not used as evidence of moisture equilibrium.

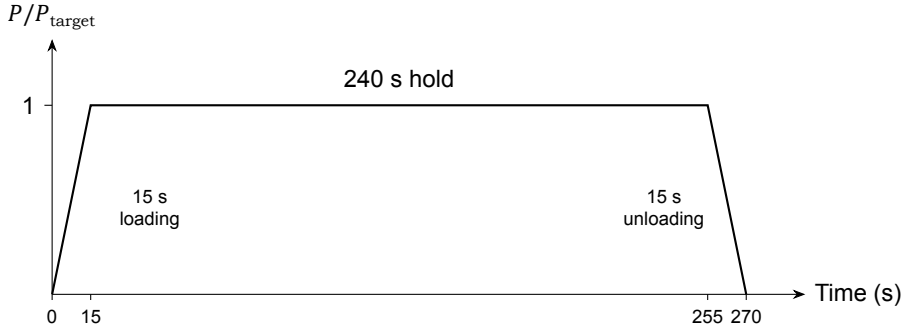

Figure 3.7: Schematic prescribed pressing cycle. The ramps are drawn as linear guides; this figure is not a recorded force trace.

Before cutting, each board was visually inspected for cracks, layer separation, warping, lateral spreading, darkening, scorching and incomplete consolidation. The formal delamination score was assigned after cutting, before the bending test. One specimen was prepared from each DOE board, and one observer examined all four exposed perimeter edges together. The observer assigned one overall ordinal score per specimen according to Table 3.6, based on the most relevant visible layering and cracking across the four edges.

Table 3.6: Criteria used for unaided visual scoring of all four perimeter edges of each specimen after cutting. One overall score was assigned per specimen based on the combined observations; scores range from 0 (least visible damage) to 3 (most visible damage).

Score	Visual observations
0	No visible delamination, or only very slight signs of layering.
1	Small visible cracks, or pronounced layering that did not involve all layers.
2	Multiple visible cracks together with visible layering, without all layers being exposed.
3	An entire layer was visible, or substantial cracking was present.

The scores describe the condition of the exposed specimen edges at the time of inspection. Cutting could reveal existing interfaces or introduce additional cracks, and the method did not measure internal bond strength or closed interfaces. The categories were ordinal: a difference of one score did not represent a fixed increase in crack size or separated area.

3.5.6. Post-DOE Confirmation and Interlayer Trials

Following the exploratory desirability analysis described in Section 4.8, six boards were manufactured at the *model-selected condition* of $185\,^{\circ}$C and 14.2 MPa, designated C185-14 (Table 3.7). The designation is a board-series name rather than the exact pressure setpoint. Two unmodified boards provided a local reference for two boards with bio-oil between the sheets and two with added pith. These six boards were not included in the 18-board factorial analysis, and the selected condition was not a statistically established optimum.

Table 3.7: Additional boards produced at the model-selected condition ($185\,^{\circ}$C and 14.2 MPa). The C185-14 suffix is a series designation, not an exact pressure value.

Board designation	Preparation and purpose	Boards
C185-14	Unmodified confirmation boards; check the response at the model-selected pressing condition.	2
C185-14-O	Bio-oil introduced between the sheets; explore the effect of an interlayer additive at the same pressing condition.	2
C185-14-P	Additional pith introduced between the sheets; explore the effect of locally increased pith at the same pressing condition.	2

The unmodified C185-14 boards were used to compare measured bending responses with those expected near the selected DOE setting. The two interlayer variants were exploratory additions to the

same base lay-up, not extra levels of the original DOE. Their preparation and material loading were tracked separately.

All six follow-up boards were made from four sheets subjected to the same hot-water pretreatment, drying, moisture adjustment and stacking procedure as the DOE boards. The nominal pressing settings were kept at $185\,^{\circ}$C and 14.2 MPa. Based on the original 90×40 mm footprint, 14.2 MPa corresponds to a nominal force target of 51.12 kN; this is a calculation rather than a measured local contact force. The oil and pith were applied between the sheets at all three interfaces, using separate application methods described below.

The two C185-14-O boards received 0.786 and 0.649 g of bio-oil, respectively. The viscous oil was scooped and spread manually onto the back faces of the sheets so that it lay at the three interfaces after assembly. Its distribution and coating thickness were not measured.

The C185-14-P boards received 1.9005 and 1.9041 g of additional fine pith. This material came from the same coconut husk supply and had been collected as loose cutting residue several months earlier. It was stored in a bag in the laboratory storeroom and selected as a fine, dust-like fraction. The pith was sprinkled onto the front faces while the sheets were stacked with their back faces down, placing added material at the three interfaces. Unlike the base sheets, the pith was not moisture-conditioned before use, and its moisture content was not measured.

The conditioned base sheets for the pith-added boards weighed 17.9970 g (bag 15) and 18.0110 g (bag E1) before pith addition. The pith portions were weighed separately, so total material loading was calculated as

$$m_{\mathrm{total}} = m_{\mathrm{sheets}} + m_{\mathrm{pith}}. \tag{3.7}$$

The resulting loads were 19.8975 and 19.9151 g, respectively, assuming negligible material loss during stacking. The complete lay-ups were not reweighed. These totals refer to the masses of the conditioned sheets and added pith at assembly, not to oven-dry mass. As the pith moisture content was unknown, the dry mass and overall moisture content of the pith-added assemblies could not be calculated.

The bio-oil used in the exploratory interlayer trials was labelled DOE-300-15-5 and originated from the hydrothermal liquefaction study of Bias [23]. It was produced from *Acacia mellifera* biomass from Namibia at $300\,^{\circ}$C with a residence time of 15 min and a hydrotalcite catalyst loading of 5 wt.% relative to the dry biomass. The exact composition and condition of the stored bio-oil used in the present experiments were not independently characterised.

3.6. Specimen Preparation and Physical Measurements

3.6.1. Whole-Board Measurement Schedule and Rationale

The physical measurements were collected to help interpret the MOR and apparent MOE results, rather than to act as independent product-compliance tests. In particular, changes in board dimensions after pressing could indicate differences in consolidation or short-term recovery between the investigated conditions. Measurements of the whole board were kept separate from the later measurements of the cut bending specimen.

For each whole board, length and width were each measured at three positions, while thickness was measured at five positions. Board mass was recorded using the laboratory balance. The same measurement counts were used at approximately 5 min, 30 min and 24 h after removal from the press (Figure 3.8). The first measurement was made as soon as practicable after handling and initial cooling; it was therefore a 5-min reference rather than an instantaneous measurement at pressure release. The 30-min observation captured further early changes, while the 24-h measurement provided a consistent first-day comparison during ambient laboratory storage.

Repeated dimension measurements are useful here because the small, unconfined husk-sheet boards could spread laterally and develop uneven thickness. Measurements at several positions reduced dependence on any single local dimension. Five thickness readings provided more spatial coverage than one central reading, while three readings in each in-plane direction offered a manageable compromise between coverage and repeated handling. The multiple readings were intended to improve the description of these small and irregular boards, not to provide an independent quality score. EN 324-1:1993 addresses dimensions of whole flat panels and uses its own measurement positions, including eight thickness points; the present five-thickness-point protocol should therefore not be described as more comprehensive or fully compliant with that standard [24]. Five-point thickness measurements have been reported for particleboard test pieces by Silva et al. [25], but this does not establish that the

present procedure is superior to measurements used in the coconut-husk literature. The 3/3/5 counts and observation times were practical adaptations for this board size.

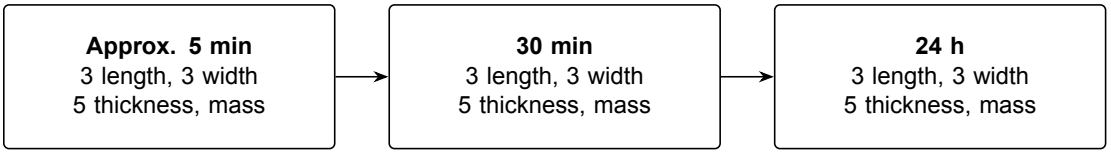

Figure 3.8: Repeated whole-board measurements following hot pressing. At each observation time, three length measurements, three width measurements, five thickness measurements and one board mass measurement were recorded. The first time point was approximately 5 min after pressing, not the instant of pressure release.

3.6.2. Whole-Board Density, Mass Change and Post-Pressing Thickness Recovery

At each observation time τ, the arithmetic mean length $\bar{l}_\tau$ was calculated from three readings, the mean width $\bar{b}_\tau$ from three readings and the mean thickness $\bar{t}_\tau$ from five readings. An approximate external board volume and whole-board density were then calculated as

$$V_\tau = \bar{l}_\tau \, \bar{b}_\tau \, \bar{t}_\tau, \qquad \rho_{\mathrm{board},\tau} = \frac{m_\tau}{V_\tau}, \tag{3.8}$$

where m_τ is the board mass at the same time point. Units were converted consistently to express density in kg m^{-3}. This volume estimate treats the board as a rectangular body described by average external dimensions; it does not describe its internal density distribution or account exactly for irregular edges and local thickness variations. The mass and dimensions were measured in the same post-pressing state, consistent with the basic mass-to-volume approach used for wood-based panel density determination in EN 323:1993 [26].

Post-pressing thickness recovery was calculated relative to the earliest post-pressing measurement, rather than relative to the uncompressed sheet stack or to the platen spacing during pressing. For a later time τ (30 min or 24 h), the percentage recovery was defined as

$$R_{t,\tau} = \frac{\bar{t}_\tau - \bar{t}_{5\mathrm{min}}}{\bar{t}_{5\mathrm{min}}} \times 100\%. \tag{3.9}$$

The percentage change in whole-board volume and mass over the same interval were calculated as

$$\Delta V_\tau = \frac{V_\tau - V_{5\mathrm{min}}}{V_{5\mathrm{min}}} \times 100\%, \tag{3.10}$$

$$G_{m,\tau} = \frac{m_\tau - m_{5\mathrm{min}}}{m_{5\mathrm{min}}} \times 100\%. \tag{3.11}$$

The pressing mass loss, using the measured prepress sheet mass as its reference, was calculated as

$$L_{m,\mathrm{press}} = \frac{m_{\mathrm{prepress}} - m_{5\mathrm{min}}}{m_{\mathrm{prepress}}} \times 100\%. \tag{3.12}$$

The terms “mass gain” and “mass loss” describe measured changes in total mass; they do not identify which constituents were removed during pressing or establish that all subsequent mass increase was due to moisture uptake. No direct moisture measurement was made at each post-pressing time point. External volume was estimated from mean dimensions; it is not a measurement of internal pore volume.

3.6.3. Interpretation of Post-Pressing Thickness Recovery

Densification studies distinguish thickness recovery occurring immediately on release of the applied pressure from dimensional changes continuing during subsequent storage [27]. Because the first thickness measurement in this study was made approximately 5 min after pressing, any recovery before that point could not be quantified. The measured response is therefore termed *post-pressing thickness recovery* and refers to the change relative to the 5-min measurement. It may include delayed mechanical relaxation and moisture-related expansion, which were not separated experimentally.

Changes in mass, thickness and calculated volume were recorded separately, allowing their time courses to be described but not the underlying processes to be isolated. Recovery driven by mechanical relaxation could change dimensions without necessarily changing mass. Sorption of moisture from ambient air could increase both mass and dimensions, but the amount of water taken up was not measured independently. Because both mechanisms may occur simultaneously, the experiment cannot apportion the measured expansion between them.

The measurements were made in ambient laboratory air without recorded relative humidity. They differ from the controlled-humidity dimensional-change procedure in EN 318:2002 and the water-immersion thickness-swelling test in EN 317:1993 [28, 29]. Their value is as descriptive short-term behaviour after pressing, not as proof of long-term dimensional stability, water resistance or a specific bonding mechanism.

3.6.4. Sequential Dry Cutting

One bending specimen was cut from each manufactured board using a Compcut ACS 600. A fixed sequence of rectangular trimming steps reduced the board through nominal dimensions of 45×83, 83×35, 35×70 and finally 70×20 mm (Figure 3.10). The predominant longitudinal fibre direction ran along the 70 mm specimen length, parallel to the bending span. The cutting sequence was applied to every board instead of selecting a region based on its appearance.

For the first DOE specimen (bag 1, B1-170-9), the final target width was larger than for the remaining specimens. Its measured average width was 25.55 mm; the later specimens were intended to be 20 mm wide and were generally measured near 21 mm. The preceding cutting steps were unchanged. All density and bending calculations used the actual measured dimensions, including the first specimen.

Preliminary cutting trials showed that wet cutting caused water-related damage, while cutting with a saw produced uneven edges and could pull fibres out of the boards. Dry cutting with the Compcut ACS 600 gave the most consistent specimen dimensions of the approaches tested. However, the grooved blade accumulated husk debris after each cut, causing it to dig into the board and jam. The blade was therefore wiped clean manually with acetone between cuts. Visible scorching along the cut edges remained. Figure 3.9 documents the equipment and specimen preparation.

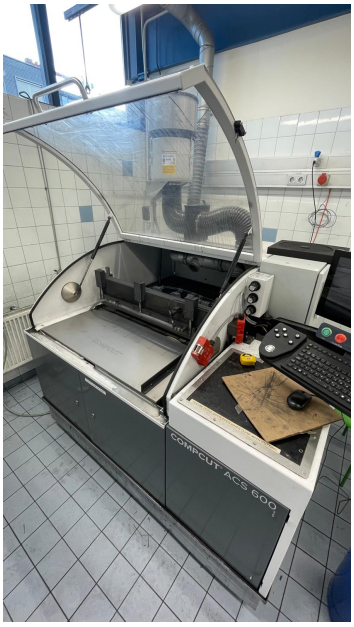

(a) Compcut ACS 600 cutting equipment



(b) Photograph from the sheet-cutting procedure

Figure 3.9: Photographs of the cutting equipment and material handling during specimen preparation. The images document the procedure but do not establish whether cutting generated particular defects.

The cutting-method comparisons were qualitative. Using the same dry-cutting and blade-cleaning procedure for all specimens improved consistency of preparation but did not establish that edge scorching or other cutting-related damage had no effect on the bending measurements or visual delamination

scores.

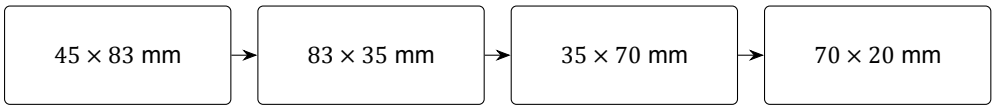

Figure 3.10: Successive nominal cutting dimensions used to prepare a single bending specimen from each board. The sequence represents dimensional reduction, not the location of the cuts on the original board. The first prepared specimen followed the same sequence but had a greater final width, as discussed in the text.

3.6.5. Cut-Specimen Dimensions and Apparent Density

After cutting, the dimensions of the bending specimens were measured separately from the whole-board measurements. Specimen length and width were each measured at three positions, near both ends and at the centre. Thickness was measured at the four corners and the centre. The mean dimensions were used to calculate specimen density and the bending properties. This repeated-point approach was intended to reduce the influence of local dimensional irregularities and is comparable in principle to five-point thickness measurements described for particleboard specimens by Silva et al. [25]. EN 324-1:1993 concerns dimensional measurements of whole boards, whereas EN 325:2025 concerns test pieces. The measurement procedure used in this study is not claimed to comply fully with either standard [30]. The repeated measurements were used to calculate mean dimensions and were not treated as independent specimens.

Apparent specimen density was calculated as

$$\rho = \frac{m}{lbt}, \tag{3.13}$$

where m is the specimen mass, l is the mean length, b is the mean width and t is the mean thickness. Mass and dimensional units were converted consistently to express apparent density in $\mathrm{kg\,m^{-3}}$. The calculation follows the mass-to-volume principle of EN 323:1993 [26], although formal compliance with the standard is not claimed because of the adapted specimen geometry and measurement procedure. Thickness is particularly relevant to the bending calculations, as MOR and MOE depend on t^2 and t^3, respectively. Whole-board density measured before cutting and cut-specimen density were therefore considered separately.

3.7. Three-Point Bending and Mechanical Data Processing

3.7.1. Test Geometry and Loading

Three-point bending tests were performed using a Zwick and Roell ProLine testing machine equipped with a 10 kN load cell. The tests followed the geometry and calculation principles of ASTM D1037 [19], adapted to the smaller specimens available. Each specimen was centred on a 60 mm support span, with the dominant longitudinal fibre direction aligned between the supports. Load was applied at mid-span at a crosshead speed of 1 $\mathrm{mm\,min^{-1}}$, while force and crosshead displacement were recorded throughout the test. Loading continued to a crosshead travel of 11 mm to observe the response after the first failure event. The outer sheet face placed towards the loading nose was not controlled or recorded.

As the expected failure loads of the coconut husk specimens were unknown before testing, the load cell already installed on the machine was used following the recommendation of the laboratory technician. After the initial tests, the same load cell was retained to maintain consistent measurement conditions and avoid introducing an additional change to the test setup. The measured failure loads were relatively low compared with its nominal capacity. Since the measurement accuracy of the load cell within this force range was not independently verified, compliance with the force-measurement accuracy requirement of EN 310:1993 cannot be confirmed [11].

The reduced specimen dimensions and crosshead-based displacement measurement should be considered when comparing the results with standard-sized board tests. EN 310:1993 specifies a three-point bending method for wood-based panels, with a conventional support span equal to 20 times the

nominal thickness and a nominal specimen width of 50 mm [11]. The approximately 5 mm-thick specimens used in this study had a span-to-thickness ratio of roughly 10–13 rather than approximately 20. EN 310 reports an apparent bending modulus because shear deformation contributes to the measured deflection. The shorter support span and use of crosshead displacement provide additional reasons to describe the calculated modulus as *apparent MOE*. A different support span could have influenced the measured response, but the contribution of shear deformation and the results for larger specimens were not determined in this study.

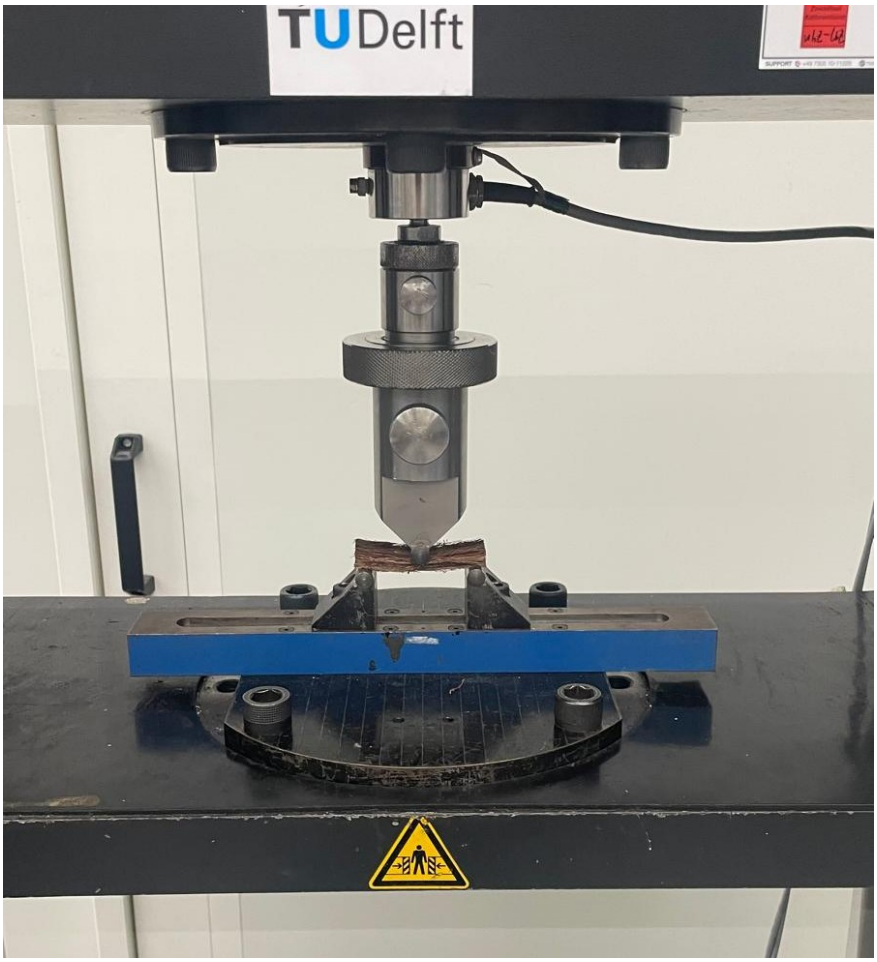

Figure 3.11: Actual three-point bending fixture with a 60 mm support span. The crosshead-displacement method was adapted to the available specimen size; testing was not carried out fully in accordance with EN 310.

3.7.2. Failure Load and Modulus of Rupture

For each specimen, the selected failure load $F_{\max}$ was defined as the first structural peak followed by a clear load drop. Some curves subsequently regained force. Those later peaks were not used when they followed an earlier substantial failure event. If a curve showed no distinct earlier drop, its highest force before final failure was selected. The same selection approach was applied to all specimens.

MOR was calculated from the selected failure load and the measured cross-section:

$$\mathrm{MOR} = \frac{3F_{\max}L}{2bt^2}, \tag{3.14}$$

where $L = 60$ mm is the support span. Force in N and dimensions in mm give MOR in MPa.

3.7.3. Displacement Reference and Modulus of Elasticity

Many force-displacement curves showed irregular contact behaviour at the start of loading. A force threshold of 5 N was chosen as a consistent reference because the traces generally became more

stable by that point. The selected threshold defines the reported displacement origin; it was not established through a separate seating-force validation.

Machine compliance was estimated from a separate metal-plate loading measurement. The slope of displacement against force between 20 and 300 N was determined by least-squares regression in Excel, giving a compliance coefficient of $c_{\mathrm{m}} = 0.00031665$ mm N^{-1}. For each recorded force F_i and displacement δ_i, the compliance-corrected displacement was calculated as

$$\delta_{\mathrm{mc},i} = \delta_i - c_{\mathrm{m}} F_i. \tag{3.15}$$

The first recorded point reaching or exceeding 5 N provided the displacement reference:

$$\delta_{\mathrm{rel},i} = \delta_{\mathrm{mc},i} - \delta_{\mathrm{mc,5N}}. \tag{3.16}$$

The subscript 5N refers to the first sampled point above the threshold, rather than an interpolated value at exactly 5 N. Subtracting this fixed offset changed the displayed displacement origin but not the slope used for MOE. The compliance correction was an estimate based on the metal-plate measurement.

The apparent MOE was calculated from a least-squares fit of force against compliance-corrected displacement over the range corresponding to 10-40% of each specimen's manually selected failure load. The relevant failure peak was identified from the force-displacement curve in Excel using the same criterion as applied for the MOR calculation. The force limits for the MOE fit were then calculated as $0.10F_{\max}$ and $0.40F_{\max}$, where $F_{\max}$ is the manually selected failure load. Only data from the ascending loading branch within this interval were included. The fitted slope k was used to calculate

$$\mathrm{MOE} = \frac{L^3}{4bt^3}k, \qquad 0.10F_{\max} \le F \le 0.40F_{\max}. \tag{3.17}$$

Here, k is the force-displacement slope in N mm^{-1}, giving MOE in MPa when the dimensions are expressed in mm. The force interval was defined relative to the selected failure load for each specimen.

3.7.4. Failure Observations

During and after bending, visible responses included tensile-side cracking, opening between sheets, local crushing and shear-like damage. The apparent failure location and the recorded force-displacement behaviour were documented together.

3.8. Visual Observations and Preliminary Cutting Check

The main visual-inspection procedure and ordinal scoring criteria are described in Section 3.5. In addition to the post-cut edge scores, intact boards were inspected after pressing for visible damage and uneven consolidation. The scores were based on the four exposed edges of one specimen per board and were assigned before bending. This distinction was retained when comparing visual observations with bending results.

3.9. Statistical Analysis

3.9.1. Data Organisation and Reporting

Each independent DOE board contributed one set of physical measurements, one bending specimen and one overall post-cut delamination score. The board ID linked the manufacturing condition and production day to its recorded platen temperatures, specimen dimensions, mass, apparent density, bending data and visual observations. Mechanical responses were calculated as described in Section 3.7. The results were reported for individual boards and as condition means with sample standard deviations (SD), calculated across independently manufactured boards. The repeated dimensional readings within a board were averaged for that board and were not treated as independent replicates.

3.9.2. Spreadsheet Processing and JMP Outputs

Raw bending-test files were processed in Microsoft Excel. The workbook combined each force-displacement trace with measured specimen dimensions, the selected structural failure load and the compliance-adjusted displacement. MOR and MOE were calculated using Equations 3.14 and 3.17 before transfer of board-level responses to the statistical dataset.

JMP was used to compare the measured responses across the nine factorial conditions and to fit exploratory response surfaces. The graph exports included measured condition summaries and model-predicted contours. For the contours, the JMP prediction formulas obtained from the DOE model were applied in a separate JMP table of pressure-temperature combinations to calculate a grid of predicted MOR and apparent MOE values. This table supplied plotting coordinates and model predictions, not new experimental observations or an independent validation dataset. Fitting was based on the board-level records rather than on group means. The contours were used to select a follow-up region, not to establish a confirmed optimum.

3.9.3. Response Surface Modelling

The effects of nominal pressing pressure and platen temperature were evaluated using quadratic response-surface models. MOR and apparent MOE were the primary responses; density, post-pressing thickness recovery and mass changes were examined as supporting responses. Pressure and temperature were treated as numerical factors. To match the coefficient parameterisation reported in the Results chapter, the fitted response was written as

$$\begin{aligned}\widehat{Y} = \beta_0 + \beta_T T + \beta_P P + \beta_{TP}(T-180)(P-12) \\ + \beta_{PP}(P-12)^2 + \beta_{TT}(T-180)^2,\end{aligned} \tag{3.18}$$

where $\widehat{Y}$ is the predicted response, T is nominal platen temperature in °C, and P is nominal pressing pressure in MPa. The interaction and quadratic terms were centred at 180 °C and 12 MPa; the linear terms are written in the original units. The observed response is understood as $Y = \widehat{Y} + \varepsilon$, where ε denotes the residual. The pressure and temperature coefficients represent local fitted slopes at the design centre. Because the linear terms are not written in centred form, β_0 alone is not the fitted response at the design centre.

The fitted domain was limited to the investigated range of 9-15 MPa and 170-190 °C. Formal statistical tests were interpreted using a 5% significance threshold. Model fit was assessed using the overall model test, R^2, adjusted R^2 and the observed residual variation. Because only two independently manufactured boards were available per pressure-temperature combination, the fitted models were used to describe trends within the investigated range and to guide the follow-up trials rather than to establish a confirmed optimum. Visual delamination was an ordinal score and was not treated as a continuous measure of interlayer bond strength.

The fitted model results and response surfaces are presented in Section 4.6.

3.10. Practical Challenges and Experimental Adaptations

Several practical challenges required adaptations to material preparation, board manufacture and mechanical testing. The nine main challenges and the responses adopted are summarised below; the cited sections describe the procedures in more detail. The remaining limitations and their implications for the results are discussed in Section 5.6.

1. **Specimen cutting.** Wet cutting caused water damage, while sawing could pull out fibres and leave uneven edges. Dry cutting gave more consistent dimensions, but the Compcut blade clogged after each cut. Wiping it with acetone allowed cutting to continue; edge scorching remained (Section 3.6.4).
2. **Limited suitable material.** Openings and missing corners reduced the supply of usable sheets. Sheet dimensions were reduced from 200×40 to 90×40 mm, and moisture content was removed as a varied DOE factor (Sections 3.3 and 3.4).
3. **Material heterogeneity.** Variations in thickness and fibre–pith distribution complicated board allocation. Visual grading and regrouping by estimated dry mass reduced some differences, but local variation remained (Sections 3.3 and 3.5.1).
4. **Uneven consolidation.** Without lateral confinement, boards spread and their edges sometimes consolidated poorly. A consistent trimming sequence was adopted, and nominal pressure was based on the initial sheet footprint (Sections 3.4 and 3.5).
5. **Moisture conditioning.** Approaching the target moisture content required repeated weighing and brief oven treatments. Moisture was estimated from mass rather than measured in every individual board (Section 3.5.1).

6. **Dry-mass calculation.** The moisture analyser's wet-basis reading was initially interpreted as a dry-basis value. The calculations were corrected retrospectively without changing the manufactured boards (Section 3.3).
7. **Bending-test setup.** The small specimens required a 60 mm support span. With failure loads initially unknown, the installed 10 kN load cell was used and retained for consistency (Section 3.7).
8. **Irregular bending traces.** Initial contact irregularities and multiple force peaks complicated data processing. A 5 N displacement reference and a consistent rule for selecting the structural failure load were applied (Section 3.7).
9. **Pressing sequence.** To avoid repeated heating and cooling, temperatures were tested in ascending order each day. Pressures were randomised within temperature blocks, but temperature remained linked to within-day production order (Section 3.5).

4

Results

4.1. Pretreatment Screening

The preliminary screening compared boards made from untreated coconut husk sheets with those treated in hot demineralised water (Demi80) or a 1 wt.% NaOH solution. The preparation and pressing procedures are described in Section 3.4.

4.1.1. Mechanical Screening Results

Figures 4.1 and 4.2 show the measured modulus of elasticity (MOE) and modulus of rupture (MOR) for the three pretreatment conditions. The Demi80-treated specimen reached 1.00 GPa and 34 MPa, respectively. The untreated control averaged 0.84 GPa and 21 MPa, while the NaOH-treated specimen reached 0.78 GPa and 23 MPa. The untreated values are based on two bending measurements; Demi80 and NaOH each have one measurement.

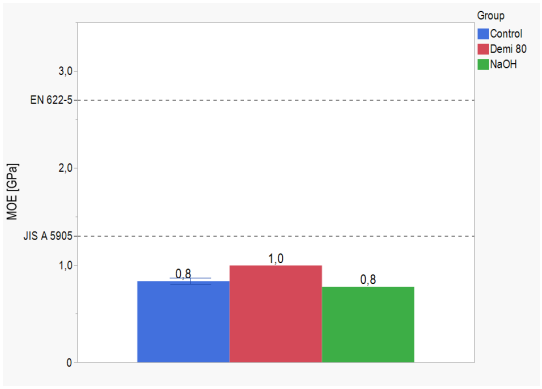

Figure 4.1: Apparent bending modulus of elasticity (MOE) in the preliminary pretreatment screening.

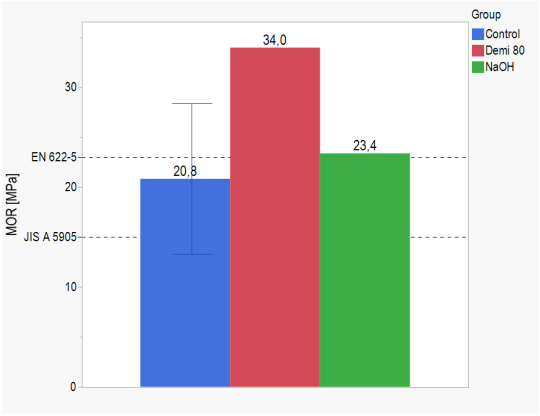

Figure 4.2: Modulus of rupture (MOR) in the preliminary pretreatment screening.

Note: The untreated control was measured twice ($n = 2$); the error bar represents sample standard deviation (SD). Demi80 and NaOH were each measured once ($n = 1$), so their SD cannot be calculated. The numerical reference lines are included for comparison only and do not establish product compliance.

4.1.2. Selection of Demi80 for the Main Experiment

Demi80 gave the highest measured MOE and MOR in the screening. Relative to the untreated control mean, its MOR was 63.0% higher and its MOE was 19.2% higher (Table 4.1). The small number of measurements does not establish a statistically significant treatment effect, but the observed performance supported the practical decision to use Demi80 for the main DOE. Pretreatment was then held constant while pressing temperature and pressure were varied.

4.1.3. FTIR Comparison of Pretreated Material

FTIR was used to compare untreated coconut husk with the Demi80- and NaOH-treated materials. Figure 4.3 shows the absorbance spectrum of untreated coconut husk, providing a reference for the main absorption regions

Table 4.1: Screening mechanical properties and differences relative to the untreated control.

Pretreatment	n	MOE (GPa)	ΔMOE (%)	MOR (MPa)	ΔMOR (%)
Untreated control	2	0.836	-	20.84	-
Demi80	1	0.996	+19.2	33.97	+63.0
NaOH	1	0.777	-7.0	23.38	+12.2

Note: n denotes bending measurements. Percentage differences are relative to the untreated control mean.

associated with lignocellulosic materials. The marked bands correspond to possible O–H, C–H, C=O, aromatic C=C and C–O/C–O–C vibrations.

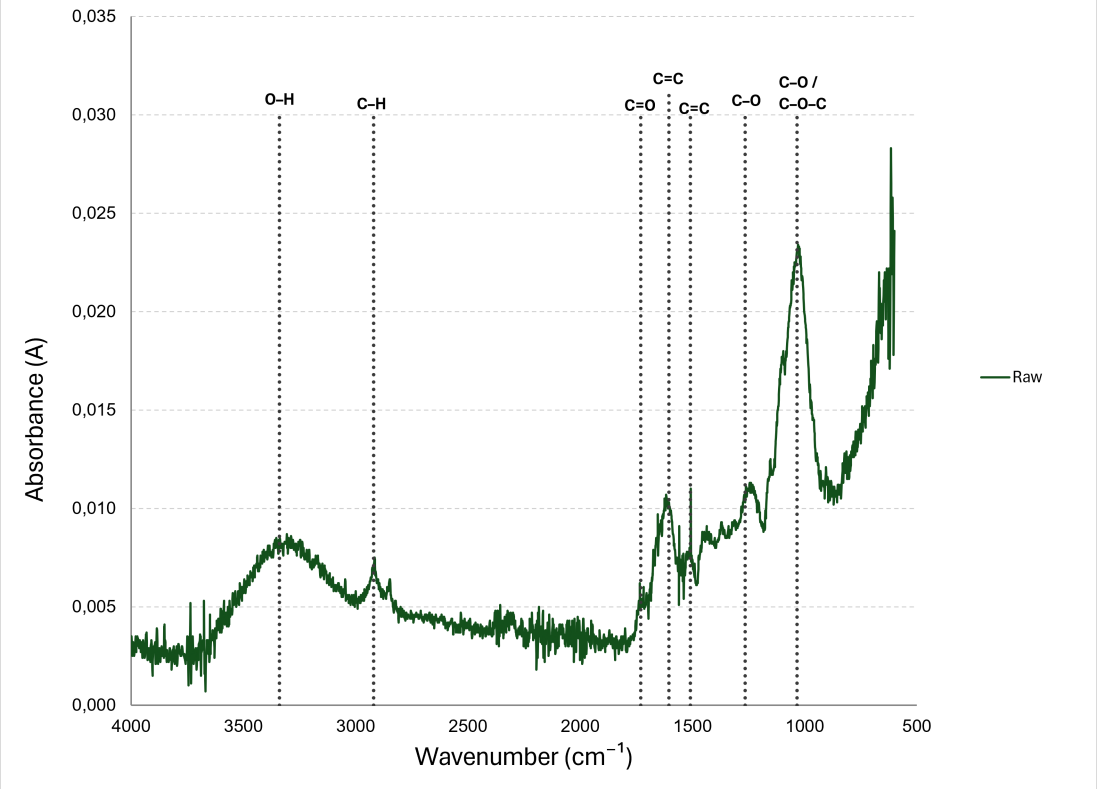

Figure 4.3: FTIR absorbance spectrum of untreated coconut husk.

Note: Vertical dotted lines indicate selected absorption regions commonly associated with lignocellulosic functional groups. These band assignments are indicative and are not unique to individual material components.

Figure 4.4 shows the differential absorbance spectra of the treated materials relative to the untreated reference. Here, $\Delta A = 0$ represents no difference in measured absorbance from the untreated material.

The NaOH-treated material showed substantially larger deviations from the untreated reference than the Demi80-treated material, particularly in the regions around 3340, 2920, 1730, 1605–1510, 1265 and 1035 cm^{-1}. The Demi80 spectrum remained closer to the untreated reference over most of the measured range, although smaller differences were also observed.

A narrow negative feature near 2350 cm^{-1} was present in the Demi80 difference spectrum. This region is associated with atmospheric CO_2 absorption, and the feature is likely related to differences in background compensation between measurements. It was therefore not interpreted as evidence of a treatment-induced chemical change.

Overall, the spectra indicate that both pretreatments produced detectable differences relative to untreated coconut husk, with NaOH producing the larger deviations. However, differences in absorbance do not directly establish changes in the concentrations of individual chemical components. The possible chemical interpretation of the selected absorption regions is discussed in Chapter 5.

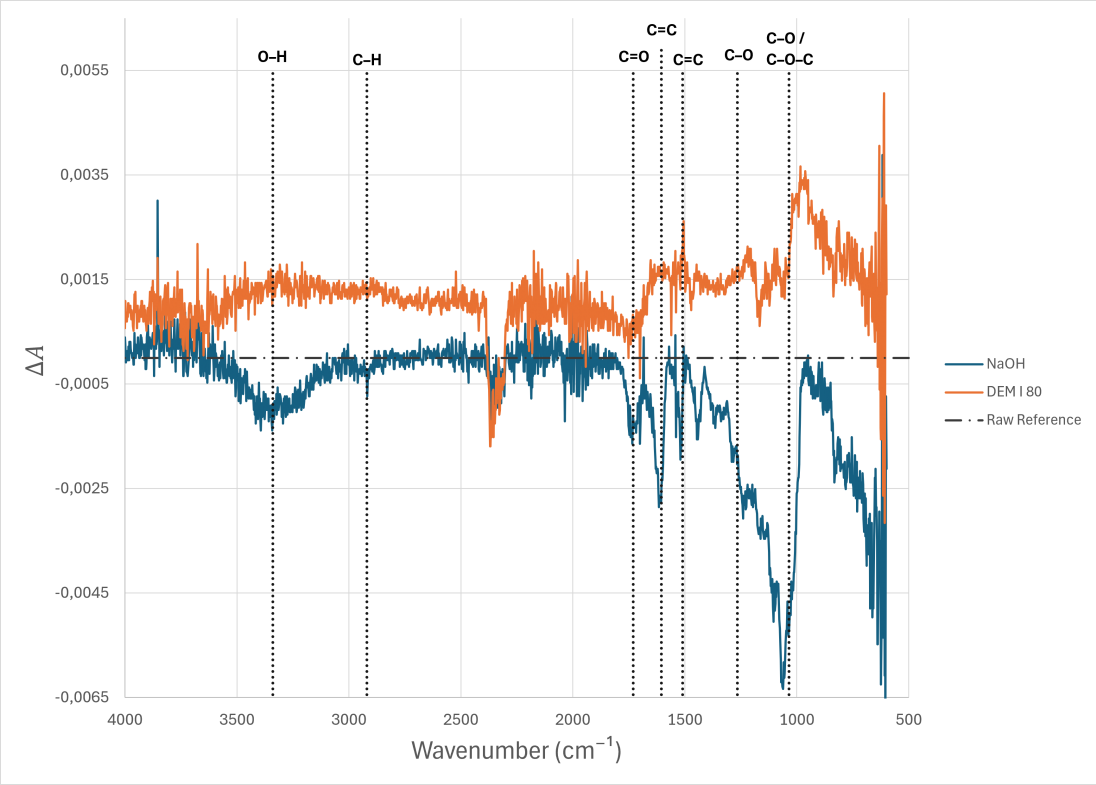

Figure 4.4: Differential FTIR absorbance spectra of Demi80- and NaOH-treated husk relative to untreated husk.

Note: The horizontal dashed line marks $\Delta A = 0$, indicating no measured absorbance difference relative to the untreated reference. Vertical dotted lines indicate selected absorption regions. The feature near 2350 cm^{-1} is likely related to atmospheric CO_2 and background compensation.

4.2. Material Preparation and Moisture Condition

4.2.1. Dry-Mass Determination and Moisture Conditioning

The moisture analyser indicated a residual moisture content of 4.49% (wet basis) in coconut husk material after drying at $70\,^{\circ}C$. This value was used to correct the reference masses when estimating dry sheet mass. A moisture content of 10.00% on a dry-mass basis was targeted before pressing. The values reported below were calculated from measured sheet masses rather than from separate moisture measurements of every board assembly.

4.2.2. Material Loading for the Main DOE

Table 4.2 presents the measured masses and calculated moisture contents for the 18 DOE assemblies. The estimated dry sheet mass was 16.346 ± 0.133 g (range 16.155-16.641 g), and the sheet mass immediately before pressing was 18.022 ± 0.148 g.

The estimated prepress moisture content averaged $(10.255 \pm 0.137)\%$, ranging from 10.007% to 10.510%. The corrected mean exceeded the nominal 10.00% target slightly because the residual moisture-analyser reading after drying at $70\,^{\circ}C$ had originally been handled with a dry-basis conversion despite being reported on a wet basis. Correcting the estimated dry masses changed the calculated DOE mean from approximately 10.01% to 10.255%; it did not change the measured masses. Despite this offset, the narrow range indicates that the estimated starting moisture contents were similar across DOE assemblies.

Table 4.2: Sheet masses and estimated prepress moisture contents for the 18 DOE boards.

Board ID	Mass at 70°C (g)	Dry sheet mass (g)	Prepress sheet mass (g)	MC (%)
B1-170-9	17.043	16.278	17.925	10.120
B2-180-15	17.241	16.467	18.151	10.227
B3-170-12	17.070	16.304	18.017	10.510
B5-180-9	16.979	16.217	17.876	10.232
B6-180-12	17.423	16.641	18.350	10.272

Continued on the next page

Table 4.2: DOE sheet masses and moisture contents (continued).

Board ID	Mass at 70°C (g)	Dry sheet mass (g)	Prepress sheet mass (g)	MC (%)
B7-190-9	17.225	16.452	18.101	10.026
B8-190-9	16.952	16.191	17.811	10.007
B9-190-15	17.213	16.440	18.155	10.431
B10-170-15	17.227	16.454	18.152	10.323
B11-170-12	17.149	16.379	18.044	10.165
B12-170-9	17.278	16.502	18.189	10.222
B13-180-9	16.972	16.210	17.878	10.290
B14-180-15	17.233	16.459	18.157	10.315
B16-180-12	17.009	16.245	17.898	10.173
B17-190-12	17.004	16.241	17.917	10.323
B18-190-12	16.914	16.155	17.836	10.408
B19-190-15	17.075	16.308	17.961	10.134
B21-170-15	17.046	16.281	17.975	10.407
Mean	17.114	16.346	18.022	10.255
Sample SD	0.139	0.133	0.148	0.137
Minimum	16.914	16.155	17.811	10.007
Maximum	17.423	16.641	18.350	10.510

Note: MC is the estimated dry-basis moisture content of the four conditioned sheets. The 4.49% wet-basis residual moisture was accounted for when estimating sheet dry masses. SD is the sample standard deviation.

4.2.3. Material Loading and Moisture at the Model-Selected Best Condition

The six boards at the model-selected best condition were evaluated separately from the DOE: two unmodified references, two with a bio-oil interlayer and two with added pith. Table 4.3 lists the conditioned sheet masses, estimated moisture contents and additional material masses.

Across these six boards, the estimated dry mass of the conditioned sheets was 16.312 ± 0.111 g, and their prepress mass was 17.984 ± 0.110 g. Estimated sheet moisture content averaged $(10.249 \pm 0.115)\%$ (range 10.146-10.393%). As in the main DOE, the mean was slightly above target, with relatively little variation between assemblies.

For the modified boards, these moisture estimates refer only to the conditioned husk sheets. The bio-oil and pith were weighed separately, and the moisture content of the additional pith was not measured.

Table 4.3: Estimated sheet moisture condition and material loading for the six boards manufactured at the model-selected best condition.

Board ID	Dry sheets (g)	Prepress sheets (g)	Sheet MC (%)	Added material (g)	Total lay-up (g)
22-C185-14	16.438	18.110	10.170	0.0000	18.1100
23-C185-14	16.163	17.843	10.393	0.0000	17.8430
24-C185-14-O	16.412	18.079	10.154	0.7860	18.8650
25-C185-14-O	16.201	17.861	10.244	0.6490	18.5100
15-C185-14-P	16.303	17.997	10.388	1.9005	19.8975
E1-C185-14-P	16.352	18.011	10.146	1.9041	19.9151
Mean	16.312	17.984	10.249	-	-
Sample SD	0.111	0.110	0.115	-	-
Minimum	16.163	17.843	10.146	-	-
Maximum	16.438	18.110	10.393	-	-

Note: The sheet moisture estimates exclude added bio-oil and pith. The added mass is zero for the unmodified references. Summary statistics refer to the six sheet assemblies before addition of oil or pith; totals include added material where applicable.

4.3. Board Production and Physical Properties

4.3.1. Recorded Pressing Conditions

Eighteen boards were manufactured for the DOE, with two independent boards at each combination of nominal platen temperature (170, 180 and 190 °C) and pressure (9, 12 and 15 MPa). All boards had a nominal 4 min pressing hold. Production took place over two days, with platen temperature increased from 170 to 190 °C on each day.

Table 4.4 summarises the platen-temperature readings taken at the start and after 2 and 4 min of pressing. The corresponding mean cycle temperatures were 170.33, 181.06 and 190.00 °C for the three nominal temperature levels. In every group, the average recorded platen temperature was higher at 4 min than at the start. Pressure is reported using the nominal setting because complete measured force records were not available for all DOE runs.

Table 4.4: Recorded platen temperatures during the DOE pressing cycles, averaged over the six boards at each nominal temperature.

Nominal T (°C)	Start (°C)	2 min (°C)	4 min (°C)	Cycle mean (°C)	Board cycle-mean range (°C)
170	169.50	170.53	170.93	170.33	169.58-171.42
180	180.12	181.43	181.62	181.06	180.50-181.50
190	188.90	190.25	190.82	190.00	189.00-191.75

Note: Start, 2-min and 4-min values are the means of the recorded average top-bottom platen temperatures ($n = 6$ boards per temperature level). The cycle mean is the arithmetic mean of these three readings for each board.

4.3.2. Board Mass, Thickness and Density

At the first post-pressing measurement, taken approximately 5 min after removal from the press, the DOE boards had a mean mass of (16.840 ± 0.195) g and a mean thickness of (4.550 ± 0.182) mm. Density calculated from whole-board mass and dimensions averaged (860 ± 42) kg/m³.

The whole-board density is an approximate descriptor of the small, unconfined panel geometry. Length and width were each sampled at three locations, and thickness at five locations; the mean dimensions were used to calculate external volume. These repeated measurements were intended to limit dependence on a single irregular edge or thickness position, not to establish compliance with EN 324-1 or a superior protocol to that reported elsewhere. Density was not a product-quality target in this study.

The density of each cut bending specimen was calculated separately. Across the 18 specimens, density averaged (1001 ± 79) kg/m³ and ranged from 897 to 1201 kg/m³. Mean specimen density increased across the nominal pressure levels, from 922 kg/m³ at 9 MPa to 1020 kg/m³ at 12 MPa and 1060 kg/m³ at 15 MPa. The highest temperature-pressure group mean was 1134 kg/m³, at $180\,^{\circ}$C and 15 MPa (Figure 4.5).

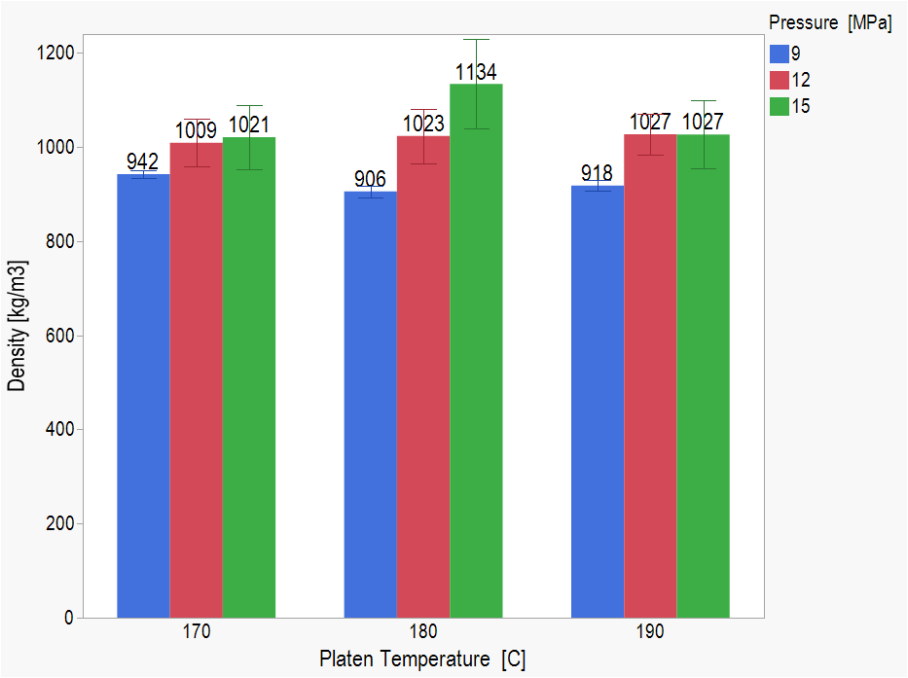

Figure 4.5: Mean cut-specimen density at the nine DOE pressing conditions.

Note: Each mean represents two independently manufactured boards ($n = 2$); error bars show sample SD. Colours distinguish nominal pressures of 9, 12 and 15 MPa. Density refers to the cut bending specimens, not the whole-board measurements.

4.3.3. Post-Pressing Mass and Dimensional Changes

Mass and thickness were measured approximately 5 and 30 min and 24 h after pressing. Mean board mass decreased from 18.022 g before pressing to 16.840 g at 5 min, corresponding to a mean pressing mass loss of 6.56% (range 5.39-7.58%). At 24 h, mean mass had increased to 17.514 g. This represented a mean gain of 4.01% (range 3.24-5.11%) relative to the 5-min measurement.

Mean board thickness increased from 4.550 mm at 5 min to 4.931 mm after 24 h. Thickness and calculated volume reflect changes in external dimensions, whereas the mass values describe a separate measured response. Neither series identifies the relative contributions from mechanical relaxation and ambient moisture sorption. Post-pressing thickness recovery averaged $(8.29 \pm 4.13)\%$, with individual values ranging from 3.66% to 22.26%. Figure 4.6 compares the group means, calculated relative to thickness at 5 min.

The highest group mean post-pressing thickness recovery was 15.1% at $170\,^{\circ}$C and 9 MPa, although the two boards differed considerably (22.26% and 7.96%). The lowest group mean was 4.9% at $190\,^{\circ}$C and 15 MPa, with individual values of 6.16% and 3.66%.

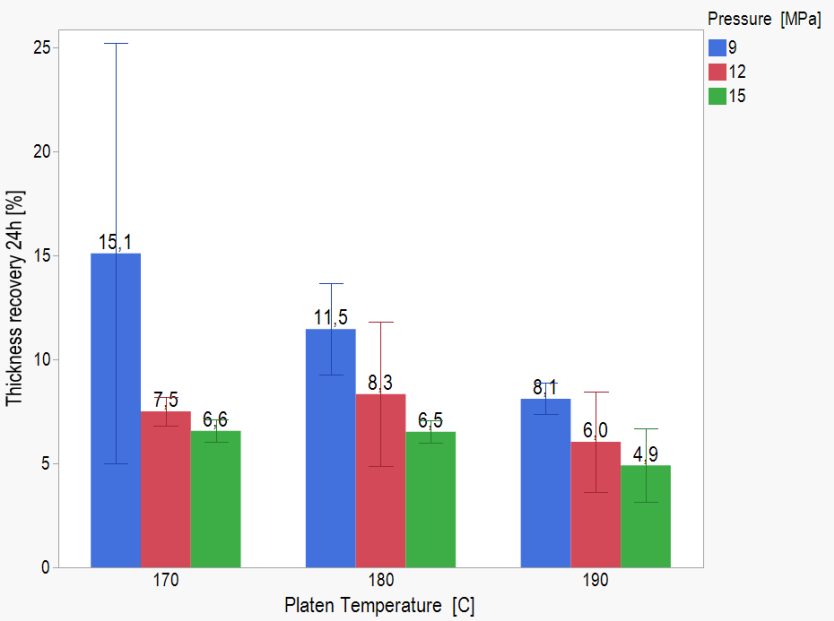

Figure 4.6: Mean 24-h post-pressing thickness recovery at the nine DOE conditions.

Note: Recovery is calculated relative to the first thickness measurement, taken approximately 5 min after pressing. Each mean represents two boards ($n = 2$); error bars show sample SD. This is not a measurement of immediate springback or water-immersion thickness swelling.



(a) Length measurement of the pressed board.

(b) Width measurement of the pressed board.

Figure 4.7: Representative DOE board after unconfined hot pressing, illustrating lateral spreading relative to the initial 40 × 90 mm lay-up. The photographed board measured approximately 48.59 mm in width and 92.00 mm in length after pressing.

Note: These photographs illustrate the external dimensions of one representative board after hot pressing without lateral confinement. Relative to the initial 40 × 90 mm lay-up, the measured board shows clear lateral spreading, particularly in width. The images are included as visual examples and do not establish the full spatial distribution of density or local pressure within the board.

4.4. Three-Point Bending Results

4.4.1. Load-Displacement Behaviour

Figure 4.8 presents representative three-point bending traces from specimens B5-180-9, B6-180-12, B17-190-12 and B21-170-15. All tests used one longitudinally oriented specimen per board and a 60 mm support span. The traces differ in initial slope, load-bearing capacity and the occurrence of force drops. B5-180-9 carried the lowest force of the four, while B21-170-15 showed an abrupt reduction followed by renewed load-bearing at higher displacement.

4.4.2. Modulus of Rupture

Across the 18 DOE specimens, modulus of rupture (MOR) averaged (18.98 ± 7.83) MPa. The lowest measured MOR was 9.53 MPa for B5-180-9, and the highest was 33.74 MPa for B17-190-12. Table 4.5 gives the individual bending results.

MOR was calculated using each specimen's measured cross-sectional dimensions and the selected structural failure load. The first specimen, B1-170-9, had a width of 25.55 mm and a thickness of 5.70 mm. The remaining specimen widths were between 20.82 and 21.07 mm. The actual dimensions were used in every calculation.

4.4.3. Modulus of Elasticity

The apparent bending modulus of elasticity (MOE) averaged (1.050 ± 0.549) GPa across the DOE. Individual values ranged from 0.266 GPa for B1-170-9 to 1.887 GPa for B2-180-15. MOE was calculated from the slope of the compliance-corrected force-displacement data within 10-40% of the selected failure load, as described in the Methodology.

4.4.4. Observed Load Drops and Recovery

Several force-displacement traces showed a sudden force drop followed by renewed load-bearing. This behaviour is visible for B6-180-12, B17-190-12 and B21-170-15 in Figure 4.8. For B21-170-15, the selected structural failure load was 176.9 N, although a higher force was recorded later. Its MOR therefore reflects the earlier selected failure event.

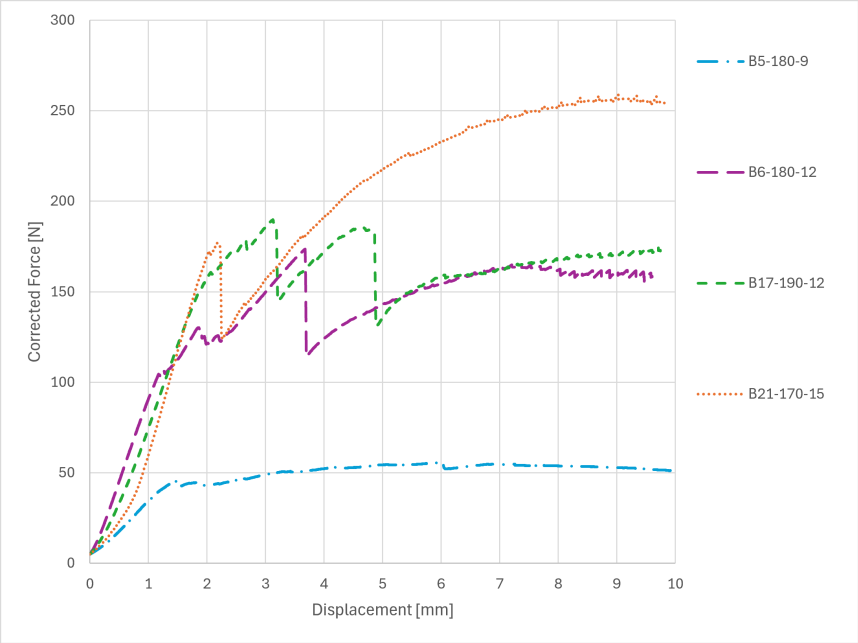

Figure 4.8: Representative three-point bending force–displacement curves from four DOE specimens.

Note: Each curve represents one cut specimen tested with a 60 mm support span. Displacement was corrected for estimated machine compliance and referenced to the first recorded point at or above 5 N. These are force–displacement curves, not stress–strain curves.

Table 4.5: Individual three-point bending results for the 18 DOE specimens.

Specimen	Width (mm)	Thickness (mm)	Failure load (N)	MOR (MPa)	MOE (GPa)
B1-170-9	25.55	5.70	97.6	10.58	0.266
B2-180-15	20.92	4.62	127.9	25.77	1.887
B3-170-12	21.04	4.97	192.7	33.38	1.790
B5-180-9	20.91	4.53	45.4	9.53	0.696
B6-180-12	21.03	5.04	130.2	21.95	1.815
B7-190-9	21.07	5.84	127.4	15.97	0.648
B8-190-9	20.93	5.56	100.3	13.95	0.625
B9-190-15	21.05	5.00	141.5	24.20	1.249
B10-170-15	20.92	5.03	70.5	11.99	0.477
B11-170-12	20.90	5.18	74.5	11.95	0.679
B12-170-9	20.92	5.57	91.9	12.74	0.822
B13-180-9	21.03	5.49	108.1	15.36	0.525
B14-180-15	20.97	5.13	126.2	20.58	1.691
B16-180-12	20.97	5.20	73.6	11.69	0.627
B17-190-12	21.00	4.91	189.8	33.74	1.715
B18-190-12	20.82	5.36	107.2	16.14	0.679
B19-190-15	20.98	5.12	137.7	22.53	1.252
B21-170-15	20.95	5.06	176.9	29.69	1.455

Note: MOR and MOE were calculated using the measured specimen dimensions. The failure load is the selected structural failure load, which may precede a later maximum in the force trace.

4.5. Effects of Pressing Temperature and Pressure

4.5.1. Measured MOR and MOE by DOE Condition

Figures 4.9 and 4.10 compare the bending results across the nine nominal pressing conditions. Each group represents two independently manufactured boards. Table 4.6 reports the group means and sample standard deviations.

At each temperature, 9 MPa produced the lowest group mean MOR and MOE. Mean MOR at 9 MPa ranged from 11.66 to 14.96 MPa, and mean MOE from 0.544 to 0.637 GPa. The groups pressed at 12 and 15 MPa

generally had higher mean values, with less consistent temperature trends.

The highest group mean MOR was 24.94 MPa at $190\,^{\circ}$C and 12 MPa, whereas the highest group mean MOE was 1.789 GPa at $180\,^{\circ}$C and 15 MPa. At 15 MPa, mean MOR increased from 20.84 MPa at $170\,^{\circ}$C to 23.18 MPa at $180\,^{\circ}$C and 23.37 MPa at $190\,^{\circ}$C. Over the same temperatures, mean MOE was 0.966, 1.789 and 1.251 GPa, respectively.

Pooling the six specimens at each nominal pressure across the three temperatures gave mean MOR values of approximately 13.02, 21.48 and 22.46 MPa at 9, 12 and 15 MPa, respectively. The corresponding mean apparent MOE values were 0.597, 1.218 and 1.335 GPa. Most of the observed increase occurred between 9 and 12 MPa; the higher overall averages at 15 MPa did not imply that 15 MPa produced the greatest response at every temperature. These pooled values are descriptive means, not separate model estimates.

The two boards at $170\,^{\circ}$C and 12 MPa differed substantially in MOR (33.38 and 11.95 MPa), giving a group mean of (22.66 ± 15.15) MPa. By comparison, specimens at $190\,^{\circ}$C and 15 MPa had MOR values of 24.20 and 22.53 MPa, with a group mean of (23.37 ± 1.18) MPa. This difference in within-condition variability is also visible in Figure 4.9.

Table 4.6: Measured MOR and MOE at the nine nominal pressing conditions, reported as mean $\pm$ sample standard deviation (SD; $n = 2$ independently manufactured boards per condition).

Temperature (°C)	Pressure (MPa)	MOR (MPa)	MOE (GPa)
170	9	11.66 ± 1.53	0.544 ± 0.393
170	12	22.66 ± 15.15	1.235 ± 0.785
170	15	20.84 ± 12.51	0.966 ± 0.692
180	9	12.44 ± 4.12	0.610 ± 0.121
180	12	16.82 ± 7.25	1.221 ± 0.840
180	15	23.18 ± 3.68	1.789 ± 0.139
190	9	14.96 ± 1.43	0.637 ± 0.016
190	12	24.94 ± 12.45	1.197 ± 0.732
190	15	23.37 ± 1.18	1.251 ± 0.002

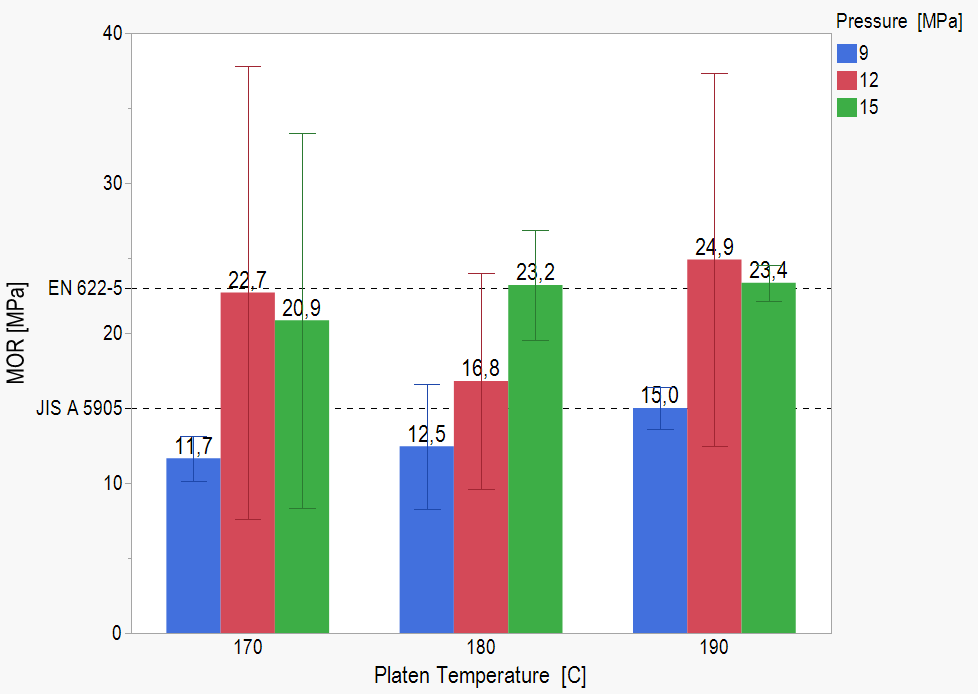

Figure 4.9: Mean modulus of rupture (MOR) by nominal pressing temperature and pressure.

Note: Bars represent the mean of two independently manufactured boards per condition ($n = 2$); error bars show sample SD. Colours distinguish the nominal pressure groups (9, 12 and 15 MPa).

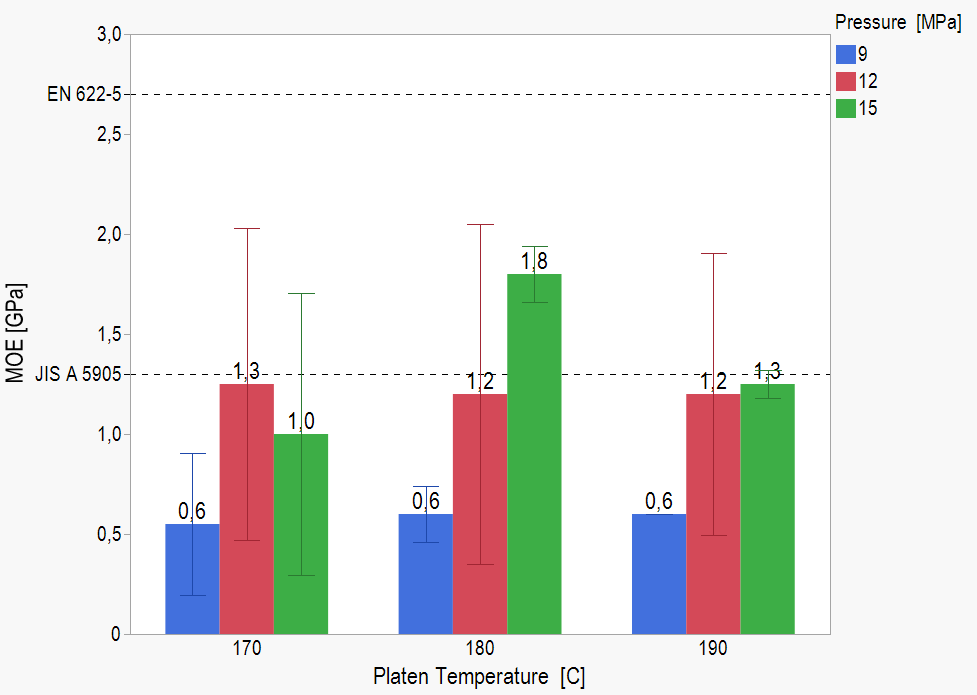

Figure 4.10: Mean apparent bending modulus of elasticity (MOE) by nominal pressing temperature and pressure.

Note: Bars represent the mean of two independently manufactured boards per condition ($n = 2$); error bars show sample SD. Colours distinguish the nominal pressure groups (9, 12 and 15 MPa).

4.6. Statistical Analysis and Fitted Responses

4.6.1. Quadratic Regression Models

Second-order regression models were fitted to the 18 DOE observations to examine how the measured responses varied with nominal pressing temperature and pressure. The same model structure was used for modulus of rupture (MOR), modulus of elasticity (MOE), cut-specimen density, post-pressing thickness recovery at 24 h, 24 h mass gain and pressing mass loss:

$$\begin{aligned}\hat{Y} = \beta_0 + \beta_T T + \beta_P P + \beta_{TP}(T-180)(P-12) \\ + \beta_{PP}(P-12)^2 + \beta_{TT}(T-180)^2,\end{aligned} \tag{4.1}$$

where T is the nominal platen temperature in °C, P is the nominal pressing pressure in MPa, and $\hat{Y}$ is the fitted response. The terms involving squared factors and their interaction are centred at $180\,^{\circ}$C and 12 MPa. The pressing hold was fixed at 4 min.

Table 4.7 lists the fitted MOR and MOE coefficients calculated from the full-precision board-level measurements. Each model contains five predictor terms. At the centre of the design ($180\,^{\circ}$C, 12 MPa), the pressure coefficient gives the local fitted change in the response per MPa. Because the linear terms are written using uncentred temperature and pressure, the intercept β_0 does not represent the predicted response at the centre of the DOE. Each coefficient p-value tests that term against a zero coefficient while retaining the other terms in the fitted model.

Table 4.7: Full-precision quadratic regression coefficients for the DOE bending responses. Estimates correspond to Equation 4.1.

Term	MOR estimate	MOR p-value	MOE estimate	MOE p-value
β_0	−23.23297	0.574	−1.117717	0.681
β_T	0.135130	0.545	0.005642	0.701
β_P	1.572943	0.0503	0.123047	0.0243
β_{TP}	−0.006460	0.943	0.001601	0.789
β_{PP}	−0.414674	0.340	−0.027908	0.331
β_{TT}	0.022607	0.559	−0.002354	0.362

4.6.2. Model Fits and Estimated Effects

Table 4.8 summarises the quadratic-model fits. The MOR and MOE models had R^2 values of 0.351 and 0.423, respectively, corresponding to adjusted R^2 values of 0.080 and 0.182. Their overall model tests yielded $p = 0.329$ for MOR and $p = 0.196$ for MOE.

Table 4.8: Fit statistics and linear-term tests for quadratic models of the main DOE responses ($n = 18$ for each response). Model and coefficient tests were calculated using the full-precision board-level data.

Response	R^2	Adjusted R^2	Overall model p	Temperature term p	Pressure term p
MOR (MPa)	0.351	0.080	0.329	0.545	0.0503
MOE (GPa)	0.423	0.182	0.196	0.701	0.0243
Cut-specimen density (kg/m³)	0.613	0.452	0.0269	0.995	0.0015
Post-pressing thickness recovery at 24 h (%)	0.526	0.329	0.0763	0.109	0.0146
Mass gain, 24 h (%)	0.825	0.751	0.0003	0.101	< 0.0001
Pressing mass loss (%)	0.681	0.548	0.0096	0.0126	0.0022

Note: The last two columns report tests of the linear terms while the interaction and quadratic terms remain in the model. Each model contains five predictor terms and an intercept, with 12 residual degrees of freedom.

The physical-property models showed stronger relationships with the nominal pressing conditions than the bending models. The cut-specimen density model had $R^2 = 0.613$ and an overall p-value of 0.0269. Its linear pressure coefficient was positive ($\beta_P = 23.05$ kg/m³ per MPa, $p = 0.0015$). For 24 h mass gain, the model had $R^2 = 0.825$ ($p = 0.0003$), with a negative pressure coefficient of -0.190 percentage points per MPa ($p < 0.0001$). Pressing mass loss was associated with both temperature and pressure ($p = 0.0126$ and $p = 0.0022$, respectively, for the linear terms). The post-pressing thickness recovery model at 24 h had a negative pressure term ($p = 0.0146$), although its overall model test yielded $p = 0.0763$.

At the design centre, the fitted linear pressure coefficients for MOE and MOR were also positive: 0.123 GPa per MPa ($p = 0.0243$) and 1.573 MPa per MPa ($p = 0.0503$), respectively. The interaction and quadratic terms affect the fitted slopes away from the centre. Although the MOE pressure term had a p-value below 0.05, neither overall bending model was statistically significant at this threshold. The fitted MOR and MOE surfaces are therefore used to explore response trends rather than to establish confirmed optimal pressing conditions. Delamination was retained as an ordinal score and is reported separately in Section 4.7.

4.6.3. Model Diagnostics

Residual-versus-fitted plots were examined for the quadratic models. Lack-of-fit tests compared the remaining model error with the pure error estimated from the replicate boards at each pressure–temperature condition. These tests did not indicate significant lack of fit for the MOR or apparent MOE models.

Considerable differences were nevertheless observed between some replicate boards produced at the same nominal condition. This variation is reflected in the relatively low adjusted R^2 values and non-significant overall model tests for MOR and apparent MOE. Production day was not included as an additional factor in the quadratic models.

4.6.4. Fitted MOR and MOE Responses

Figures 4.11 and 4.12 show the fitted quadratic response surfaces across the investigated range of 170–190 °C and 9–15 MPa. The contours describe the fitted models between the experimental conditions; no additional boards were manufactured at these intermediate settings.

Neither the MOR nor the apparent MOE model was statistically significant overall, so the surfaces were used only to explore trends within the experimental range. They informed the subsequent selection of an exploratory follow-up pressing condition (Section 4.8) rather than establishing a confirmed optimum.

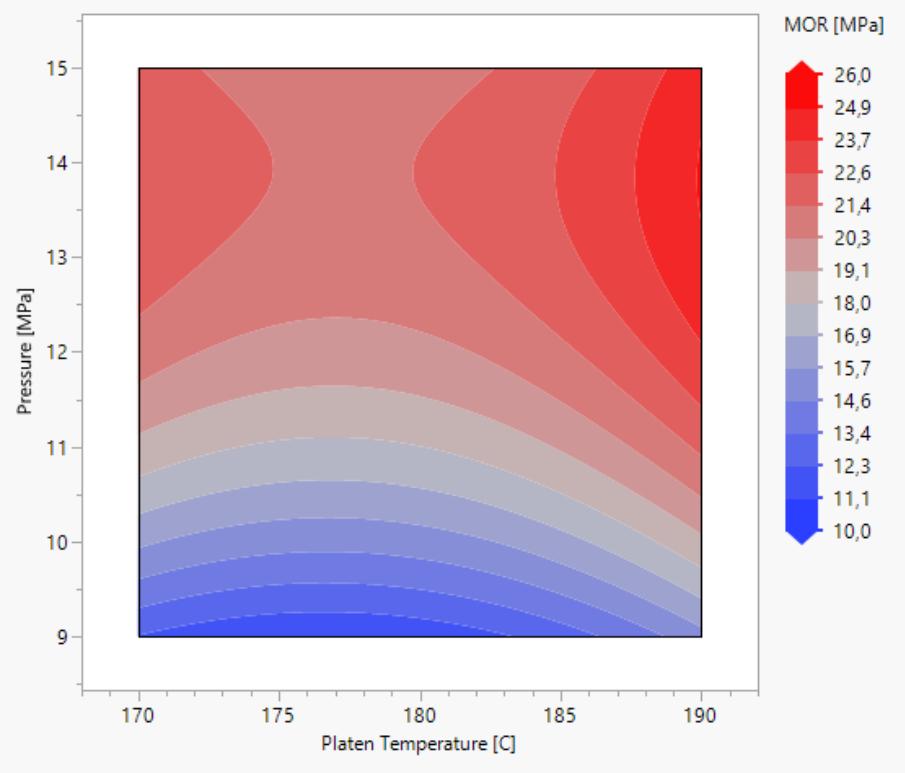

Figure 4.11: Fitted quadratic response surface for modulus of rupture (MOR).

Note: Contours show fitted MOR in MPa across the DOE range (170–190 °C; 9–15 MPa), not additional measured results. The overall MOR regression was not statistically significant ($p = 0.329$).

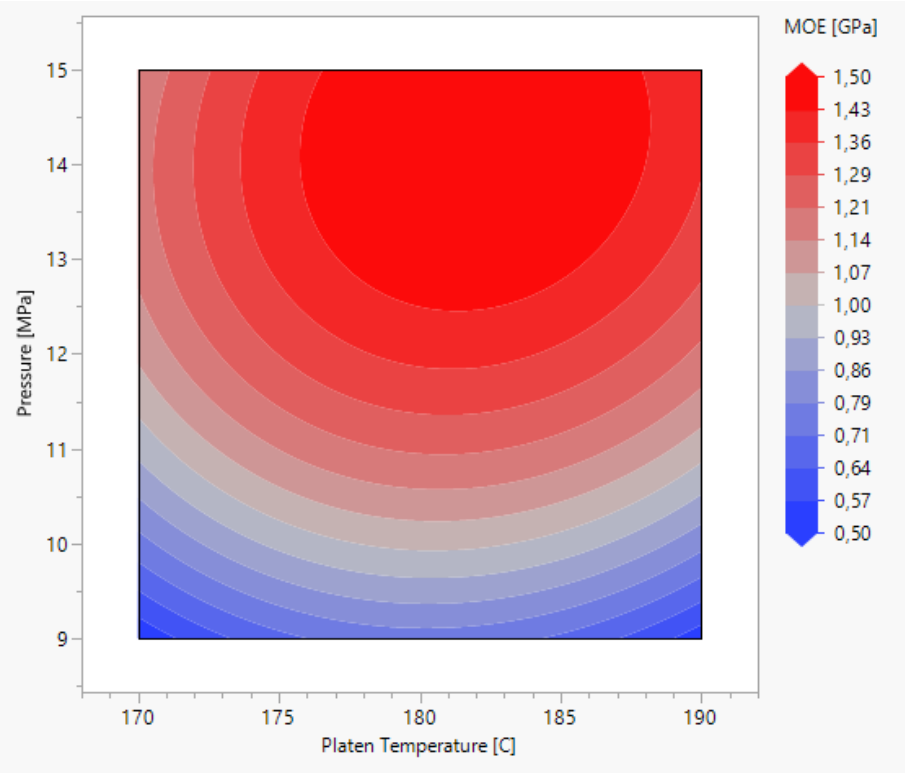

Figure 4.12: Fitted quadratic response surface for apparent bending modulus of elasticity (MOE).

Note: Contours show fitted MOE in GPa across the DOE range (170–190 °C; 9–15 MPa), not additional measured results. The overall MOE regression was not statistically significant ($p = 0.196$).

4.7. Visual Board Quality

4.7.1. Distribution of Delamination Scores

One bending specimen was prepared from each of the 18 DOE boards. Following cutting, the four exposed edges were assessed together to assign one visual delamination score per specimen on a scale from 0 to 3.

Score 0 represented no visible delamination or only faint layering; score 1 indicated minor cracks or limited visible layering. Scores 2 and 3 described more extensive cracking or separation between layers. The full scoring criteria are given in the Methodology.

Of the 18 specimens, two were assigned score 0, five score 1, seven score 2 and four score 3 (Table 4.9).

Table 4.9: Distribution of visual delamination scores among the 18 DOE specimens.

Delamination score	Number of specimens	Percentage (%)
0	2	11.1
1	5	27.8
2	7	38.9
3	4	22.2
Total	18	100.0

Figure 4.13 summarises the scores for the nine nominal temperature-pressure combinations. Each bar represents the mean score of two boards, with error bars showing sample SD. Since the scores form an ordinal scale, these group statistics are used only for descriptive comparison. No consistent pressure–temperature pattern or association with bending performance was evident from the descriptive scores.

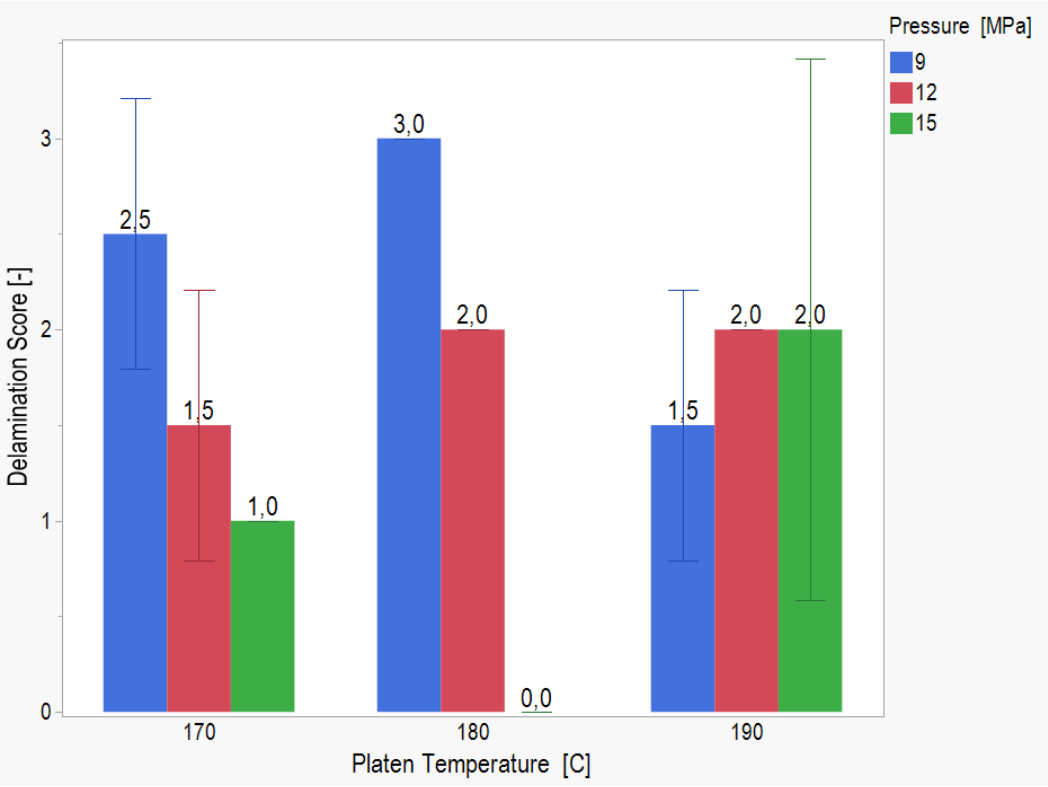

Figure 4.13: Mean visual delamination score at the nine DOE pressing conditions.

Note: Each mean is calculated from two board-level scores ($n = 2$); error bars show sample SD. Scores are ordinal (0–3), based on visible features of four cut edges, and are descriptive rather than measurements of internal bond strength.

4.7.2. Representative Delamination Observations

Figure 4.14 shows selected edge photographs illustrating differences in visible layering, cracking and layer separation between specimens. The photographs show individual edge views and are included to illustrate the appear-

ance of the layered structure. The formal delamination score for each specimen was assigned from the combined observation of all four exposed perimeter edges, as described in the Methodology.



(a) Example of limited visible layer separation

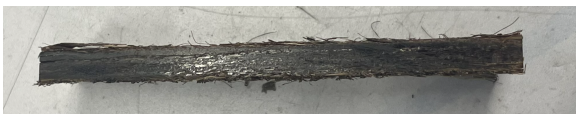

(b) Board 25: visible layering



(c) Board 15: cracking and local layer separation



(d) Board 17: extensive opening between layers

Figure 4.14: Representative cut-edge photographs showing layering, cracking and sheet separation.

Note: Each panel shows one photographed edge, whereas the visual score was assigned after examining all four cut edges. The photographs illustrate different appearances of the layered structure; Board 17 is from the main DOE.

4.8. Desirability-Based Selection of the Follow-up Condition

The fitted quadratic models were used in an exploratory multi-response desirability analysis in JMP to select a practical pressure–temperature condition for the additional boards. MOR and apparent MOE were set to be maximised, while the post-cut visual delamination score was set to be minimised. Table 4.10 lists the desirability anchors entered in the analysis. These settings express the chosen response preferences, not measured material limits or product-standard requirements.

Table 4.10: Value-desirability anchors used in the exploratory desirability analysis. The values in parentheses are desirability scores, not measured responses.

Response	Goal	Low: value (d)	Middle: value (d)	High: value (d)
MOR (MPa)	Maximise	15 (0.01)	23 (0.50)	25 (0.99)
Apparent MOE (GPa)	Maximise	1.3 (0.01)	1.4 (0.50)	1.5 (0.99)
Visual delamination score	Minimise	0 (0.99)	1 (0.80)	3 (0.01)

In the first profiler run, MOR, apparent MOE and delamination were all assigned an importance of 1. In the second run, delamination was given zero importance while the bending-response settings remained unchanged. Table 4.11 compares the pressing conditions selected by the two profiles.

Table 4.11: Pressing conditions selected by two exploratory desirability profiles. Delamination has importance 1 in the first profile and 0 in the second; MOR and MOE have importance 1 in both.

Profile	Temperature (°C)	Pressure (MPa)
MOR, MOE and delamination	184.81	14.50
MOR and MOE only	184.74	14.21

The two profiles selected similar pressure–temperature regions, differing by approximately $0.07\,^{\circ}$C and 0.29 MPa. Giving delamination zero importance therefore had little effect on the selected region under the specified desirability settings. Because the bending models were not significant overall, and the delamination score was ordinal, these settings were regarded as exploratory manufacturing guides rather than confirmed optima.

The six additional boards were manufactured at $185\,^{\circ}$C and 14.2 MPa, close to both selected settings. Their measured physical and bending properties are reported in the following section.

4.9. Boards Produced at the Model-Selected Best Condition

Six boards were manufactured at the model-selected best condition of $185\,^{\circ}\mathrm{C}$ and 14.2 MPa, using the same Demi80 pretreatment as the DOE. Two unmodified boards provided a local reference, while two boards each were manufactured with a bio-oil interlayer or additional pith. These boards were evaluated separately and were not included in the DOE regression models.

4.9.1. Material Additions and Visual Quality

The bio-oil boards, 24-C185-14-O and 25-C185-14-O, contained 0.786 and 0.649 g of added oil, respectively. The added-pith boards, 15-C185-14-P and E1-C185-14-P, contained 1.9005 and 1.9041 g of additional coconut husk pith. The moisture content of the additional pith was not measured.

Both added-pith specimens received a visual delamination score of 2. A pronounced blister and local layer separation were observed on board E1-C185-14-P before specimen cutting (Figure 4.15). This pre-cut damage was recorded separately from the score assigned after examining the specimen edges.



Figure 4.15: Blistering and local sheet separation on added-pith board E1-C185-14-P.

Note: The photograph was taken before cutting. This pre-cut observation is distinct from the ordinal delamination score subsequently assigned using the specimen edges.

4.9.2. Comparison of Unmodified and Interlayer Variants

Table 4.12 summarises the measured properties of the six boards at the model-selected best condition. The reported densities refer to the cut bending specimens, while board mass and thickness were measured approximately 5 min after pressing.

Table 4.12: Measured physical and mechanical properties of the six boards manufactured at the model-selected best condition.

Board ID	Mass 5 min (g)	Thickness 5 min (mm)	Specimen density (kg/m^3)	MOR (MPa)	MOE (GPa)	Delam. score
22-C185-14	16.931	4.194	1124	14.61	1.42	1
23-C185-14	16.731	4.214	1109	22.26	2.04	2
24-C185-14-O	16.859	4.476	1108	24.92	2.74	2
25-C185-14-O	16.613	4.486	1144	15.05	1.42	1
15-C185-14-P	18.705	4.898	1148	36.79	3.22	2
E1-C185-14-P	18.612	5.124	1080	31.52	2.04	2

Measured Bending Responses at the Selected Condition

Figures 4.17 and 4.18 compare the measured mean MOR and apparent MOE for the three variants. The unmodified reference boards reached (18.43 ± 5.41) MPa for MOR and (1.73 ± 0.43) GPa for MOE. The bio-oil boards reached (19.98 ± 6.98) MPa and (2.08 ± 0.93) GPa, respectively. The added-pith boards had the highest group means, with MOR of (34.15 ± 3.72) MPa and apparent MOE of (2.63 ± 0.84) GPa. Values are reported as mean $\pm$ sample standard deviation (SD) from two boards per variant.

Relative to the unmodified references, the added-pith boards had an 85.3% higher mean MOR and a 51.8% higher mean MOE. The corresponding differences for the bio-oil boards were 8.4% and 20.3%. The two bio-oil boards differed considerably in both bending responses, while apparent MOE also varied between the added-pith specimens. Both added-pith specimens exceeded the MOR of each unmodified board, although board E1 exhibited a pronounced blister before cutting. With only two boards per variant and different material loadings, these comparisons remain descriptive and do not establish an improvement in intrinsic interlayer bonding.



(a) Unmodified reference (b) Bio-oil (c) Added pith

Figure 4.16: Photographs of the unmodified, bio-oil and added-pith board variants manufactured at the model-selected best condition.

Note: All variants were manufactured at 185 °C and 14.2 MPa. The photographs illustrate the appearance of individual boards, rather than the mean bending performance of each group.

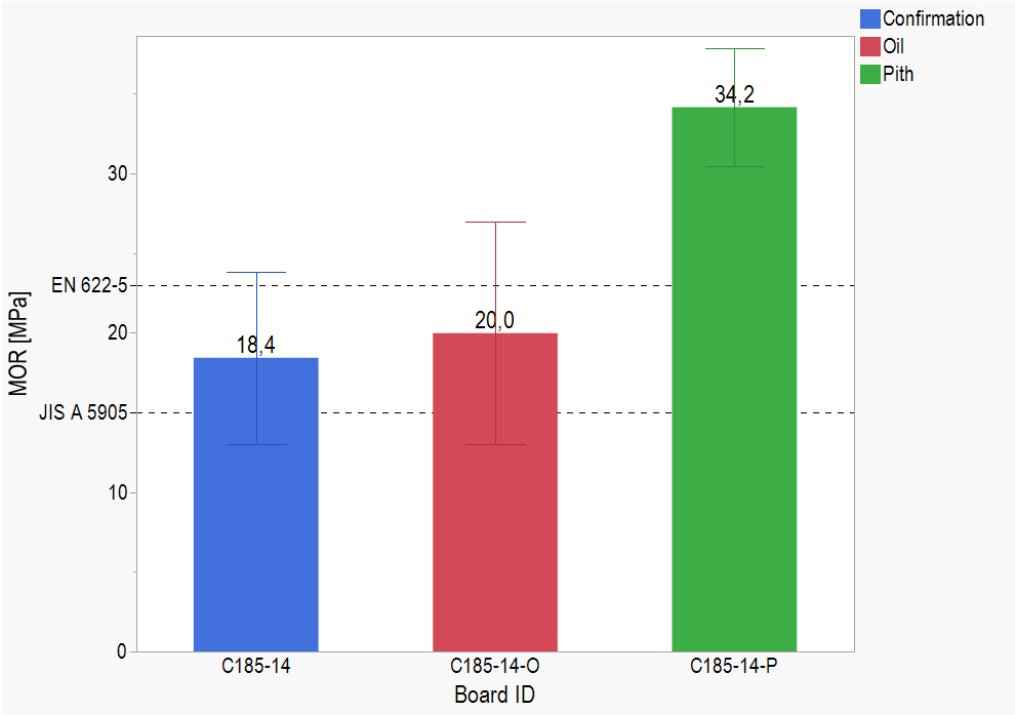

Figure 4.17: Mean modulus of rupture (MOR) of the three follow-up board variants.

Note: Each variant includes two independently manufactured boards ($n = 2$) at 185 °C and 14.2 MPa; error bars represent sample SD. Any JIS or EN lines are numerical bending benchmarks, not compliance assessments.

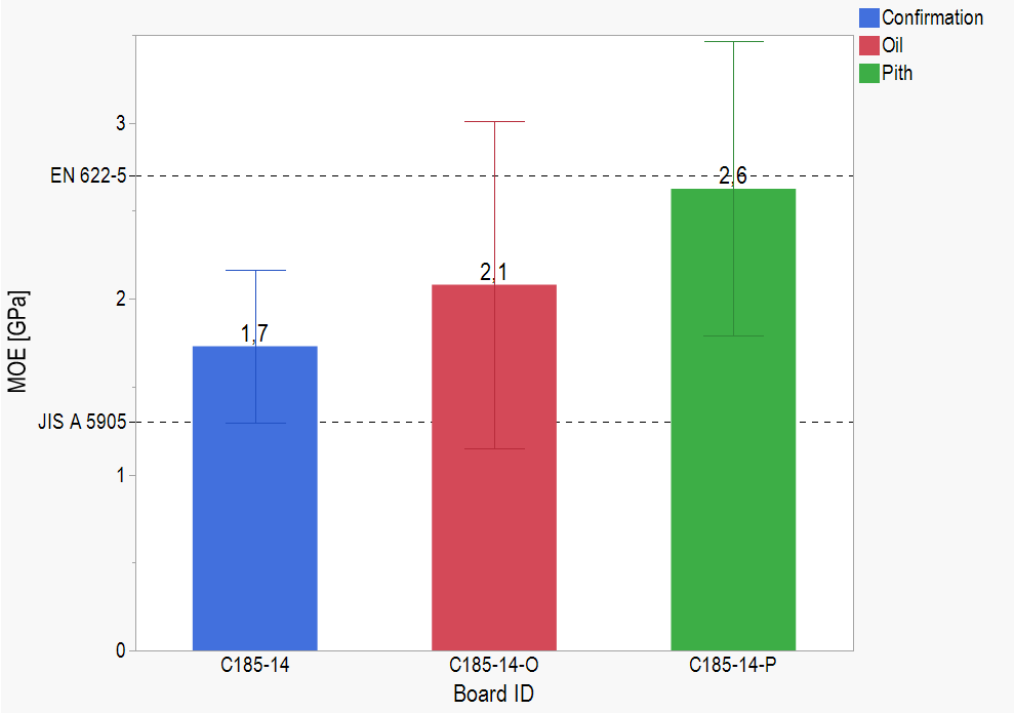

Figure 4.18: Mean apparent bending modulus of elasticity (MOE) of the three follow-up board variants.

Note: Each variant includes two independently manufactured boards ($n = 2$) at $185\,^{\circ}$C and 14.2 MPa; error bars represent sample SD. Any product-standard reference lines are numerical comparisons only.

Comparison with Model Predictions

The quadratic MOR and apparent MOE expressions fitted to the 18 DOE boards (Equation 4.1 and Table 4.7) were evaluated at the manufactured follow-up setting of $T = 185\,^{\circ}$C and $P = 14.2$ MPa. At this setting, $(T - 180) = 5$ and $(P - 12) = 2.2$. Substitution of the reported coefficients gives

$$\begin{aligned}\widehat{\mathrm{MOR}} &= -23.23297 + 0.135130(185) + 1.572943(14.2) \\ &\quad - 0.006460(5)(2.2) - 0.414674(2.2)^2 + 0.022607(5)^2 \\ &= 22.59\ \mathrm{MPa}, \end{aligned} \tag{4.2}$$

$$\begin{aligned}\widehat{\mathrm{MOE}} &= -1.117717 + 0.005642(185) + 0.123047(14.2) \\ &\quad + 0.001601(5)(2.2) - 0.027908(2.2)^2 - 0.002354(5)^2 \\ &= 1.497\ \mathrm{GPa}. \end{aligned} \tag{4.3}$$

Table 4.13 compares these model predictions with the measured means of the two unmodified confirmation boards. The mean measured MOR was 18.4% below the predicted value, while the mean apparent MOE was 15.6% above it. These differences are calculated relative to the respective model predictions.

Table 4.13: Quadratic-model predictions at $185\,^{\circ}$C and 14.2 MPa compared with the two unmodified confirmation boards.

Response	Model prediction	Measured mean $\pm$ SD	Difference (%)
MOR (MPa)	22.59	18.43 ± 5.41	-18.4
Apparent MOE (GPa)	1.497	1.73 ± 0.43	$+15.6$

Note: Difference $= (\bar{Y}_{\mathrm{measured}} - \hat{Y})/\hat{Y} \times 100\%$. Measured values are means and sample standard deviations from two independently manufactured unmodified boards ($n = 2$). These are local descriptive comparisons, not a statistical validation of either response surface.

The predictions and observed means were broadly comparable in magnitude, but the differences between the two confirmation boards and the non-significant overall DOE bending models prevent a conclusion that the response surfaces reliably predict performance. The six follow-up boards were not used to refit the regression models.

4.9.3. Numerical Comparison with Development Benchmarks

For an indicative comparison, EN 622-5:2009 lists a bending-strength reference of at least 23 MPa and a bending-modulus reference of at least 2.7 GPa for general-purpose, dry-use MDF of nominal thickness greater than 4 and up to 6 mm [16]. JIS A 5905:2022 Type 15 MDF has a bending-strength requirement of at least 15 MPa, while its 1.3 GPa bending-modulus value is informative rather than mandatory [17, 18]. These are fibreboard product benchmarks, not acceptance criteria that were fully tested here.

Five of the 18 DOE specimens reached or exceeded the numerical 23 MPa EN reference in the present MOR calculation, and none reached the 2.7 GPa MOE reference. These comparisons address only a single measured bending specimen per board, not panel-level pass rates or product compliance. Both added-pith specimens exceeded 23 MPa in MOR, while one also exceeded 2.7 GPa in apparent MOE; the bio-oil group contained one specimen above each of these numerical references. The adapted specimen dimensions, 60 mm span and crosshead-based MOE calculation prevent a formal standards-compliance claim. Internal bond strength and water-immersion thickness swelling were not tested.

The added-pith boards also had greater total prepress material masses and higher postpress thicknesses than the unmodified reference boards. These differences are considered in the Discussion when evaluating the measured mechanical properties.

4.10. Summary of Main Findings

Demi80 gave the highest observed MOR and apparent MOE in the limited pretreatment screening and was selected for the DOE. The 18-board DOE showed the lowest mean bending properties at 9 MPa, but large differences between some replicate boards and non-significant overall MOR and apparent MOE models prevented confirmation of a unique pressing optimum. The exploratory desirability analysis guided the selection of $185\,^{\circ}$C and 14.2 MPa for six additional boards. Density and post-pressing measurements provided supporting evidence about consolidation, rather than a complete explanation of bending response. Among the exploratory interlayer variants, added pith gave the highest group mean MOR and apparent MOE; the limited sample size and different material loading prevent assigning the improvement to interlayer bonding alone.

5

Discussion

5.1. Pretreatment Choice and FTIR Interpretation

The untreated coconut husk spectrum (Figure 4.3) provides a reference for interpreting the pretreatment results. Its broad absorption around 3340 cm^{-1} is consistent with O–H stretching, while the feature near 2920 cm^{-1} is associated with aliphatic C–H stretching. The region near 1730 cm^{-1} may contain carbonyl vibrations associated with hemicellulose, and the bands around 1605 and 1510 cm^{-1} are commonly assigned to aromatic skeletal vibrations, mainly from lignin. Absorption around 1265 and 1035 cm^{-1} includes overlapping C–O and C–O–C contributions from lignocellulosic components. These are tentative assignments of spectral regions, not measurements of individual constituent concentrations.

Relative to this reference, the NaOH-treated material showed larger absorbance differences than Demi80 (Figure 4.4). The narrow feature near 2350 cm^{-1} in the Demi80 difference spectrum is likely related to atmospheric CO_2 and background compensation rather than a change in the husk itself. Differences in sample contact, baseline and material heterogeneity may also affect the spectra. The larger NaOH deviations therefore cannot be taken as evidence of more effective bonding or quantified removal of lignin or hemicellulose.

In the bending screening, Demi80 had the highest observed MOR of 33.97 MPa and apparent MOE of 0.996 GPa. These values were above the untreated control means, whereas NaOH produced a smaller MOR increase and a lower apparent MOE. Only one board was tested for each treated condition and two for the untreated control, so treatment superiority was not established. The selection of Demi80 for the DOE was a practical choice based on these observations. Comparisons with Faria et al. [13] and Alharbi et al. [14] are limited by differences in pretreatment conditions and material forms; neither study directly represents the retained-sheet boards investigated here.

5.2. Pressing Conditions and Mechanical Response

At every investigated temperature, the 9 MPa boards had the lowest group mean bending properties. Pooling specimens by nominal pressure gave mean MOR values of 13.02, 21.48 and 22.46 MPa at 9, 12 and 15 MPa, respectively; apparent MOE increased from 0.597 to 1.218 and 1.335 GPa. Most of the observed improvement occurred between 9 and 12 MPa. This is consistent with pressure improving consolidation, although the smaller additional gain at 15 MPa does not demonstrate that a pressure threshold was reached or that interface properties became the sole limiting factor.

Temperature had no equally consistent relationship with bending performance over 170–$190\,^{\circ}$C. Moreover, large differences remained between boards made at the same nominal condition: the two specimens pressed at $170\,^{\circ}$C and 12 MPa had MOR values of 33.38 and 11.95 MPa. The quadratic models were not significant overall for either MOR ($p = 0.329$; adjusted $R^2 = 0.080$) or apparent MOE ($p = 0.196$; adjusted $R^2 = 0.182$). Although the fitted linear pressure term for apparent MOE was positive ($p = 0.0243$), the overall model does not provide a reliable basis for predicting bending performance. The non-significant models do not establish that temperature or pressure has no effect.

Local fibre–pith distribution, sheet thickness, interface contact and moisture variation are plausible contributors to the unexplained variation. Loading-face orientation and damage during specimen preparation may also have influenced the measurements. None of these factors was assessed separately, while the temperature sequence was repeated in increasing order on both production days. Similarly, bonding mechanisms proposed in the literature, including thermal softening and intrinsic bonding [5, 12], cannot be confirmed without local temperature or chemical measurements.

5.2.1. Interpretation of the Model-Selected Best Condition

The desirability analysis identified a *model-selected best condition* according to the fitted models and specified response preferences, rather than a statistically confirmed manufacturing optimum. The two profiles identified nearby settings of $184.81\,^{\circ}$C and 14.50 MPa, and $184.74\,^{\circ}$C and 14.21 MPa (Section 4.8). Six additional boards were subsequently manufactured at $185\,^{\circ}$C and 14.2 MPa, including two unmodified confirmation boards.

At this manufactured condition, the DOE regression expressions predicted an MOR of 22.59 MPa and an apparent MOE of 1.497 GPa (Section 4.9.2). The corresponding measured unmodified means were (18.43 ± 5.41) MPa and (1.73 ± 0.43) GPa. Relative to the predictions, the measured MOR mean was 18.4% lower and apparent MOE was 15.6% higher. The predictions were therefore broadly comparable in magnitude to the observed means at this single setting.

This local comparison is useful for describing the subsequent boards but is not evidence that the response surfaces have been validated. Only two unmodified confirmation boards were manufactured, their measured responses differed, and neither overall bending model was statistically significant. The selected condition consequently remains an exploratory manufacturing choice rather than a demonstrated reproducible optimum.

5.2.2. Reduced Bending Geometry and Possible Shear Effects

Material availability limited the bending specimens to approximately 70×20 mm and a 60 mm support span. For measured thicknesses of about 4.5–5.8 mm, the span-to-thickness ratio was approximately 10–13. EN 310 specifies a span of 20 times nominal thickness for bending tests on wood-based panels, normally with 50 mm-wide specimens [11]. The present procedure was adapted from ASTM D1037 and did not conform to EN 310 [19].

At a relatively short span, shear deformation can contribute more strongly to the measured displacement. In a layered board, relative movement between incompletely bonded sheets may provide an additional source of compliance. Machine-compliance correction was applied, but crosshead displacement could not separate these contributions from bending deflection. A longer-span test might therefore yield a different apparent MOE; it would not necessarily produce a higher MOR because the failure mode and defects sampled could change. Tests at multiple span-to-thickness ratios, using direct specimen deflection measurements and complementary internal bond or interlaminar shear tests, are needed to evaluate the role of the interfaces.

5.3. Consolidation and Changes after Pressing

Mean cut-specimen density increased from 922 to 1020 and 1060 kg/m³ at 9, 12 and 15 MPa. The density model was significant overall ($p = 0.0269$), supporting an association between nominal pressure and consolidation. Density was nevertheless a supporting process descriptor, not a target property or a direct measure of interface strength.

For the whole boards, length and width were each measured at three positions and thickness at five positions to estimate external volume from mean dimensions. This adapted approach accounted partly for the irregular shape of the unconfined boards, but was not a standard EN 324-1 measurement or demonstrably more accurate than methods used in other studies [24]. Whole-board density averaged 860 kg/m³ at approximately 5 min after pressing, compared with 1001 kg/m³ for later cut bending specimens. Their different geometry, measurement times and trimming histories prevent direct equivalence; no spatial density profile was obtained. Nominal pressure was calculated from the starting lay-up area, and lateral spreading meant that local contact pressure remained unknown.

The post-pressing measurements describe both mass and dimensional changes. Mean mass decreased by 6.56% from before pressing to approximately 5 min afterwards, then increased by 4.01% relative to the 5-min value over 24 h. Mean thickness increased from 4.550 to 4.931 mm during the latter interval, corresponding to $8.29 \pm 4.13\%$ post-pressing thickness recovery. Because the first measurement was taken after unloading and initial cooling, this is neither instantaneous springback nor water-immersion thickness swelling under EN 317 [29].

Delayed mechanical relaxation could increase thickness without increasing mass, whereas moisture uptake from ambient air could increase both. Both processes may have occurred, and pressing mass loss cannot be assumed to consist entirely of water. The thickness-recovery model had a negative linear pressure term ($p = 0.0146$), but was not significant overall ($p = 0.0763$); a relationship between pressure, dimensional recovery and bending performance therefore remains unconfirmed. Repeated measurements under controlled dry and humid conditions, together with direct moisture measurements, would help separate relaxation from moisture-driven expansion and determine which mechanism is most relevant to dimensional stability.

5.3.1. Layer Integrity and Vapour Escape

The four-sheet arrangement contains three sheet-to-sheet interfaces. Visible cracks and openings on cut edges suggest that contact was not always continuous, but the ordinal delamination scores were assigned after cutting and do not measure internal bond strength. Cutting may have exposed or enlarged defects. No consistent relationship between these visual ratings and nominal temperature, pressure or bending performance was established. Board 17 showed substantial layer separation (Figure 4.14), while added-pith Board E1 had a pronounced blister

before cutting (Figure 4.15). Its bending specimen nevertheless reached 31.52 MPa MOR, illustrating why the performance of one specimen cannot establish the integrity of an entire board.

Unconfined pressing allowed lateral spreading and provided short paths from the small board interiors to free edges. In larger panels, the greater distance to an edge could make vapour escape more difficult, depending on permeability and pressure-release conditions. This is a scale-up concern, not an observed size effect. A lateral mould could control dimensions but might also restrict venting; mould design and vapour management should therefore be evaluated separately. The controlled degassing investigated by Böger et al. [8] provides a relevant process comparison, but does not establish a suitable release procedure for retained sheets.

5.4. Exploratory Interlayer Additions

The six boards at the model-selected best condition included two unmodified references, two with bio-oil and two with added pith. Relative to the unmodified group, mean MOR and apparent MOE were 8.4% and 20.3% higher for bio-oil, and 85.3% and 51.8% higher for added pith. The two bio-oil specimens differed considerably, whereas both added-pith specimens had MOR values above those of either reference specimen. These are descriptive comparisons of two boards per variant, not established treatment effects.

Additional pith may have filled gaps between uneven sheets and improved local load transfer, consistent with the potential binding role of coconut pith discussed in the literature [3, 10]. However, each pith board contained approximately 1.9 g of additional material, had a different thickness, and received pith of unmeasured moisture content. Mean cut-specimen densities were similar for the reference and pith groups (approximately 1117 and 1114 kg/m^3), so density alone does not explain their different mean bending responses. The observed blister on E1 also shows that higher local bending performance need not imply improved whole-board integrity. Both interlayer approaches merit controlled follow-up work, with added pith giving the stronger initial bending response.

5.5. Comparison with Existing Boards and Product Requirements

Most published binderless coconut-husk boards use milled or mechanically opened furnish rather than intact flattened sheets. The present boards were produced with a 4 min pressure hold within a prescribed 4.5 min press operation. Van Dam et al. reported approximately 50 MPa MOR and 5 GPa MOE for dense boards around 1300–1400 kg/m^3 [3], while Böger et al. reported 19.3 ± 3.1 MPa MOR for 12 mm milled-husk boards near 900 kg/m^3 [8]. Differences in furnish, density, thickness, pressing procedure and bending-test geometry prevent a direct ranking against the present results. Retaining long fibres may preserve continuous reinforcement, but the sheet interfaces introduce another possible weakness. Whether avoiding milling leads to a simpler or stronger overall production route has not yet been established.

For general-purpose dry-use MDF above 4 and up to 6 mm thick, EN 622-5:2009 specifies numerical reference values of 23 MPa MOR and 2.7 GPa MOE [16]. JIS A 5905:2022 Type 15 specifies 15 MPa MOR, with 1.3 GPa MOE given as an informative reference [17, 18]. Some DOE specimens reached these bending-strength levels, and both added-pith specimens exceeded the EN MOR benchmark. These comparisons indicate development potential, not product compliance: the reduced-span bending tests were adapted, and standard panel sampling, internal bond testing, immersion swelling, water resistance and fire-performance measurements were not completed.

5.6. Limitations and Remaining Uncertainty

The practical challenges and adaptations are summarised in Section 3.10. Their remaining consequences for the interpretation of the results are considered here. Table 5.1 brings together the principal limitations of the experimental design, board manufacture and measurement procedures.

Table 5.1: Principal experimental limitations and their implications for interpreting the results.

Limitation	Consequence for interpreting the results
Limited time and mould availability	A lateral-confinement mould could not be implemented. Spreading and uneven edge consolidation mean that nominal pressure, calculated from the initial lay-up area, does not describe the local contact pressure.
Limited number of independent replicates	The limited supply of suitable sheets allowed only two independently manufactured boards per DOE condition, with one bending specimen per board. Variability was therefore estimated imprecisely, and within-board bending variation was not assessed.
Natural material heterogeneity	Differences in fibre and pith distribution, sheet thickness and local defects remained despite grading and material allocation. These uncontrolled differences may have contributed to the variation in bending performance.
Visual material selection	Only sheets without substantial visible openings or missing corners were selected. The results therefore may not represent the full variability of the supplied husk.
Reduced three-point bending geometry	The 60 mm span and span-to-thickness ratio of approximately 10–13 increased the potential contribution of shear and interlayer movement to displacement. Apparent MOE was based on compliance-corrected crosshead displacement and is not a standard EN 310 result.
Load-cell accuracy	The accuracy of the 10 kN load cell at the relatively low measured forces was not independently verified. Its contribution to force-measurement uncertainty could not be quantified.
Cutting-related damage	Visible edge scorching remained after dry cutting. Possible fibre damage or additional cracking could not be separated from pre-existing board defects, and their influence on bending results was not assessed.
Moisture-content uncertainty	Prepress moisture was estimated from masses and representative residual-moisture corrections, without a direct measurement for each board. Local moisture differences may have contributed to the observed variability.
Fixed temperature sequence	Temperature was increased in the same order on both production days. Possible within-day process drift could not be separated completely from temperature effects.
Visual delamination assessment	Ordinal scores were assigned from the cut specimen edges. Cutting could affect the visible damage, and the method could neither identify closed internal interfaces nor quantify internal bond strength.
Short-term dimensional measurements	The first measurements were made approximately 5 min after pressing, missing any earlier recovery. Ambient humidity was not recorded, so moisture-driven expansion and mechanical relaxation could not be separated.

Taken together, these limitations permit descriptive comparisons within the investigated pressure–temperature range, but reduce confidence in attributing differences to the pressing factors alone. They also limit the reliability of the fitted response surfaces and their transferability to larger boards or other husk supplies. The *model-selected best condition* should therefore be interpreted as an exploratory choice rather than a validated manufacturing optimum. The following Recommendations chapter addresses measurements and experimental changes that could reduce these uncertainties.

6

Conclusions

This study examined whether mechanically flattened coconut husk sheets could be converted into binderless flat boards with a short hot-pressing operation and how preparation, nominal pressure and platen temperature related to their bending properties. The experiments included pretreatment screening, an 18-board pressure–temperature DOE, supporting physical measurements and six exploratory interlayer boards. The principal conclusions concern measured MOR and apparent MOE; product durability and full board qualification were not assessed.

6.1. Material Pretreatment

Demi80 pretreatment, consisting of immersion in demineralised water at $80\,^{\circ}$C for 1 h, gave the highest measured screening MOR (33.97 MPa) and apparent MOE (0.996 GPa). These were 63.0% and 19.2% above the untreated control means, respectively. Demi80 was therefore selected as the common preparation condition for the DOE. With only one bending observation for each treated condition, the experiment did not establish a reproducible pretreatment advantage. Relative FTIR differences were detected after both Demi80 and NaOH treatment but did not identify a bonding mechanism explaining the mechanical observations.

6.2. Pressing Conditions and Mechanical Performance

At every investigated temperature, the 9 MPa group had the lowest mean MOR and apparent MOE. The pooled mean MOR values were 13.02, 21.48 and 22.46 MPa at 9, 12 and 15 MPa, while apparent MOE increased from 0.597 to 1.218 and 1.335 GPa. Most of the descriptive increase occurred between 9 and 12 MPa. Cut-specimen density also increased with pressure, consistent with greater consolidation, but the gain in bending response was not proportional and substantial differences remained between nominally identical boards. Platen temperature showed no consistent bending trend over 170–$190\,^{\circ}$C.

The quadratic model was not statistically significant overall for MOR ($p = 0.329$) or apparent MOE ($p = 0.196$), so no reliable pressure–temperature optimum was established. The six additional boards were produced at the *model-selected best condition* of $185\,^{\circ}$C and 14.2 MPa, chosen from the exploratory JMP desirability analysis (Section 4.8). At this setting, the DOE models predicted 22.59 MPa MOR and 1.497 GPa apparent MOE, compared with measured unmodified means of (18.43 ± 5.41) MPa and (1.73 ± 0.43) GPa (Section 4.9.2). The measured means were 18.4% below and 15.6% above the respective predictions. This local comparison did not validate the response surfaces or establish a reliable manufacturing optimum.

6.3. Supporting Physical Changes and Board Integrity

Between approximately 5 min and 24 h after pressing, mean board thickness increased by $8.29 \pm 4.13\%$ and mass increased by 4.01% relative to the 5-min measurements. This post-pressing thickness recovery is neither immediate springback nor standard water-immersion swelling. Delayed mechanical relaxation and moisture sorption may both have contributed, but their separate effects were not determined.

Visible layering, cracks and local separation occurred at several specimen edges. No consistent association between these ordinal visual scores and pressing pressure, temperature or bending properties was established. The scores did not measure internal bond strength and could have been affected by cutting. With a 60 mm support span and approximately 10–13 span-to-thickness ratios, shear and relative movement between retained sheets may also have contributed to the measured bending response. The adapted test cannot determine the magnitude of that contribution or predict values for larger, standard-size specimens.

6.4. Exploratory Interlayer Additions

At the model-selected best condition, the added-pith boards reached mean MOR and apparent MOE of 34.15 ± 3.72 MPa and 2.63 ± 0.84 GPa, compared with 18.43 ± 5.41 MPa and 1.73 ± 0.43 GPa for the unmodified references. The bio-oil boards also had higher group means (19.98 ± 6.98 MPa and 2.08 ± 0.93 GPa), although their results varied more considerably. Each variant contained only two independent boards. Added pith changed total material loading and board thickness, its moisture content was unknown, and one pith-added board developed a pronounced pre-cut blister. Neither addition was therefore established to improve intrinsic interlayer bond strength reliably. Both remain relevant exploratory routes, with pith showing the larger observed increase in MOR.

6.5. Overall Conclusion

Four mechanically flattened coconut husk sheets were consolidated into testable binderless boards using a 4 min pressure hold within a prescribed 4.5 min press operation. This establishes laboratory-scale feasibility for the investigated material and dimensions, but not a repeatable or industrially validated process. Higher pressure was generally associated with better average bending performance, whereas temperature effects were less consistent. Differences between nominally identical boards and visible defects indicate that reliable interlayer integrity remains unresolved. Added pith showed the strongest exploratory potential for improving bending performance, although its contribution to bonding was not isolated.

Some specimens reached numerical JIS A 5905 and EN 622-5 bending-strength benchmarks, but the adapted tests and absence of internal-bond, water-immersion and fire-performance measurements prevent product-compliance claims [11, 17, 16]. Published milled-husk boards also achieve high bending values, so retaining long fibres cannot yet be claimed to improve strength or overall processing efficiency. Further development should establish reproducible interface performance and evaluate standard-size boards before the route is considered for a specific product.

7

Recommendations

The next development stage should test whether the higher bending values obtained in selected retained-sheet boards can be reproduced without compromising whole-board integrity. The priorities below address the main unresolved questions: sheet-interface load transfer, specimen geometry, post-pressing dimensional changes and scale-dependent vapour escape.

7.1. Priority 1: Interlayer Bonding and Controlled Pith Addition

Repeat the unmodified, added-pith and bio-oil variants using more independently manufactured boards at the model-selected best condition of $185\,^{\circ}$C and 14.2 MPa, while recording full material masses and moisture conditions. For pith trials, condition and characterise the added pith before use, record its dry mass and distribute it consistently across the three interfaces. Include comparisons that distinguish the effects of extra material loading from those of interlayer pith placement; a constant-base-sheet comparison alone cannot isolate bonding from an increase in total mass. For bio-oil trials, verify the material identity and condition, measure the amount applied to each interface and develop a repeatable application method.

Determine internal bond strength and document representative cross-sections before and after mechanical testing. These measurements could test whether higher MOR accompanies improved contact or load transfer between sheets, rather than simply a change in thickness or material loading. Record the location and severity of whole-board blisters independently of post-cut edge scores, so that bending performance and board integrity remain separate outcomes.

7.2. Priority 2: Bending Geometry, Failure Mode and Reproducibility

Increase independent replication and balance production order across temperatures. Standardise sheet grading, fibre orientation, lay-up sequence, material loading, trimming and the outer face presented to the bending nose. Record production day and individual board condition.

Once this procedure is repeatable, compare parallel and cross-oriented lay-ups or deliberate pith placement using comparable dry material loading and sufficient independent boards. Assess bending in both principal directions, failure modes and internal bond strength rather than assuming that fibre continuity or cross-orientation improves performance.

Prepare larger and properly conditioned bending specimens and test them using EN 310 geometry and measurements where feasible [11]. At a nominal thickness near 5 mm this implies an approximately 100 mm support span and longer, wider specimens than the present setup. Recording direct mid-span deflection and examining more than one span-to-thickness ratio would help assess whether shear deformation or interlayer movement contributed to the current apparent MOE. It would not be appropriate to assume that larger specimens necessarily produce higher MOR.

7.3. Priority 3: Post-Pressing Recovery and Vapour Management

Separate delayed mechanical relaxation from moisture-dependent expansion in a dedicated experiment. Record mass, thickness and external volume immediately after safe handling and at consistent later times, with temperature and relative humidity logged. Compare otherwise equivalent boards stored in dry or moisture-restricted conditions with boards exposed to controlled humidities. Independent moisture measurements and a longer conditioning period would indicate whether the recorded mass increase reflects moisture uptake and how much of the

dimensional recovery persists without humidity exchange. These tests should remain distinct from the standard 24 h water-immersion swelling procedure.

Investigate venting and pressure-release profiles alongside dimensional control. The present small, unconfined boards had short paths to their free edges, unlike the central region of a larger panel. Larger trial boards may develop different internal vapour-pressure behaviour, but an increase in central blistering has not yet been demonstrated. Where feasible, measure board-core temperature, record complete force histories and compare vented and unvented pressure-release schedules. A lateral restraint or mould may improve geometry but should not be presumed to prevent blistering; its effect on moisture escape must also be assessed.

7.4. Priority 4: Mechanical and Product Validation

After manufacturing repeatability has improved, evaluate multiple specimens from each full-size board and compare the measured properties with relevant JIS A 5905 and EN 622-5 product benchmarks [17, 16]. The present bending results provide numerical development indications only. Product classification will require the applicable standard sampling, conditioning and test procedures, including internal bond strength, standard-size bending, water absorption and 24 h water-immersion thickness swelling. Reaction-to-fire performance and any other properties required for the intended non-load-bearing interior wall-panel use should be investigated separately rather than inferred from the current data.

Targeted FTIR and, if feasible, thermal analysis could provide additional information about pretreatment and pressing, but should be interpreted alongside mechanical tests and cross-sectional observations; spectral differences alone cannot identify an intrinsic bonding mechanism. A controlled sheet-versus-milled-furnish comparison with matched raw material, dry mass, conditioning and bending geometry would be needed to assess whether retaining long fibres provides a mechanical or process advantage.

A

Supporting comparison data for non-coconut lignocellulosic materials

This appendix contains reference studies on non-coconut lignocellulosic materials. These sources are not treated as coconut-husk product-route evidence. They are included only to support comparison with related agricultural residues or to evaluate the potential transferability of high-frequency dielectric heating.

A.1. Purpose of the appendix

The main literature review focuses on coconut husk, coir fibre, pith and whole-husk products. However, some non-coconut studies are useful as references. Bagasse is useful because it was tested in the same insulation-board study as coconut husk. Rice straw and MDF are useful because they provide high-frequency or dielectric-heating data, while direct coconut-husk high-frequency pressing studies were not found in the reviewed sources. General binderless-board reviews are used only for mechanism and process interpretation.

A.2. Reference materials and relevance

Table A.1: Non-coconut reference studies used as supporting comparison data.

Ref. ID	Material	Product / system	Binder	Density (kg/m^3)	Thickness (mm)	Heating method	Relevance to this thesis	Source
REF1	Bagasse	Low-density insulation board	None	250-450	25	Hot pressing	Direct comparison material tested in the same study as coconut husk.	[9]
REF2	Rice straw	Insulation board	MDI	200-350	40	High-frequency hot pressing	Shows high-frequency hot pressing for low-density insulation-board production.	[31]
REF3	MDF furnish	Medium-density fibreboard	UF	609; 705; 801	-	High-frequency curing	Shows that high-frequency curing can improve internal bond compared with hot-platen curing.	[32]
REF4	MDF mat	MDF model / experiment	UF	-	50; 70; 80	13.56 MHz dielectric heating	Provides dielectric-heating model data and cycle-reduction potential for thick mats.	[33]
REF5	Wood-based composites	Review	Various	-	-	Hot pressing	Supports interpretation of heat and mass transfer in hot pressing.	[34]
REF6	Lignocellulosic fibres	Binderless material review	None	-	-	Thermo-compression	Supports interpretation of binderless bonding mechanisms.	[6]
REF7	Agricultural residues	Binderless fibreboard review	None	-	-	Thermo-compression	Provides broader context for binderless agricultural-residue fibreboards.	[35]

A.3. Bagasse comparison from the Panyakaew and Fotios study

Bagasse is not a coconut-husk material, but it is retained in the appendix because Panyakaew and Fotios [9] tested bagasse boards alongside coconut-husk boards. This makes it useful for evaluating

whether coconut husk behaves differently from another agricultural residue under similar low-density board conditions.

Table A.2: Bagasse process and property values used only as comparison data.

Ref. ID	Material	Temp. (°C)	Time (min)	Pressure (MPa)	Density (kg/m^3)	k (W/mK)	MOR (MPa)	Result / note	Source
REF1-A	Bagasse	160-200	7-13	14.7	250	0.049-0.055	0.43	Low-density comparison set	[9]
REF1-B	Bagasse	160-200	7-13	14.7	350	0.049-0.055	1.51	Met JIS except thickness swelling at 200 °C / 13 min	[9]
REF1-C	Bagasse	160-200	7-13	14.7	450	-	4.16	Highest bagasse strength set	[9]

A.4. High-frequency and dielectric-heating reference studies

The high-frequency and dielectric-heating studies in this appendix are not coconut-husk product evidence. They are included because they indicate how volumetric heating may influence thick lignocellulosic mats, internal bond development and press-cycle time. Any transfer to coconut husk should be experimentally validated because dielectric heating depends strongly on moisture content, density, salt content, thickness and dielectric properties.

Table A.3: High-frequency and dielectric-heating reference values from non-coconut materials.

Ref. ID	Material / product	Freq. (MHz)	Time	MC (%)	Density (kg/m^3)	Thickness (mm)	Reported effect	Source
REF2	Rice-straw insulation board	-	shortened	14	200-350	40	High-frequency hot pressing produced insulation boards with reported k-values of 0.051-0.053 W/mK.	[31]
REF3	MDF furnish	-	-	-	609; 705; 801	-	High-frequency-cured MDF had higher internal bond than hot-platen-cured MDF.	[32]
REF4	MDF model / experiment	13.56	0-240 s	variable	-	50; 70; 80	Modelled internal temperature development and showed potential for reduced press cycle.	[33]

B

Supplementary Quadratic Regression Results

Tables B.1 and B.2 summarise the quadratic regression expressions and their reported fit statistics for the six continuous responses discussed in Section 4.6. The model form follows Equation (4.1):

$$\hat{Y} = \beta_0 + \beta_T T + \beta_P P + \beta_{TP}(T - 180)(P - 12) + \beta_{PP}(P - 12)^2 + \beta_{TT}(T - 180)^2. \tag{B.1}$$

Here, T and P are the nominal platen temperature (°C) and nominal pressing pressure (MPa). The terms $\beta_T T$ and $\beta_P P$ are written in un-centred form, while the interaction and squared terms are centred on 180 °C and 12 MPa. All models were fitted to the 18 independently manufactured DOE boards; no follow-up boards were included.

Table B.1: Coefficients of the quadratic prediction expressions for the main DOE responses. Values are displayed to six decimal places; MOR and apparent MOE correspond to Table 4.7.

Response	β_0	β_T	β_P	β_{TP}	β_{PP}	β_{TT}
MOR (MPa)	-23.232973	0.135130	1.572943	-0.006460	-0.414674	0.022607
Apparent MOE (GPa)	-1.117717	0.005642	0.123047	0.001601	-0.027908	-0.002354
Cut-specimen density (kg/m^3)	765.185219	-0.010972	23.052327	0.252910	-3.160315	-0.303348
Thickness recovery, 24 h (%)	49.288417	-0.168703	-0.927192	0.044431	0.164702	-0.007392
Mass gain, 24 h (%)	8.652709	-0.014288	-0.190175	-0.001824	0.013395	0.001911
Pressing mass loss (%)	2.308241	0.033931	-0.149633	0.000639	-0.003151	-0.000656

Note. Coefficients were obtained from the JMP prediction expressions fitted to the 18 DOE boards. The fitted domain is $170 \le T \le 190$ °C and $9 \le P \le 15$ MPa. The models are exploratory and have not been independently validated. Model fit statistics and individual coefficient p-values are reported in Table B.2.

Table B.2: Model fit statistics and individual coefficient p-values for the six main DOE responses ($n = 18$).

Response	R^2	Adj. R^2	Model p	p_T	p_P	p_{TP}	p_{PP}	p_{TT}
MOR (MPa)	0.351	0.080	0.329	0.545	0.0503	0.943	0.340	0.559
Apparent MOE (GPa)	0.423	0.182	0.196	0.701	0.0243	0.789	0.331	0.362
Cut-specimen density	0.613	0.452	0.0269	0.995	0.0015	0.719	0.349	0.319
Thickness recovery, 24 h	0.526	0.329	0.0763	0.109	0.0146	0.287	0.398	0.670
Mass gain, 24 h	0.825	0.751	0.0003	0.101	< 0.0001	0.589	0.404	0.195
Pressing mass loss	0.681	0.548	0.0096	0.0126	0.0022	0.201	0.890	0.750

Note. Model fit statistics and linear-term p-values are also reported in Table 4.8. The remaining individual coefficient p-values were obtained from the JMP Parameter Estimates output. Each model includes an intercept and five predictor terms, with 12 residual degrees of freedom. Individual coefficient p-values test each term conditional on the other fitted terms and do not replace the overall model significance test. The ordinal visual-delamination score is excluded from these continuous-response models.

Bibliography

[1] Anjana J. Atapattu et al. “Upcycling Coconut Husk By-Products: Transitioning from Traditional Applications to Emerging High-Value Usages”. In: *Agricultural Waste to Value-Added Products*. Ed. by R. Neelancherry et al. Springer Nature Singapore, 2024, pp. 249–273. DOI: 10.1007/978-981-97-2535-9_12.

[2] Alan Portal D’Almeida and Tiago Lima de Albuquerque. “Coconut Husk Valorization: Innovations in Bioproducts and Environmental Sustainability”. In: *Biomass Conversion and Biorefinery* 15 (2025), pp. 13015–13035. DOI: 10.1007/s13399-024-06080-5.

[3] Jan E. G. van Dam, Martien J. A. van den Oever, and Edwin R. P. Keijsers. “Production Process for High Density High Performance Binderless Boards from Whole Coconut Husk”. In: *Industrial Crops and Products* 20.1 (2004), pp. 97–101. DOI: 10.1016/j.indcrop.2003.12.017.

[4] Jan E. G. van Dam et al. “Process for Production of High Density/High Performance Binderless Boards from Whole Coconut Husk. Part 2: Coconut Husk Morphology, Composition and Properties”. In: *Industrial Crops and Products* 24.2 (2006), pp. 96–104. DOI: 10.1016/j.indcrop.2005.03.003.

[5] Jan E. G. van Dam et al. “Process for Production of High Density/High Performance Binderless Boards from Whole Coconut Husk. Part 1: Lignin as Intrinsic Thermosetting Binder Resin”. In: *Industrial Crops and Products* 19.3 (2004), pp. 207–216. DOI: 10.1016/j.indcrop.2003.10.003.

[6] Thibaud Pintiaux et al. “Binderless Materials Obtained by Thermo-Compressive Processing of Lignocellulosic Fibers: A Comprehensive Review”. In: *BioResources* 10.1 (2015), pp. 1915–1963.

[7] Claus Uhrenholt Jensen et al. “Fundamentals of Hydrofaction™: Renewable Crude Oil from Woody Biomass”. In: *Biomass Conversion and Biorefinery* 7.4 (2017), pp. 495–509. DOI: 10.1007/s13399-017-0248-8. URL: https://doi.org/10.1007/s13399-017-0248-8.

[8] Thomas Böger et al. “Binderless Boards Made of Milled Coconut Husk: An Analysis of the Technical Feasibility and Process Restraints”. In: *International Wood Products Journal* 9.1 (2018), pp. 3–8. DOI: 10.1080/20426445.2017.1400756.

[9] Satta Panyakaew and Steve Fotios. “New Thermal Insulation Boards Made from Coconut Husk and Bagasse”. In: *Energy and Buildings* 43.7 (2011), pp. 1732–1739. DOI: 10.1016/j.enbuild.2011.03.015.

[10] Martin H. B. Snijder et al. *Coir Based Building and Packaging Materials: Final Report of Project CFC/FIGHF/11*. CFC Technical Paper 43. Amsterdam, The Netherlands: Common Fund for Commodities, 2005.

[11] European Committee for Standardization. *EN 310:1993: Wood-based panels – Determination of modulus of elasticity in bending and of bending strength*. CEN, 1993. URL: https://www.nen.nl/en/nen-en-310-1993-en-10293.

[12] Ngesa Ezekiel et al. “Effect of Temperature and Durations of Heating on Coir Fibers”. In: *Industrial Crops and Products* 33.3 (2011), pp. 638–643. DOI: 10.1016/j.indcrop.2010.12.030.

[13] Douglas Lamounier Faria, Lourival Marin Mendes, and José Benedito Guimarães Junior. “Effect of surface treatment on the technological properties of coconut fiber-reinforced plant polyurethane composites”. In: *Environmental Science and Pollution Research* (2023). DOI: 10.1007/s11356-023-25946-1.

[14] Mohammed Abdullah Hamad Alharbi et al. “Effects of chemical composition, mild alkaline pretreatment and particle size on mechanical, thermal, and structural properties of binderless lignocellulosic biopolymers prepared by hot-pressing raw microfibrillated Phoenix dactylifera and Cocos nucifera fibers and leaves”. In: *Polymer Testing* 84 (2020), p. 106384. DOI: 10.1016/j.polymertesting.2020.106384.

[15] Jose A. Espinoza Montero et al. “Preparation of Thermal Insulation Panels from Coconut Husk Using Polylactic Acid (PLA) as Agglutinative”. In: *InterSedes* 23.48 (2022), pp. 290–307. DOI: 10.15517/isucr.v23i48.49852.

[16] European Committee for Standardization. *EN 622-5:2009: Fibreboards – Specifications – Part 5: Requirements for dry process boards (MDF)*. CEN, 2009. URL: https://www.nen.nl/en/nen-en-622-5-2009-en-141122.

[17] Japanese Standards Association. *JIS A 5905:2022: Fiberboards*. Japanese Standards Association, 2022. URL: https://webdesk.jsa.or.jp/books/W11M0090/?bunsyo_id=JIS+A+5905%3A2022.

[18] Japan Fibreboard and Particleboard Manufacturers Association. *MDF: Quality Requirements Based on JIS A 5905*. Industry summary; reference values are distinguished from mandatory specification values. 2022. URL: https://jfpma.jp/product/mdf.html.

[19] ASTM International. *ASTM D1037-12(2020): Standard Test Methods for Evaluating Properties of Wood-Base Fiber and Particle Panel Materials*. West Conshohocken, PA: ASTM International, 2020. DOI: 10.1520/D1037-12R20.

[20] Joana Mendes Ferraz et al. “Effects of Treatment of Coir Fiber and Cement/Fiber Ratio on Properties of Cement-Bonded Composites”. In: *BioResources* 6.3 (2011), pp. 3481–3492. URL: https://bioresources.cnr.ncsu.edu/resources/effects-of-treatment-of-coir-fiber-and-cementfiber-ratio-on-properties-of-cement-bonded-composites/.

[21] R. Hari Setyanto et al. “A Preliminary Study: The Influence of Alkali Treatment on Physical and Mechanical Properties of Coir Fiber”. In: *Journal of Materials Science Research* 2.4 (2013), pp. 80–88. DOI: 10.5539/jmsr.v2n4p80.

[22] Tiancheng Xiong et al. “Simultaneously enhancing strength and toughness of coir fiber through NaOH and sodium alginate treatment”. In: *Industrial Crops and Products* 222 (2024), p. 119668. DOI: 10.1016/j.indcrop.2024.119668.

[23] Nikos Bias. “Catalytic hydrothermal liquefaction of invasive species: A case study of Namibia’s Encroacher Bush”. Master’s thesis. Delft University of Technology, June 2023.

[24] European Committee for Standardization. *EN 324-1:1993: Wood-based panels – Determination of dimensions of boards – Part 1: Determination of thickness, width and length*. 1993. URL: https://www.nen.nl/en/nen-en-324-1-1993-en-10350.

[25] Luana Cristal Lirya Silva et al. “Heat Transfer and Physical-Mechanical Properties Analysis of Particleboard Produced with ZnO Nanoparticles Addition”. In: *BioResources* 14.4 (2019), pp. 9904–9915. DOI: 10.15376/biores.14.4.9904-9915. URL: https://bioresources.cnr.ncsu.edu/resources/27803/.

[26] European Committee for Standardization. *EN 323:1993: Wood-based panels – Determination of density*. 1993. URL: https://www.nen.nl/en/nen-en-323-1993-en-10080.

[27] John Paul Cabral et al. “Densification of timber: a review on the process, material properties, and application”. In: *Journal of Wood Science* 68 (2022), p. 20. DOI: 10.1186/s10086-022-02028-3. URL: https://doi.org/10.1186/s10086-022-02028-3.

[28] European Committee for Standardization. *EN 318:2002: Wood based panels – Determination of dimensional changes associated with changes in relative humidity*. 2002. URL: https://www.nen.nl/en/nen-en-318-2002-en-68314.

[29] European Committee for Standardization. *EN 317:1993: Particleboards and fibreboards – Determination of swelling in thickness after immersion in water*. 1993. URL: https://www.sis.se/en/produkter/wood-technology/woodbased-panels/fibre-and-particleboards/ssen317/.

[30] European Committee for Standardization. *EN 325:2025: Wood-based panels – Determination of dimensions of test pieces*. 2025. URL: https://www.nen.nl/nen-en-325-2025-en-345270.

[31] Kangcheng Wei et al. “Development and Performance Evaluation of a New Thermal Insulation Material from Rice Straw Using High Frequency Hot-Pressing”. In: *Energy and Buildings* 87 (2015), pp. 116–122. DOI: 10.1016/j.enbuild.2014.11.026.

[32] Robert R. Stevens and George E. Woodson. “High-Frequency and Hot-Platen Curing of Medium-Density Fiberboards”. In: *Forest Products Journal* 27 (1977), pp. 46–50.

[33] Celeste M. C. Pereira et al. “High Frequency Heating of Medium Density Fiberboard (MDF): Theory and Experiment”. In: *Chemical Engineering Science* 59.4 (2004), pp. 735–745. DOI: 10.1016/j.ces.2003.09.038.

[34] Peixing Wei et al. “Hot Pressing of Wood-Based Composites: A Review”. In: *Forest Products Journal* 66.7–8 (2016), pp. 419–427. DOI: 10.13073/FPJ-D-15-00047.

[35] M. Nasir et al. “Recent Development in Binderless Fiber-board Fabrication from Agricultural Residues: A Review”. In: *Construction and Building Materials* 211 (2019), pp. 502–516. DOI: 10.1016/j.conbuildmat.2019.03.279.